

**An Investigation on the Optimum Aging
Condition for HFQ-processed AA6082
Aluminium Alloy**



A thesis submitted to the University of Birmingham for the degree of
MSc by research

by

Yuan Liang

School of Metallurgy and Materials
College of Engineering and Physics Science
University of Birmingham

November 2016

UNIVERSITY OF
BIRMINGHAM

University of Birmingham Research Archive

e-theses repository

This unpublished thesis/dissertation is copyright of the author and/or third parties. The intellectual property rights of the author or third parties in respect of this work are as defined by The Copyright Designs and Patents Act 1988 or as modified by any successor legislation.

Any use made of information contained in this thesis/dissertation must be in accordance with that legislation and must be properly acknowledged. Further distribution or reproduction in any format is prohibited without the permission of the copyright holder.

SYNOPSIS

The innovative solution heat treatment, forming and in-die quenching (HFQ) process combines die forming and quenching in one operation to reduce thermal distortion and spring back effects. However, the hardness of aged HFQ processed AA6082 components varied with the positions and the peak hardness of the product is lower than AA6082 in T6 condition.

In this project, a Gleeble machine was used to simulate HFQ process to produce deformed AA6082 specimens with the strain ranging from 0 to 30%; a wide range of aging time at 180°C was employed to identify the optimal aging time for a given strain; and a series of materials characterisation techniques were used to investigate the mechanism involved including XRD, optical microscopy, SEM, EDX, TEM.

The experimental results have demonstrated that the pre-deformation introduced by Gleeble tensile testing after solution heat treatment has a significant impact on the response of the deformed AA6082 material to subsequent aging at 180°C. In general, the optimal aging time corresponding to the peak hardness for HFQ-simulated samples decreases with increasing the strain because the plastic deformation induced defects (such as voids and dislocations) accelerate the aging process. The pre-deformation reduced the peak hardness from 120HV0.3 for T6 conditioned AA6082 to about 105HV0.3 due to the accelerated transformation of β'' to β' in severely deformed areas. The mechanisms involved are discussed based on TEM studies and the optimal aging time at 180°C for different strains is identified.

ACKNOWLEDGEMENTS

This work has been carried out in the Surface Engineering Group, Department of Metallurgy and Materials, University of Birmingham. I would like to take this opportunity to thank the following individuals for their contribution towards the success of this project.

Firstly, I would like to thank my supervisor Prof. H. Dong and co-supervisor Dr. X. Li for their patient guidance, continuous help throughout my MSc by research project. Their enthusiastic and professional attitudes towards my project and valuable suggestions motivated me to complete this project successfully.

Thanks to Q. Liu, Y. Dong and Q. Chen who provided expertise and assistance during this research.

I would like to thank all the members of the Surface Engineering Group for their kind help and precious discussions in my research work.

Many thanks to the technique staff in the Department of Metallurgy and Materials who helped me train Gleeble machine and other related experimental equipment.

Finally, I also would like to thank my parents for supporting and encouraging my study in University of Birmingham.

CONTENTS

CHAPTER I INTRODUCTION.....	1
CHAPTER II LITERATURE REVIEW	4
2.1 Aluminium Alloy Categories	4
2.1.1 Cast Aluminium Alloys Designation	6
2.1.2 Wrought Aluminium Alloys Designation.....	7
2.1.2.1 6XXX Series Aluminium Alloy.....	10
2.1.2.2 6082 Aluminium Alloy	11
2.2 Heat Treatments of AA6082.....	13
2.2.1 Aluminium Temper Designation System.....	13
2.2.2 Annealing.....	16
2.2.3 Solution Heat Treatment.....	20
2.2.4 Aging Treatment	22
2.2.5 Precipitation Hardening Mechanism.....	27
2.3 Forming Methods of Aluminium Alloy	30
2.3.1 Cold Forming	30
2.3.2 HFQ Process	32
2.4 Effect of Pre-deformation Before Aging on Precipitate Hardening.....	37
2.5 Inclusion Phase Transformation During Heat Treatments	41
CHAPTER III EXPERIMENTAL METHODS	43
3.1 Materials and Sample Preparation.....	43
3.2 Heat Treatment	48
3.2.1 Solution Heat Treatment.....	48
3.2.2 Aging Treatments.....	50
3.3 Gleeble Test.....	52
3.3.1 Equipment and Sample Settings	52
3.3.2 Evaluation of Temperature Difference	54
3.3.3 Setting up of HFQ Simulation Tests.....	55
3.4 Post-treatment Characterization	59
3.4.1 Sample Preparation for the Aging of Dog-bone Shaped Specimens	59
3.4.2 Micro-hardness Test.....	60
3.4.3 Microstructure Characterisation.....	61

3.4.3.1 Optical Microscope Observation.....	61
3.4.3.2 SEM (EDS) Observation.....	61
3.5 XRD and TEM Detect	62
3.5.1 XRD Analysis	62
3.5.2 TEM Characterisation.....	63
3.5.2.1 Sample Preparation	63
3.5.2.2 TEM Observation.....	64
CHAPTER IV RESULTS.....	65
4.1 Characterisation of As-received Material.....	65
4.1.1 Microstructure of As-received AA6082 Samples.....	65
4.1.2 XRD and TEM characterisation.....	68
4.2 Hardness of Solution Heat Treated Samples	72
4.3. Effect of Pre-strain.....	74
4.3.1 Hardness of Aged HFQ-simulated Samples	74
4.3.2 Optimal Aging Time for Peak Hardness.....	77
4.4 Microstructure Characterisation of HFQ-simulated Samples	82
4.4.1 Optical and SEM microstructure	82
4.4.2 XRD patterns of HFQ-simulated Samples	86
4.4.3 TEM and EDS Analysis.....	89
4.4.3.1 Solution Heat Treated and 180°C-8h Aged Sample	89
4.4.3.2 HFQ Process Simulated AA6082 Samples	91
CHAPTER V DISCUSSION.....	97
5.1 The Relationship between Optimum Aging Time and Strains.....	97
5.2 Reduced Peak Hardness of HFQ-simulated Samples After Aging	100
5.3 Optimised Aging Condition Applied in HFQ-processed AA6082 Alloy	104
CHAPTER VI CONCLUSIONS AND SUGGESTED FUTURE WORK	107
6.1 Summary and Conclusions	107
6.2 Recommendations for Future Work	110
REFERENCES.....	111

CHAPTER I INTRODUCTION

Aluminium and aluminium alloys are the leading non-ferrous metals widely used in food and beverage containers, package, automotive vehicles, architectures and energy transportation (www.constellium.com). These broad applications are owing to the advantages of their properties, for instance, low strength to weight ratio, high corrosion resistance, excellent electrical and thermal conductivity as well as high toughness (www.aalco.co.uk).

To overcome the shortage of relatively low strength compared with steels, especially in transport applications, aluminium alloys are artificially aged to enhance their strength by precipitation hardening. However, aged aluminium alloys with enhanced hardness have problems in forming process, such as spring back and shrinkage, because of low toughness and poor formability after aging treatment (LoCoLite, 2013). A novel forming method called HFQ process is then designed for high strength heat-treatable aluminium alloys, which combines die forming and quenching together. It is known that aluminium alloys possess high toughness and formability after solution heat treatment, and thus HFQ process solves the problems during forming (Zhang, 2014).

AA6082 alloy is a heat-treatable aluminium alloy, which contains such primary elements as Al, Mg and Si. After being artificially aged to T6 condition, it possesses a high hardness about 120 HV (Zhang, 2014). A component of car door inner structures was produced by AA6082 alloy via HFQ process and then underwent aging treatment to T6 condition. However, as shown in Fig.1-1, compared with AA6082 alloy in T6

condition, the hardness of the cross-section area of two marked area in yellow dotted squares dropped significantly and different areas of the component showed varying hardness.

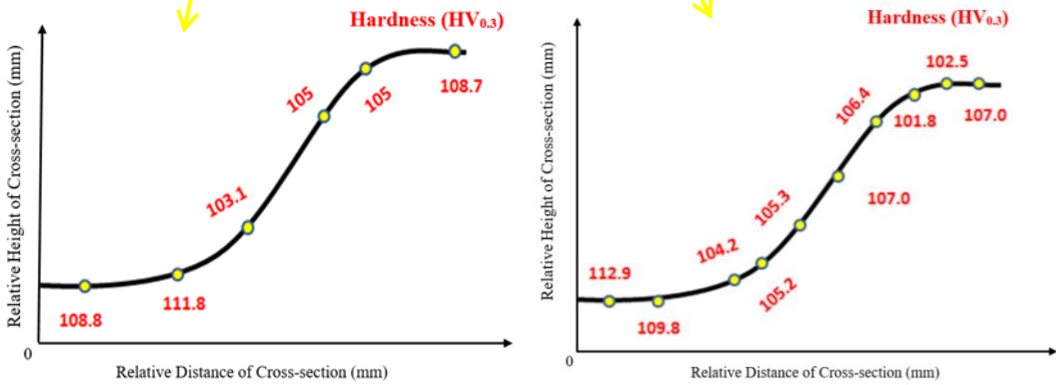


Figure 1-1 Cross-section hardness of marked area in HFQ-processed and aged AA6082 components, unit: HV, loads 300g.

Researches carried out by Birol (2006) discovered via DSC analysis that deformation introduced by punching after solution heat treatment was able to accelerate the precipitation kinetics of β'' and β' metastable second phases, thus leading to a significant change in the peak arrangement of the DSC curve. But it was also discovered that the sample punched before solution heat treatment showed enhanced peak hardness after aging, which was opposite from the hardness results showed in HFQ-processed and aged AA6082 door inner component. It was supposed that T6 condition was no longer the optimal aging condition for the HFQ-processed AA6082 components. However, no research has been done on the impact of deformation introduced during HFQ process on the subsequent aging process, as well as the final properties of AA6082 material.

Therefore, the aim of this project was to study the optimum aging condition for HFQ-processed AA6082 components to reach (or approach to) the hardness of AA6082 alloy in T6 condition. However, it is known that the strain of a HFQ-processed component varied with its position. Hence, in order to apply the HFQ process in automotive vehicles manufacture, it is a timely task from both a scientific and a technological point-of-views to study the optimal aging conditions as a function of strain introduced by HFQ process. In addition, this project also explored the effect HFQ processing on the hardness of HFQ-processed and peak-aged samples as compared with the hardness of T6 conditioned AA6082 alloy.

CHAPTER II LITERATURE REVIEW

2.1 Aluminium Alloy Categories

Aluminium is now the second most widely used metal in the world after iron. Compared with other metals, pure aluminium has the advantages of low weight (low density), easy machinability, excellent corrosion resistance, superior thermal and electrical conductivity (www.aluminiumdesign.net). Therefore, it is the main raw material for conductor cables and foil (Woodward, 2001).

However, pure aluminium is unable to meet the requirement for high strength applications in most cases. To overcome this, aluminium is alloyed with some elements, for instance, boron, copper, lithium, magnesium, manganese, silicon, tin, and zinc commonly (Woodford, 2016). Small quantities of chromium, zirconium, titanium, iron, lead, nickel and bismuth are also added in pure aluminium (www.azom.com, 2015). Besides high strength, aluminium alloys possess other enhanced mechanical properties as well, as shown in Fig.2.1-1 For example, by alloying aluminium with copper, the new material is able to survive at elevated temperature, which is suitable to be used in plane or car engine. Alloying aluminium with magnesium to enhance machinability, the alloy is easy to shape and seal and applied in packaging. Aluminium alloy containing boron is the common raw material used in power plants to carry electricity in long distance (Woodford, 2016).



Figure 2.1-1 Alloy elements effects on aluminium alloy properties (www.aluminiumdesign.net).

Aluminium alloys are commonly categorised into different groups according to the mechanical properties and characteristics of the material, for instance, the main elements alloyed in the pure aluminium, its degree and sensitivity of response to mechanical and thermal treatment. Besides the identification principle above, the cast and wrought aluminium alloys also have different systems of identification. The wrought alloys are marked with a 4-digit system, while the castings have a 3-digit and 1-decimal place system (www.alcotec.com). Details are introduced as below.

2.1.1 Cast Aluminium Alloys Designation

The first digit of its 3 digit-plus decimal designation identification system indicates the principal alloying element alloyed in the material. Different numbers stand for different elements as shown in Table 1 (www.alcotec.com). The digits on second and third positions are random numbers used to identify a specific alloy in the series. If the decimal digit is 1 or 2, it indicates that the alloy is an ingot while 0 following the decimal point means the alloy is a casting. Sometimes a prefix capital letter added stands for a modification to a specific alloy (www.alcotec.com).

Table 1 Cast aluminium alloy designation system (Brown et al., 1985).

Alloy Series	Principal Alloying Element
1xx.x	99.000% minimum Aluminium
2xx.x	Copper
3xx.x	Silicon Plus Copper and/or Magnesium
4xx.x	Silicon
5xx.x	Magnesium
6xx.x	Unused Series
7xx.x	Zinc
8xx.x	Tin
9xx.x	Other Elements

In terms of alloying elements proportion, wrought alloys only contain alloying elements less than 4 percentages in total, which is much lower than that of cast aluminium alloys. Cast alloys contain alloying elements in greater quantities, but the elements alloyed are quite similar to wrought ones (Brown et al., 1985).

Apart from chemical composition differences, mechanical properties of cast and wrought aluminium alloys are also different at elevated temperatures. When the

solidus temperature of the alloy is reached, intergranular regions of eutectic composition start to melt, which leads to brittleness of cast aluminium alloys at high temperatures. However, most wrought alloys have a much higher solidus temperature (generally over 600⁰C) than cast aluminium alloys, which ranges from 520⁰C to 580⁰C. As a result, while the wrought alloys remain ductile in a certain temperature range, cast aluminium alloys tends to be separated into small pieces (Brown et al., 1985).

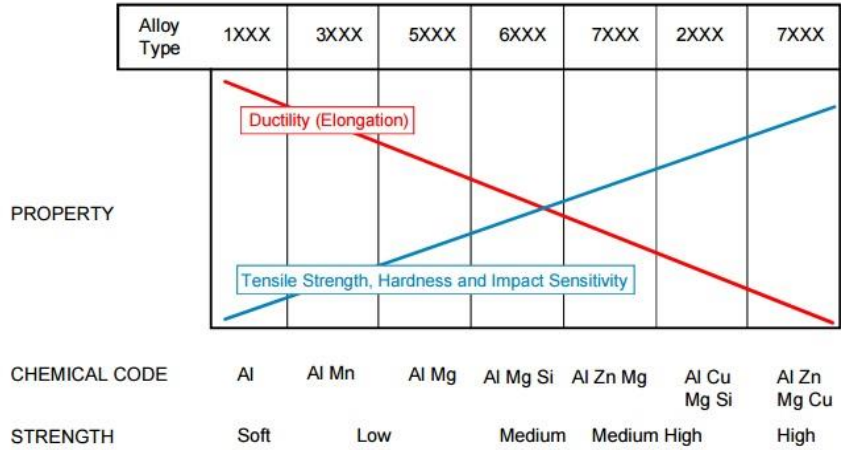
2.1.2 Wrought Aluminium Alloys Designation

The first digit of its 4 digit code designation identification system indicates the principal alloying element in the material. Different elements are marked by different numbers as shown in Table 2 (www.alcotec.com). If the number in the second position differs from 0, it indicates a modification to a specific alloy. The two digits following on the right are random numbers used to identify a specific alloy in the series (www.alcotec.com). However, an exception of the principle needs to be mentioned here that, for 1XXX series, the third and fourth digits indicate the minimum aluminium percentage above 99%. Besides, minor changes in the chemical composition of a certain alloy due to national variations are indicated by a suffix capital letter following the 4-digit code (Cobden et al., 1992).

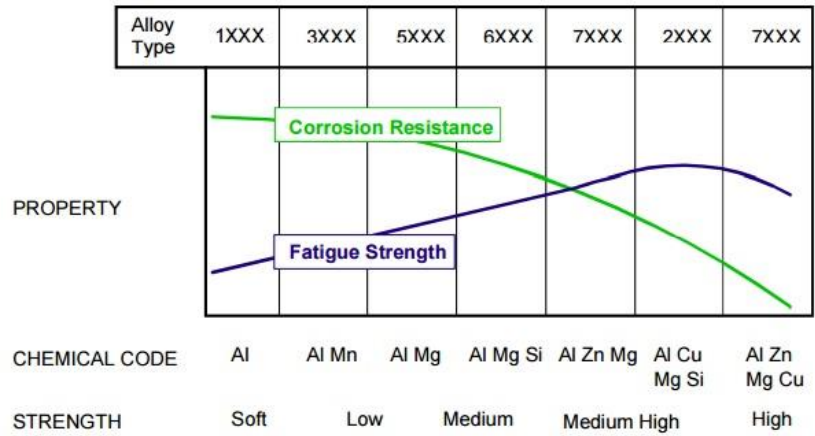
Table 2 Wrought aluminium alloy designation system (www.alcotec.com).

Alloy Series	Principal Alloying Element
<i>1xxx</i>	99.000% Minimum Aluminium
<i>2xxx</i>	Copper
<i>3xxx</i>	Manganese
<i>4xxx</i>	Silicon
<i>5xxx</i>	Magnesium
<i>6xxx</i>	Magnesium and Silicon
<i>7xxx</i>	Zinc
<i>8xxx</i>	Other Elements

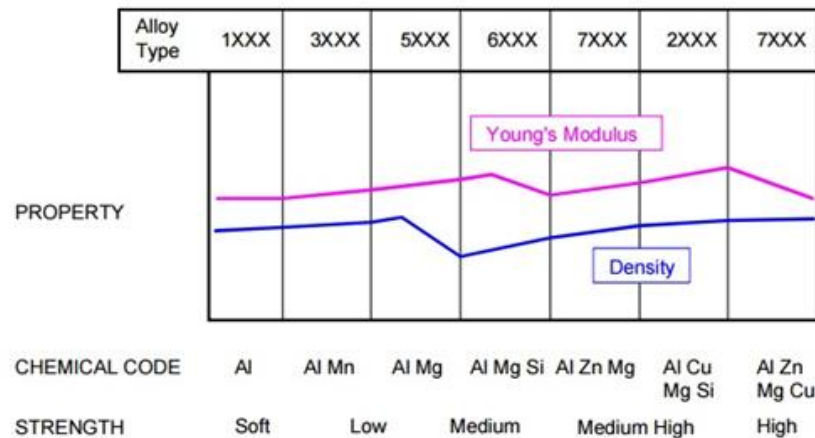
Differences in chemical composition lead to variation in properties and characteristics. Elongation of the alloy decreases obviously as the first digit number increases in a linear relationship except for 2xxx series. Some alloys of 7xxx series reach the minimum elongation value, while 2xxx alloy series show the second lowest ductility in the sequence. In terms of hardness, tensile strength and impact sensitivity, the rise tendency is consistent with decline of elongation, shown as Fig.2.1-2 (a) below. However, for fatigue strength, 2xxx series aluminium alloys possess the highest strength and then it declines with the decrease of the first digit in designation system (Fig.2.1-2 (b)). Corrosion resistance exhibits a parabola going downwards consistently with ductility of each alloy. It is shown apparently in Fig.2.1-2 (c) that the Young's modulus of 1xxx series is lower than other series, whilst the maximum values lie in 6xxx series, 2xxx series and some of 7xxx series (containing copper as main alloying elements). In addition, different alloys in the same series show diverse modulus due to different principal alloying elements proportion (Cobden et al., 1992).



(a)



(b)



(c)

Figure 2.1-2 The effect of alloying elements on alloy (a) ductility, tensile strength, hardness and impact sensitivity; (b) corrosion resistance and fatigue strength; (c) Young's modulus and density (Cobden et al., 1992).

2.1.2.1 6XXX Series Aluminium Alloy

6xxx series belong to high strength aluminium alloy, which are heat-treatable and strengthened by precipitation hardening but weaker than the 7xxx and 2xxx series. Compared with other wrought aluminium alloy series, the alloys also exhibit good formability and weldability, with ultimate tensile strength (UTS) in the range of 18-58 ksi (124-400MPa) approximately (www.alcotec.com). The principal alloying elements of this series are silicon (mostly ranges from 0.3 to 1.5 wt%) and magnesium (www.aluminium.matter.org.uk). Magnesium and silicon alloyed in pure aluminium combines to form a compound of magnesium-silicide precipitates. The precipitates enable the material to undergo solution heat treatment for strength improvement (www.alcotec.com). Furthermore, Si contributes to improving corrosion resistance and fluidity of the molten alloy, whilst magnesium enhances the material weldability. However, excessive Si reduces the machinability when the Si content is more than 13% (www.aluminium.matter.org.uk).

These aluminium alloys are predominantly applied in extruded form for machined products and widely used throughout the welding fabrication industry. Normal form of the preliminary cold worked products and their corresponding alloy codes are shown in Table 3 (Zhang, 2014). Owing to the solidification crack sensitivity, the materials are prevented to be arc welded without filler materials. According to the application and service requirements, 4xxx and 5xxx are used as general filler materials (www.alcotec.com).

Table 3 Products from various 6xxx aluminium alloys (Zhang, 2014).

Products	Aluminium alloy
Sheet	6009 6010 6951 6061 6063 6082
Plate	6951 6061 6082
Drawn tubing	6101 6951 6053 6061 6262 6063
Extruded tube and pipe	6101 6053 6061 6262 6066 6070
Extruded shapes	6006 6262 6101 6063 6105 6351 6066 6053 6061 6071
Rolled shapes	6101 6061
Wire	6201 6151 6951 6053 6061 6262
Rod	6101 6201 6951 6053 6061 6262 6066
Rivers	6151 6053 6061
Forgings	6101 6151 6053 6061 6066
Impacts	6151 6053 6061 6063 6043

2.1.2.2 6082 Aluminium Alloy

Aluminium alloy 6082 (AA6082) is also equivalent to EN AW-6082, A96082 and ISO: AlSi1MgMn (Zhang, 2014). The chemical composition of as-received AA6082 is shown in Table 4. Temper is available for AA6082, of which excellent mechanical strength after heat treatment is at the top for 6xxx series. It is also shown in Table 5 that the elongation of the material ranges from 6% to 13%, moderate among 6xxx series aluminium alloy (Zhang, 2014). Furthermore, these alloys possess good corrosion resistance and fusion weldable. The alloy is generally used in the form of plate, sheet, rod and bars, applied in structural parts or welded components of cars, railways, trucks, shipbuilding and aerospace (www.aviometal.com).

Table 4 Chemical composition of AA6082 (Zhang, 2014).

Element	Element Range/ %	Actual Element / %
Si	0.7-1.3	0.9
Fe	0-0.5	0.38
Cu	0-0.1	0.08
Mn	0.4-1.0	0.42
Mg	0.6-1.2	0.7
Cr	0-0.25	0.02
Zn	0-0.2	0.05
Ti	0-0.1	0.03
Others Each	0-0.05	0.02
Others Total	0-0.15	0.03

Table 5 Mechanical Properties of 6082 (Zhang, 2014).

	Yield Strength/MPa	Tensile Strength/MPa	Elongation/%
Min	210	310	6
Actual	309	344	13

2.2 Heat Treatments of AA6082

2.2.1 Aluminium Temper Designation System

Even the alloys with completely same composition are able to possess diverse mechanical properties after undergoing thermo-mechanical processing during production or post-production, which will further influence the applications (www.aluminium.matter.org.uk). As a result, another designation system is created to identify two distinctly different types of aluminium alloy, heat treatable groups and non-heat treatable alloys, shown as Fig.2.2-1 (www.alcotec.com).

In terms of heat treatable aluminium alloys, their optimal mechanical properties are obtained through thermal treatment at the beginning of the work hardening process (www.aluminium.matter.org.uk). The most common heat treatments are solution heat treatment and artificial aging. 2xxx, 6xxx, 7xxx series and part of 4xxx series wrought aluminium alloys belong to heat-treatable group. For cast aluminium alloys, 2xx.x, 3xx.x, 4xx.x and 7xx.x series are heat treatable. Temper methods vary drastically by changing treatment temperature and time in order to acquire a wide variety of mechanical properties (www.alcotec.com).

Non-heat treatable alloys are only able to enhance their properties by strain hardening mechanism through cold working such as rolling, forging, extrusion, drawing and so on. This group contains 1xxx, 3xxx, part of 4xxx and 5xxx wrought aluminium alloys series (www.aluminium.matter.org.uk).

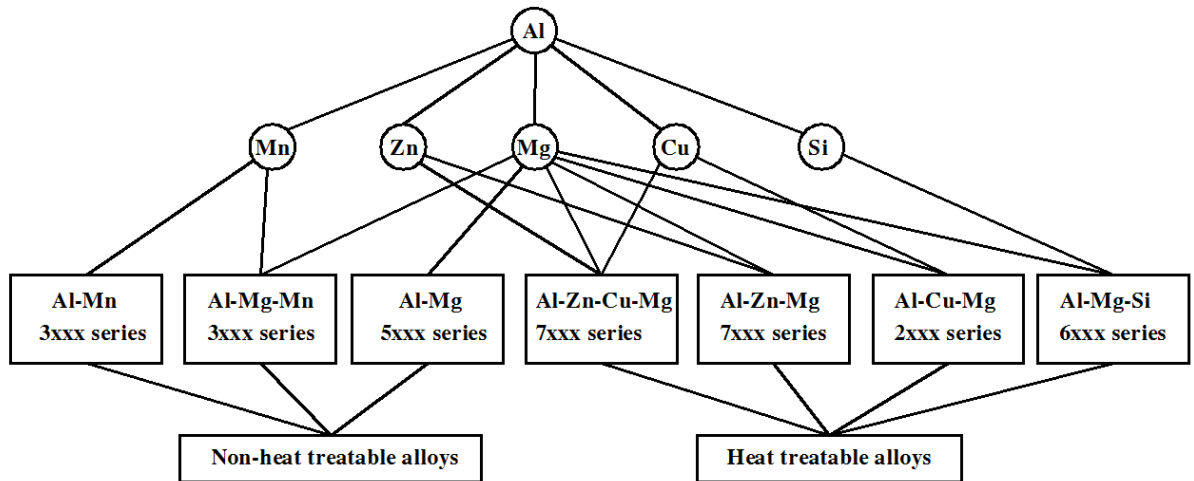


Figure 2.2-1 Diagram of aluminium alloy categories and chemical composition (Zhang, 2014)

Table 6 Basic Temper Designations (www.alcotec.com).

Letter	Meaning
F	As fabricated – Applies to products of a forming process in which no special control over thermal or strain hardening conditions is employed
O	Annealed – Applies to product which has been heated to produce the lowest strength condition to improve ductility and dimensional stability
H	Strain Hardened – Applies to products that are strengthened through cold-working. The strain hardening may be followed by supplementary thermal treatment, which produces some reduction in strength. The “H” is always followed by two or more digits (see subdivisions of H temper below)
W	Solution Heat-Treated – An unstable temper applicable only to alloys which age spontaneously at room temperature after solution heat-treatment
T	Thermally Treated - To produce stable tempers other than F, O, or H. Applies to product that has been heat-treated, sometimes with supplementary strain-hardening, to produce a stable temper. The “T” is always followed by one or more digits (see subdivisions of T temper below)

In temper identification system, some specific captain letters are used to stand for different treatment conditions aluminium alloys undergo. Detailed explanations are shown in Table 6.

In this project, the supplied specimens were made from AA6082 alloy on T6 condition, which stands for thermal treated condition. T condition includes 10 types of heat treatment processes as described below in Table 7.

Table 7 Subdivisions of T Temper (www.alcotec.com).

T1	Naturally aged after cooling from an elevated temperature shaping process, such as extruding.
T2	Cold worked after cooling from an elevated temperature shaping process and then naturally aged.
T3	Solution heat-treated, cold worked and naturally aged.
T4	Solution heat-treated and naturally aged.
T5	Artificially aged after cooling from an elevated temperature shaping process.
T6	Solution heat-treated and artificially aged.
T7	Solution heat-treated and stabilized (overaged).
T8	Solution heat-treated, cold worked and artificially aged.
T9	Solution heat treated, artificially aged and cold worked.
T10	Cold worked after cooling from an elevated temperature shaping process and then artificially aged.

2.2.2 Annealing

Cold working brings about a distorted and dislocated structure of aluminium alloys, which is not stable and tends to revert into strain-free state. In terms of aluminium alloys, these structural variations take place at high temperature during annealing process (www.totalmateria.com, 2006). Annealing, aiming to soften metallic materials, is a process consisting of heating the materials to 310-400°C, holding for 0.5 to 3 hours subject to alloy size and type, after that, cooling at a suitable rate to room temperature (AZoM, 2004).

- Recovery

The number of dislocations decreases most dramatically at the centre of grain fragments during this stage. Subgrain formation takes place with a mass of dislocations concentrated on the boundary of subgrain structure initially. As heat treatment goes on, polygonization recovers and the size of subgrain grows as well. At the end of the stage, most subgrains have boundaries without dislocation tangles (www.totalmateria.com, 2006). However, the grain size remains the same and internal stresses introduced by cold working are partly removed (Zhang, 2014), which causes an initial rapid but slight decrease in hardness (www.totalmateria.com, 2006).

- Recrystallization

As heating time lasts and temperature rises on the basis of recovery stage, recrystallization occurs with gradual formation of new strain-free grains. This process totally follows the principles of equation: $\frac{1}{t} = k e^{-a/T}$, in which k and a are constants, e is the base of natural logarithms (approximately 2.7183), t is time and T is the absolute temperature. The constant a is equivalent to Q/R, where Q stands for

energy term, much like activation energy, and R is the gas constant (www.totalmateria.com, 2006).

During this process, new grains nucleate and replace distorted original grains caused by internal stress until the former grains are totally transformed, shown as Fig.2.2-2 below (Zhang, 2014). Meanwhile, the grain size of strain-free grains newly formed is under the effect of alloy composition. It is proved that Cu, Fe, Mg and Mn reduce grain size. It is also discovered that in rolled sheet, new grains reorient which is different from the principal deformed texture (www.totalmateria.com, 2006). Accompanying these changes, the alloy turns to a stable status with low free energy. Large amounts of dislocations are eliminated, thus the ductility and strength of the material increasing dramatically (Zhang, 2014).

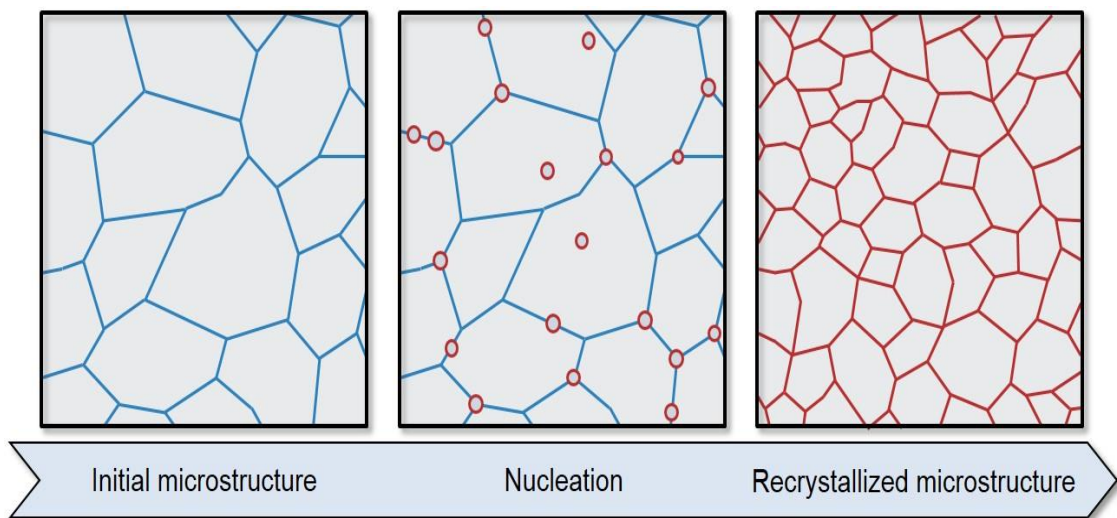


Figure 2.2-2 Recrystallization process (www.hhallberg.com, 2014).

- Grain growth

After the first two stages complete, grains start to grow quickly and coarsely when the material is heated continuously. One of coarsening forms is slow growth and uniform grain size increase, which is identified as normal grain growth. When grains grow preferentially and annex the surrounding grains, which causes a bimodal distribution of recrystallized grain sizes, this situation is called abnormal grain growth (Zhang, 2014). In commercial aluminium alloys, impurity phases and the composition of intermetallic compounds restricts the normal grain growth process. For instance, manganese and chromium pin the grain boundaries, prevent further movement and thus slow down homogeneous growth. However, in terms of abnormal grain growth, inhibited elements, for example, iron, manganese and chromium lose the negative effects on the process due to elevated temperatures (www.totalmateria.com, 2006). This stage results in apparent drop of the strength, thus the decrease in the hardness of the aluminium alloy (Zhang, 2014).

Under industrial conditions, AA6082 aluminium alloys are usually annealed at 415°C for 1 hour holding and then cooled to 260°C gradually at a constant speed which takes about 5.5 hours. The cooling rate from 260°C to room temperature has no effect on alloy microstructure and mechanical properties, as demonstrated in Fig.2.2-3 (Zhang, 2014). It can be seen from Fig.2.2-4 that the strength, thus the hardness of the materials declines sharply while the ductility goes up significantly after annealing process.

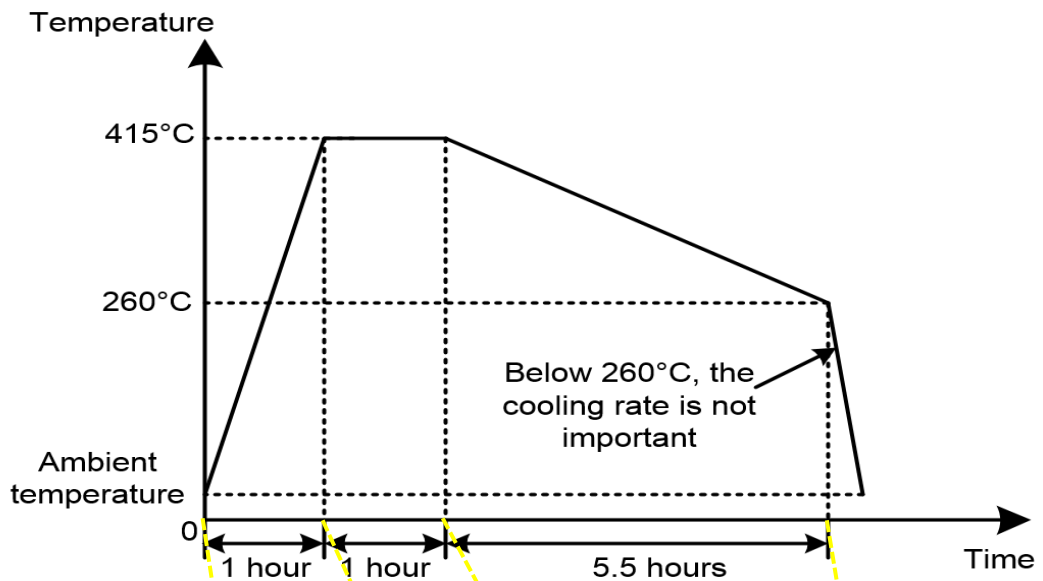


Figure 2.2-3 Typical O annealing condition of AA6082 (Zhang, 2014).

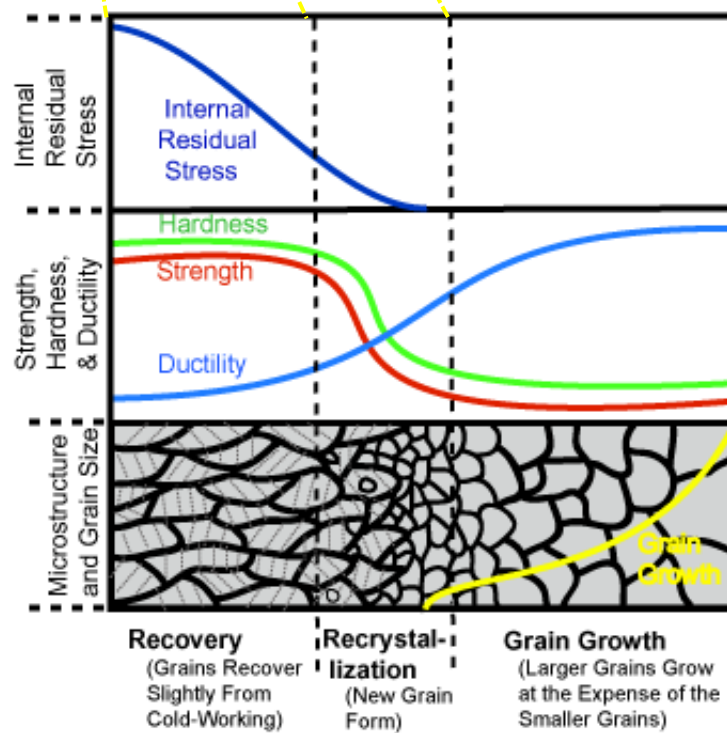


Figure 2.2-4 Variations of mechanical properties during annealing process (www.gatesolution-metallurgicalengineering.blogspot.co.uk).

2.2.3 Solution Heat Treatment

Solution Heat Treatment (SHT) is defined as a thermal process that holds the material at an elevated temperature above the solvus for a sufficient period to take the alloying elements fully into the solid solution by dissolving soluble precipitates into aluminium matrix (Zhang, 2014). At the start of a SHT process, precipitates already exist in as-received aluminium alloys owing to the pre-treatments of the sheet material during forming, solution heat treatment and ageing process. For AA6082 type, the precipitates mainly consist of magnesium silicide compounds and Si (Garrett et al., 2005).

In the beginning of solution heat treatment, precipitates in diverse sizes are concentrated along grain boundaries preferentially, which offer flow barriers during deformation. When the aluminium alloy is heated continuously at a high temperature, the precipitation phase magnesium silicide starts to dissolve into the aluminium matrix gradually, accompanied by barriers reduction to the flow of the material. Thus, it is impossible to form micro-voids around second phases in plastic deformation. It has been proved that during this stage, material ductility and formability is enhanced but the flow stress, as well as residual stress are reduced. With sufficient treatment time, the microstructure of the alloy transforms to a homogeneous single phase (Garrett et al., 2005). The whole process is demonstrated schematically in Fig.2.2-5.

As discovered by some researchers, coarsening, rounding and transforming of alloying elements also occur. Hard non-dissolvable particles with sharp edges are rounded off as well during solution heat treatment, thus improving the ductility of the material (Garrett et al., 2005).

The other vital purpose for SHT is to introduce a large amount of vacancies. Vacancies accelerate diffusion in the aluminium matrix, which is beneficial for homogenization process. The concentration of vacancies in equilibrium phase is calculated as: $C_v = C_0 e^{-\frac{E_v}{kT}}$, where E_v is the energy barrier to introduce a vacancy, k is Boltzmann's constant, T is Kelvin temperature and C_0 is a constant (Granholt, 2012).

As reported, the SHT holding temperature should be set as close as possible to the solidus of the alloy to ensure the fast diffusion rate (Garrett et al., 2005). The liquidus temperature for AA6082 alloy is about 650°C, while the over-heating temperature range is proved to be between 575°C (solidus temperature) to 585°C. When AA6082 is heated and hold above 590°C in solution heat treatment, the reduction of material mechanical performance takes place (Zhang, 2014).

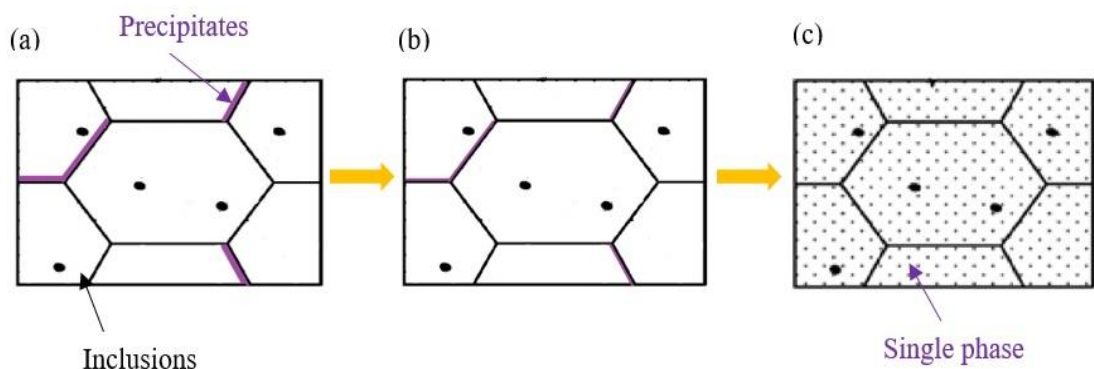


Figure 2.2-5 The microstructure evaluation during solution heat treatment (a) start of SHT; (b) intermediate SHT; (c) close to finishing SHT (Garrett et al., 2005).

2.2.4 Aging Treatment

Following SHT, generally, the material is rapidly quenched by cold water to obtain a super saturated solid solution (SSSS) with high vacancy concentration because no sufficient time is offered to form new equilibrium phase. The super saturated solid solution (SSSS) results in a driving force for second phase precipitation to form the two-phase region in the phase diagram (Granholt, 2012).

During aging, the alloying elements in SSSS diffuse through the voids of the vacancies towards the clusters formed by the excess vacancies and condensate on them (Zhang, 2014). With the help of atom probe field ion microscope (APFIM), it is found that separated Mg and Si-clusters, as well as Mg-Si co-clusters exist in the early stage of aging (Fang et al., 2010). This leads to the formation of Guinier-Preston (GP) zones which are solute-rich groups with thickness of only one or two atom planes. The formation of the Guinier-Preston (GP) zones demands much lower energy barriers than the equilibrium phase, and thus they have priority to nucleate and grow into a spherical shape at a rapid speed. The GP zones possess quite low interfacial and strain energy and are fully coherent with the aluminium matrix. Then, the GP zones transform to the metastable precipitate phases (Zhang, 2014). General sequence of precipitate phase transformation is exhibited as: super saturated solid solution (SSSS) → G.P. zones → metastable β'' → metastable β' → stable equilibrium β phase. The respective features of each phase are summarised in Table 8 below.


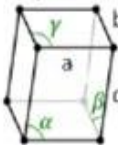

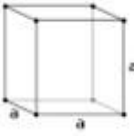
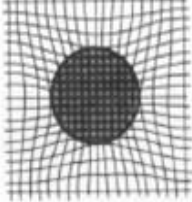
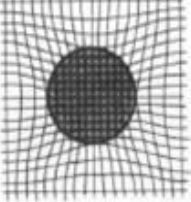
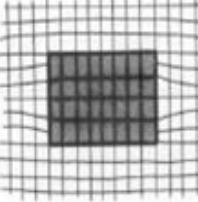
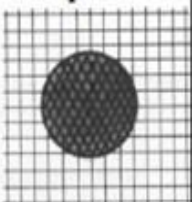
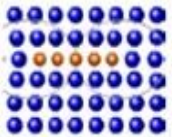
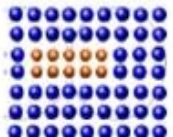
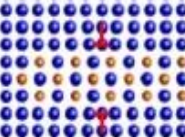

It is claimed that nano-sized metastable precipitates nucleate in a composition close to $\text{Mg}_2\text{Si}_2\text{Al}_7$ with a framework provided by Si pillars. Besides the varied second phases mentioned above, it is also found that pre- β'' phase exist shortly as most developed G.P. zones just before the formation of β'' phase with the composition of $(\text{Al}+\text{Mg})_5\text{Si}_6$.

The Al atoms are able to be replaced by Mg and Si atoms during annealing (Fang et al., 2010). β'' phase provides the primary hardening effect in AA6082 alloy. It is needle-like precipitates and elongated along the $\langle 100 \rangle_{Al}$ direction coherently. It grows semi-coherently in the two other directions as well (Granholt, 2012). The chemical formula of metastable β'' is detected as Mg_5Si_6 (Fang et al., 2010) or $Mg_5Al_2Si_4$ in general (Granholt, 2012).

The appearance of β' precipitation follows behind. Metastable β' phase possesses a hexagonal structure, a rod-like shape and aligns along $\langle 100 \rangle_{Al}$ directions as well. It has been discovered by energy dispersive spectroscopy (EDS) that for β' phase, Mg : Si ratio is approximately 1.68. Recently, a new finding is reported that β' phase has an hcp microstructure with composition as Mg_9Si_5 (Fang et al., 2010).

The stable equilibrium phase β in plate-like shape grows along $\{100\}_{Al}$ planes in a CaF_2 type f.c.c. structure. According to the previous research results, when the atomic ratio of Mg to Si is less than 2, the equilibrium Si phase will nucleate along the equilibrium phase β at the end of second phase transformation sequence (Fang et al., 2010).

Table 8 Structure and feature of the four second phases (Zheng, 2014).

	GP Zone	β''	β'	β
Composition	Clusters or co-clusters of Mg, Si atoms	Mg_3Si_6	$Mg_{1.8}Si$	Mg_2Si
Shape	Spherical 	Monoclinic(Needles) $\beta \neq 90^\circ$ $\alpha, \gamma = 90^\circ$ 	Hexagonal(Rods) 	Cubic(Plates) 
Size/nm	Not defined	$a=1.534nm$ $b=0.405nm$ $c=0.683nm$ $\beta=106^\circ$	$a=0.705nm$ $c=0.405nm$	$A=0.639nm$
Stable Size/nm	1-2nm	9-15nm	30-250nm	Not defined
Status	Coherent 	Coherent 	Semi-Coherent 	Structure part 
Growth process				
Precipitate Temperature	70-110°C	240-250°C	290-320°C	450°C
Start Time	10min	24min	30min	45min

In sum, aging process is a heat treatment to increase material strength by finely dispersed coherent or semi-coherent precipitates nucleating and growing. Based on the hardness values after ageing, 3 status are identified as: under-aged, peak-aged and over-aged. Among them, peak-aged is the ideal condition with optimum material mechanical properties (as shown in Fig.2.2-6). The aged alloy can obtain its peak hardness when needle-shaped precipitates Mg_5Si_6 are in the maximum density (Fang et al., 2010). In this condition, the second phases of AA6082 –T6 are a coexisting mixture of β'' , β' and β phase, but the β'' precipitates occupy the largest proportion (Zhang, 2014). T6 temper condition of AA6082 is holding 8-9 hours at 180°C.

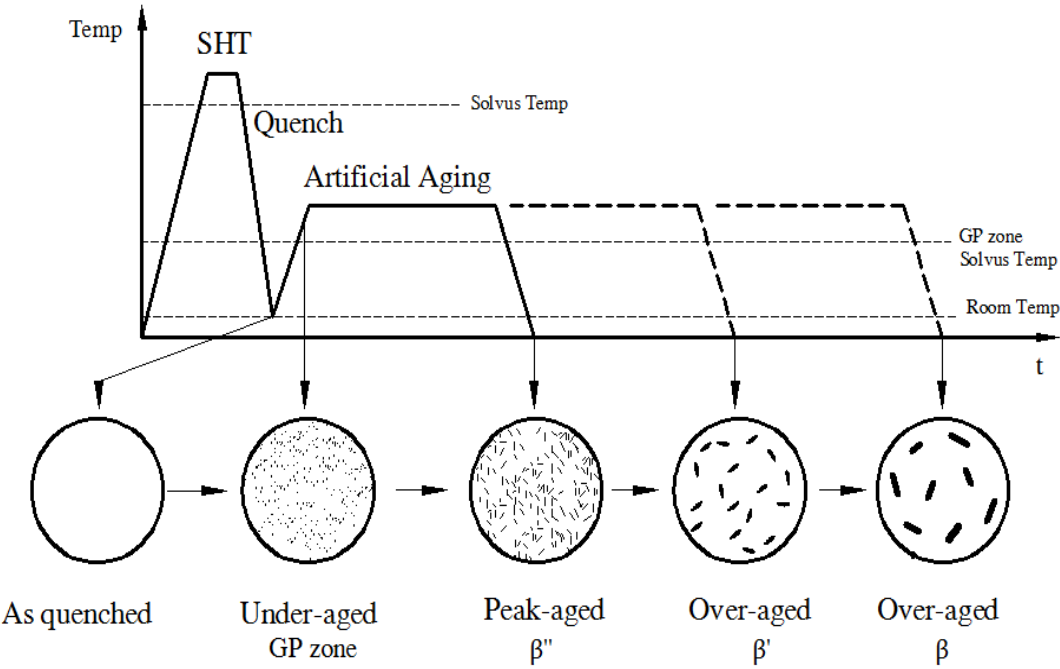


Figure 2.2-6 Schematic properties sequence in microstructure domain (Zheng, 2014).

Fig.2.2-7 shows the image of peak-aged AA6082 samples observed via TEM (transmission electron microscope). It can be clearly seen that β'' needles are finely and homogeneously dispersed all over the Al matrix. Along $\langle 100 \rangle_{\text{Al}}$ directions, needle-like β'' phases are observed in both cross-section sides, lying vertically or horizontally. For the β'' needles form perpendicularly to the observation direction, they are only shown as dark spots in the TEM image. The inset demonstrates the pattern of $\langle 100 \rangle_{\text{Al}}$ zone axis (Wenner, 2014).

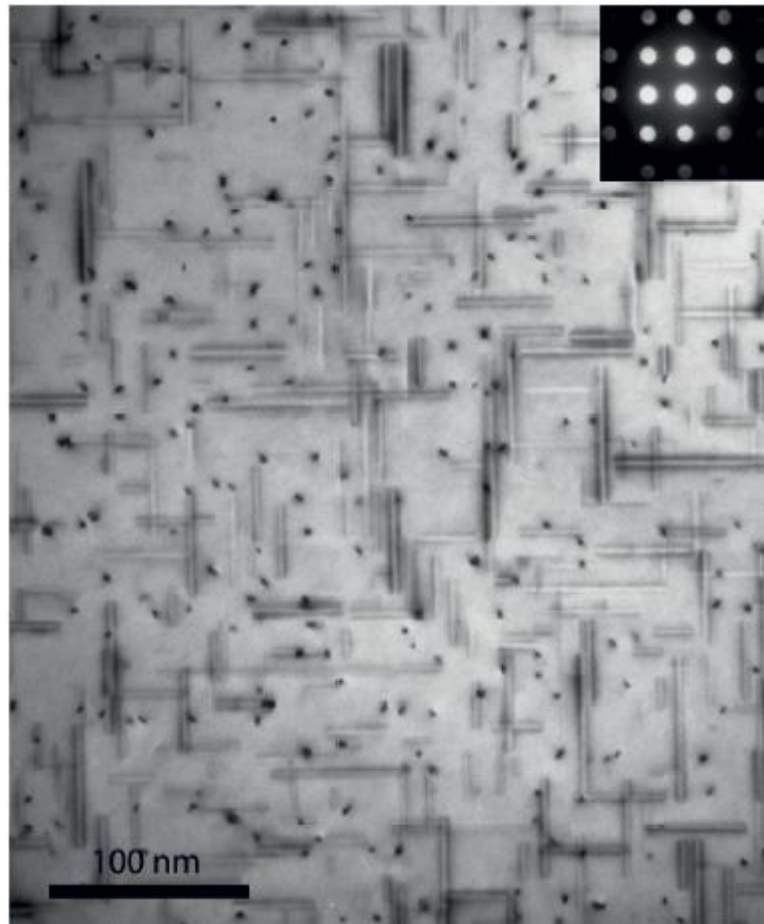


Figure 2.2-7 TEM image of peak-aged AA6082 material (Wenner, 2014).

2.2.5 Precipitation Hardening Mechanism

Precipitation hardening aims to control the distributions and proportions of second phases in aluminium alloys. High volume fraction of precipitates and fine grain sizes are both able to decrease the particle spaces and thus enhance material strength. Main types of strengthening mechanisms related in aging stage are: coherency strain hardening, chemical hardening and Orowan hardening.

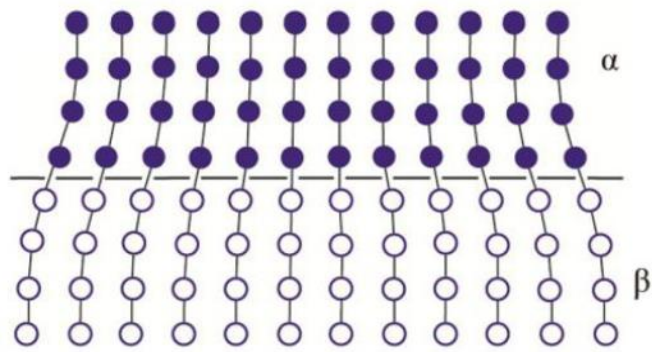
For coherency strain hardening, the lattice mismatch between the aluminium matrix and the precipitate phases, as can be seen in Fig.2.2-8 (a), resists dislocation and thus strengthen the alloy. Two main factors have effects on coherency strain hardening, which are the number and sizes of the GP zones and precipitates, as well as the degree of strain created (Zhang, 2014). This kind of strengthening reaches the highest value when the radius of dislocation line equals to the distance between particles (Zheng, 2014).

Chemical hardening, also known as cutting, is suitable for the situation when a larger stress is applied and dislocations go through precipitates, as shown in Fig.2.2-8 (b) (Zhang, 2014). Dislocation lines will cut precipitates first. The energy demanded to shear the precipitates increases with the precipitation particle size, thus cutting becomes more difficult. An equation shows the relationship between material strength and cutting effect: $\tau = \frac{\pi r \gamma}{bL}$, where τ is the strength of material, r is precipitate particle radius, γ stands for the surface energy, b is the magnitude of Burgers vector while L represents the distance between pinning points. Therefore, it is inferred that the strength of the alloy is proportional to precipitate particle size and inversely proportional to the distance of pinning points (Zheng, 2014).

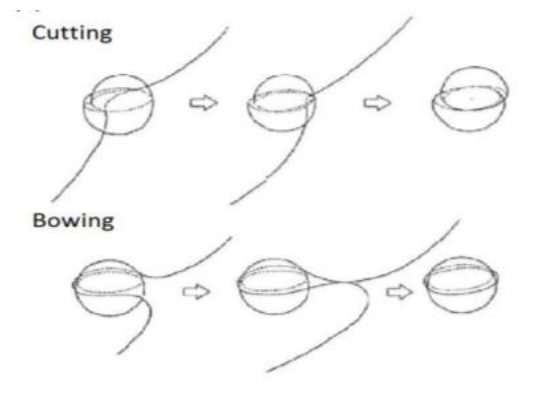
If the size or strength of precipitate size increases, the passing of the moving dislocation transforms from cutting (shearing) to bypassing (looping), as it can be seen in Fig.2.2-8 (b) (Zhang, 2014). Bowing leaves a loop around precipitates. Its effect on material strength can be described with the equation: $\tau = \frac{Gb}{L-2r}$, where G is shear modulus, b is the magnitude of Burgers vector, L stands for the distance between pinning points, r means precipitate particle radius (Zhang & Chen, 2006).

It can be clearly seen in Fig.2.2-8 (c) that, when the precipitate radius is small, shearing dominates for the hardening mechanism, while looping dominates if the precipitate radius is large (Zhang, 2014). The material strength increases at first with the increase of precipitate particle size, then drops owing to the change from chemical hardening to Orowan strengthening.

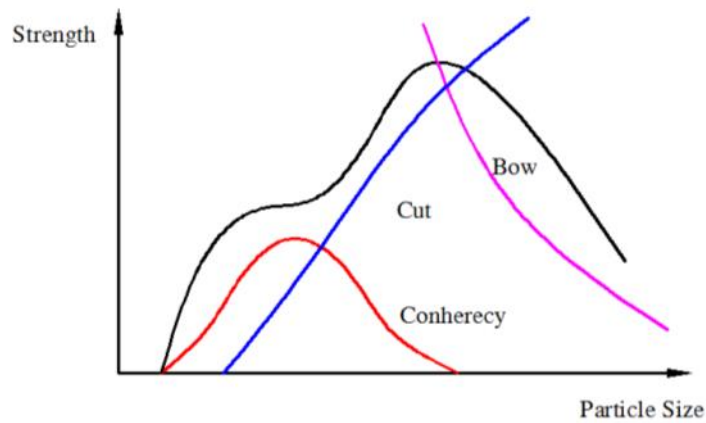
It is discovered that the size of β'' precipitate phase obtains the optimum particle size, which is not only big enough to provide high resistance for cutting, but also properly small to avoid bowing. That is the reason why aging aims to obtain the largest volume fraction of finely dispersed β'' Mg-Si second phase (Zheng, 2014). As it is known, over-aged condition leads to coarse precipitates which are non-shearable, and thus the moving of the dislocation changes to bypassing and results in strength decline of the aluminium alloy (Zhang, 2014).



(a)



(b)



(c)

Figure 2.2-8 Mechanism of precipitation hardening. (a) lattice mismatch between precipitates & matrix; (b) dislocation passing through precipitates by cutting and bowing; (c) strength contributions from different hardening (Zheng, 2014).

2.3 Forming Methods of Aluminium Alloy

2.3.1 Cold Forming

Cold forging is a production process carried out by forward and backward cold forging combination, and also requires high concentricity and close tolerances. It is the traditional forming method for aluminium alloys (Jensrud & Pedersen, 1998). In terms of non-heat treatable aluminium alloys with relatively low strength, the slugs are commonly required to be fully annealed (usually holding at 345 °C) before cold forming, aiming to remove the effects of strain hardening and softening the metal. The possible un-dissolved precipitates exist as coarse grains by slow cooling after annealing. The formability of alloy is enhanced and the forming load required is small. In some special cases, solution heat treatment and quenching are added just before cold forming for heat treatable aluminium alloys. Compared with fully annealed condition, the ductility and the yield stress of solution heat treated and quenched alloy are similar, but the large residual stresses which quenching brings are avoided, hence distortions and local coarse grains in the final formed part are mostly eliminated. After that, the part undergoes further precipitation hardening process (Bay, 1997).

However, as demonstrated in Fig.2.3-1, the AA6082 specimens received have already been artificially aged. Considering industry efficiency, most 6xxx series aluminium alloy sheets are precipitation hardened before forming (Bay, 1997). Nevertheless, this process results in the two major bottle-neck problems, low formability and spring back, which made cold forging only available for simple shape parts of high strength aluminium alloys with high manufacturing and assembly cost. For products with complex shapes, they are replaced with multiple simple parts and then assembly or

laser welded together after forming, which not only increases processing costs but also destroys the structural integrity (LoCoLite, 2013).

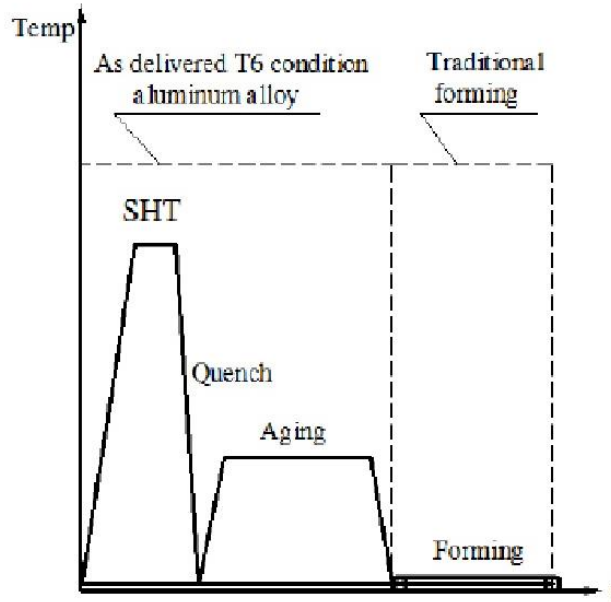


Figure 2.3-1 Temperature profile of traditional forming process for AA6082 alloy (Zheng, 2014).

Some research studies have been carried out to solve the problems. One primary method is to combine heat treatment and forming process together to improve the material formability. It is discovered that aluminium alloys processed by hot blow forming are enhanced on ductility. In hot blow forming, the sheets are first heated then stretched with a high-pressure gas and are provided good stretch formability in which Mn and Cr contents are adjusted properly. Besides, warm forming is also designed based on the same mechanism. Different from hot blow forming, warm forming enhances material shape fixability by dynamic recovery but do not impart high ductility to the aluminium alloy (Takata, 2013). However, it is possible to destroy the desirable microstructure and material properties. Superplastic forming

techniques and creep age forming are both effective solutions, but are not appropriate to be put into practice.

2.3.2 HFQ Process

The limited formability of aluminium alloy at room temperature, especially for high strength types, restricts shaping demand and application range. To overcome these obstacles suffered in traditional forming methods, an innovative solution heat treatment, forming and in-die quenching (HFQ) process is designed for high strength aluminium alloys, such as AA6082. It combines die forming and quenching in one operation, and thus carries out shaping and heat treatment simultaneously (LoCoLite, 2013). The initial status of Al alloy in HFQ process is T6 temper, which means peak-aged condition, as shown in Fig.2.3-2. During HFQ process, the blank undergoes solution heat treatment at first to form a super saturated solid solution (SSSS) microstructure with homogeneous single phase. As a result, the ductility and hence the formability of the material are significantly enhanced owing to the reduced obstacles to moving dislocations and the decreased yield stress. Next, the blank is transferred into a cold die, pressed into complex shapes and held in the tool for a few seconds to provide a rapid cooling rate or quenching. The purpose is to prevent precipitates forming in the microstructure and remain super saturated solid solution (SSSS) microstructure, as shown in Fig.2.3-3. It has also been proved that thermal distortion and spring back effects are minimized by high cooling rate and lower material strength during forming on account of holding the pressed part in cold mould (Fakir et al., 2014). The deformed aluminium alloy parts are artificially aged afterwards.

The HFQ process is influenced by factors, for instance, temperature, ram speed and blank holding forces (Fakir et al., 2014). It not only reduces production steps, but also facilitates the production of high precision and complex-shaped parts using high strength aluminium alloys (5xxx, 6xxx and 7xxx series), as it can be observed in Fig. 2.3-4. It is a kind of highly-efficient and cost-effective forming technologies, which contributes to expanding aluminium alloys application scopes. In terms of products with complex shapes, high strength aluminium alloys are able to replace sheet steels with much lower required press forces. Thus, HFQ process is beneficial to reduce tool wear, increase tool life and reduce energy. Compared with common forming process, spring back and shrinkage are eliminated by the novel HFQ process (shown in Fig.2.3-5), which reduces the tool design costs, and no assembling is required because complex cross-section can be formed only by one pressing which also lower the fabrication costs (LoCoLite, 2013).

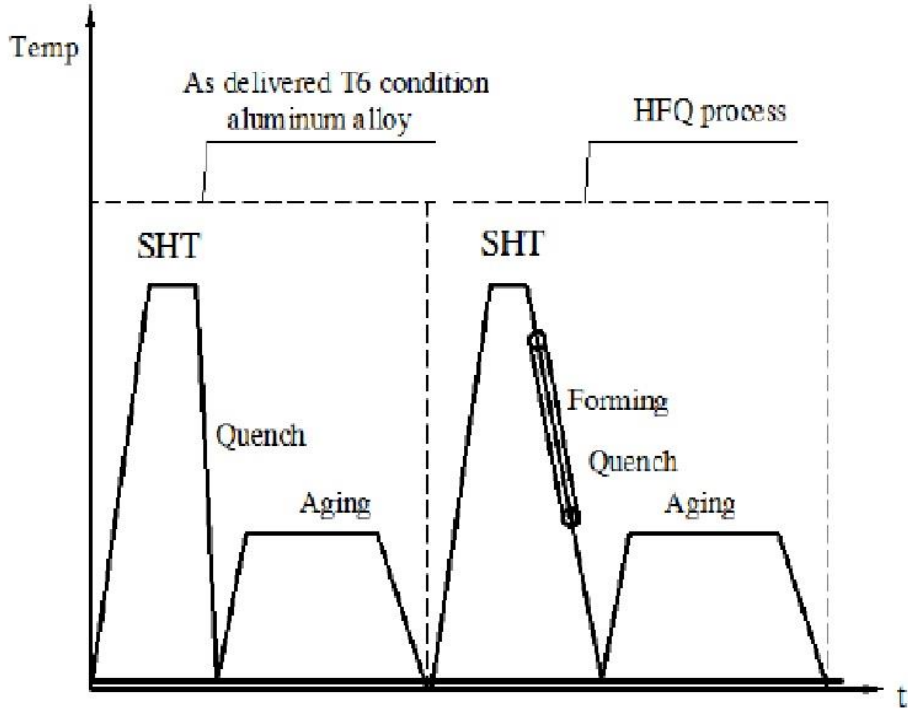


Figure 2.3-2 Temperature profile of HFQ process for AA6082 alloy (Zheng, 2014).

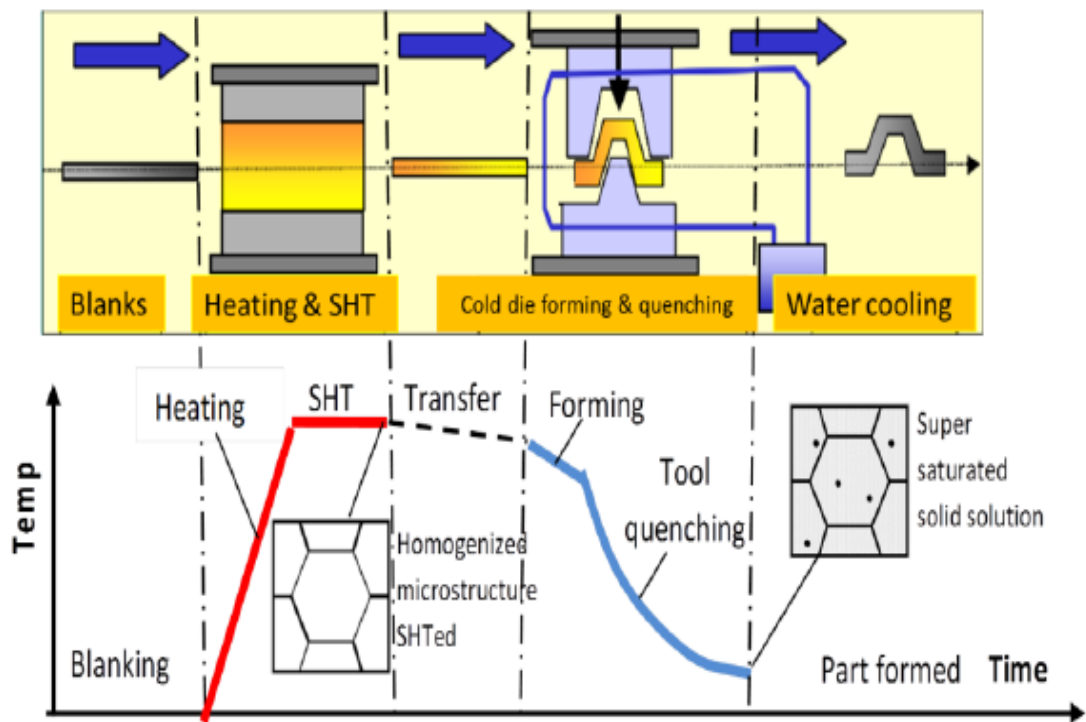
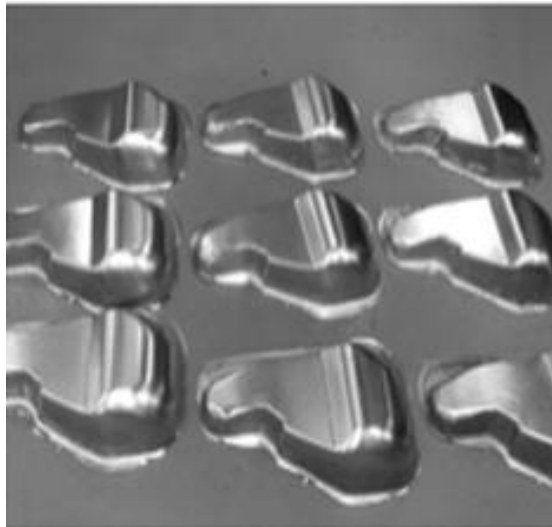
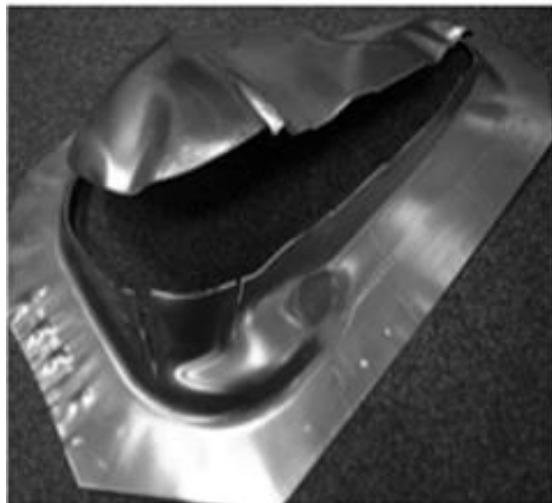


Figure 2.3-3 The integrated HFQ process (LoCoLite, 2013).



(a)

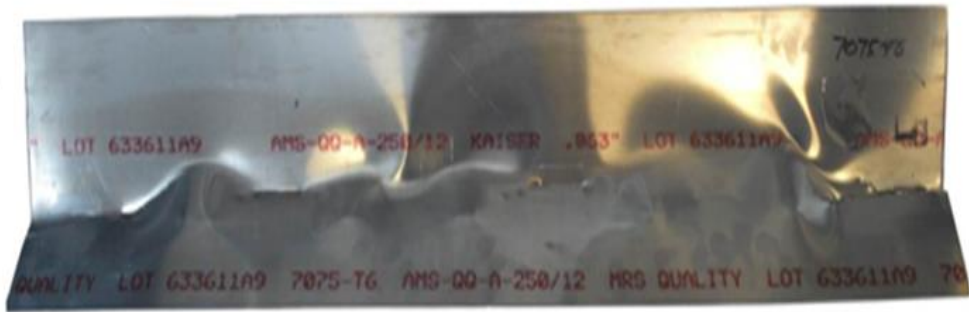


(b)

Figure 2.3-4 AA6082 T6 alloy bulkhead pressed by HFQ process and conventional forming at room temperature (Sellers, 2013).



(a)



(b)

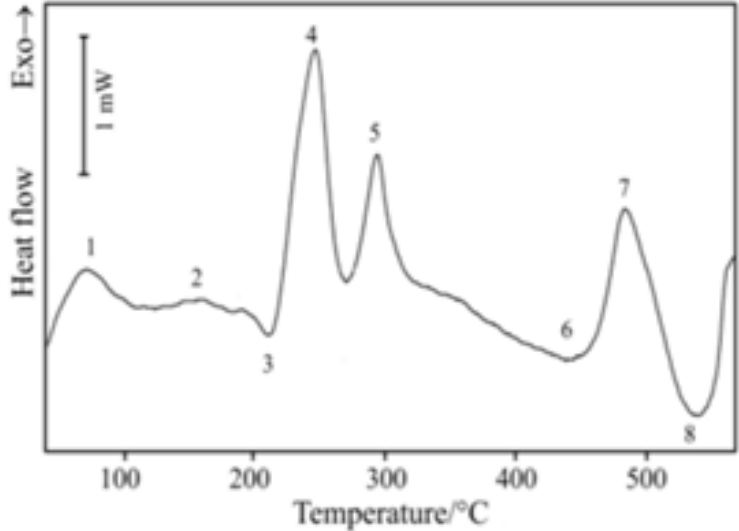
Figure 2.3-5 Forming of complex shaped component under (a) HFQ and (b) cold forming conditions (www.localite.net, 2014).

2.4 Effect of Pre-deformation Before Aging on Precipitate Hardening

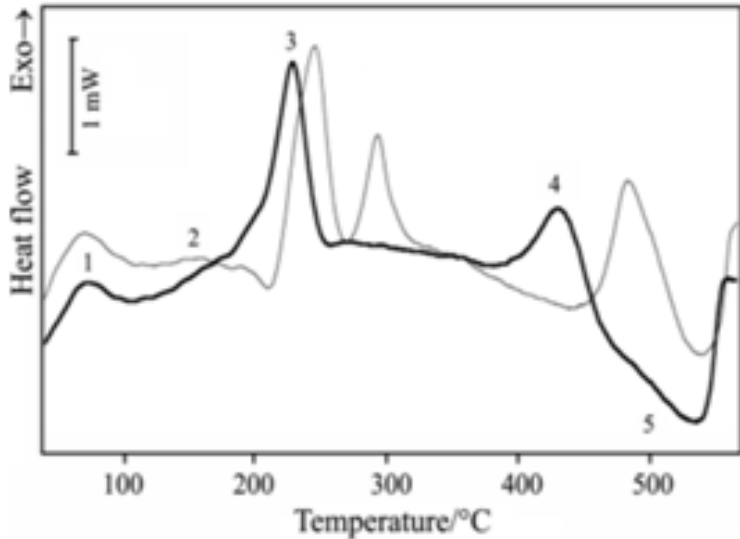
A research has been carried out on AA6082 specimen, which was punched after solution heat treatment, and then aged in a differential scanning calorimetry (DSC) cell to 600°C. With the help of the DSC technology, the precipitates formation of pre-deformed AA6082 aluminium alloy during aging process can be explored. The findings are beneficial to analyse the mechanical properties of HFQ-formed samples after aging, as well as to find the corresponding optimum aging conditions. Even though the specimen disc size is intentionally small to exaggerate the punching deformation effect, the deformation degree is still limited with no exact values on strain can be demonstrated (Birol, 2006).

Comparing the DSC curves in Fig.2.4-1 for two samples, which were punched before or after solution treatment, it is observed that compared with the sample which was punched before SHT, the clustering at low temperatures was suppressed whilst the precipitation kinetics at elevated temperatures were accelerated in the sample which was punched after SHT. Dislocations had little effects on clusters and GP zones but caused vacancy sinks which reduced significantly the amount of quenched-in vacancies. Therefore, the clustering activities were restricted and thus clustering was restrained. The elements of Mg and Si were still mainly dissolved in the aluminium matrix and with the heterogeneous nucleation sites offered by dislocation for GP zones. Already formed GP zones became the stable nuclei for metastable β'' phase. As a result, the formation of β'' precipitates was facilitated. It was also found that deformation, just after SHT but prior to aging, contributes to promoting the formation of metastable β'' phase and accelerating its transformation to rod-like metastable β'

phase as well. Pre-deformation after solution heat treatment introduced rather high dislocation density, which led to that β'' phase lost coherency with the aluminium matrix and transformed to semi-coherent β' phase (Birol, 2006).



(a)



(b)

Figure 2.4-1 (a) DSC curve of AA6082 disc samples punched before SHT; (b) DSC curve of AA6082 disc samples punched after SHT and heated at 10 °C min⁻¹ (Birol, 2006)

Hardness test was also conducted on the two AA6082 samples punched before and after solution heat treatment separately during heating in DSC cells. It is clearly demonstrated in Fig.2.4-2 that, sample punched after SHT possessed a lower peak hardness but the corresponding heating temperature, as well as heating time was reduced (Birol, 2006). Therefore, it was proposed that deformation introduced prior to aging and after SHT was able to accelerate the subsequent aging process but decreased the sample peak hardness after aging. However, because aging process is different from continuous heating in DSC, the results can not be applied to HFQ-processed and aged samples directly.

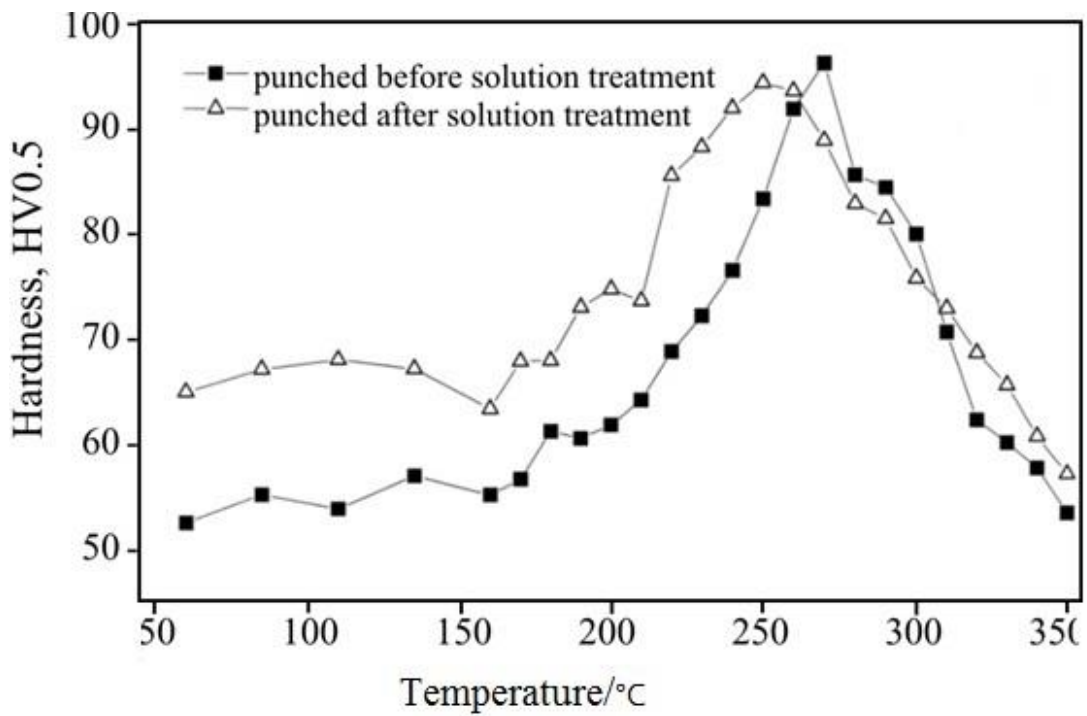


Figure 2.4-2 Hardness of punched before and after SHT AA6082 samples, heated in DSC cells at $10^{\circ}\text{C min}^{-1}$ in Argon atmosphere (Birol, 2006).

It was also discovered in another DSC analysis experiments that dislocation introduced by pre-deformation after solution heat treatment suppressed the formation of Mg-Si co-clusters during subsequent aging. As shown in Fig.2.4-3, in which the DSC curves were shifted upwards to prevent overlapping, owing to the acceleration effect of pre-deformation prior to aging, the exothermic β''/β' peak was shifted to lower temperature with increasing deformation rate while β peak existed at the same temperature for four sample DSC curves. However, there was a distinct trough at the beginning of β''/β' peak for naturally aged sample, which were not able to be seen for pre-deformed samples. This trough appeared due to the dissolution of Mg-Si co-clusters which were formed during natural aging. It was also followed with a higher temperature of exothermic β''/β' peak, which resulted in the slowing down of precipitation hardening process. Therefore, it is supposed that the Mg-Si co-clusters are restrained to form due to the annihilation of quenched-in vacancies (Kolar et al., 2011).

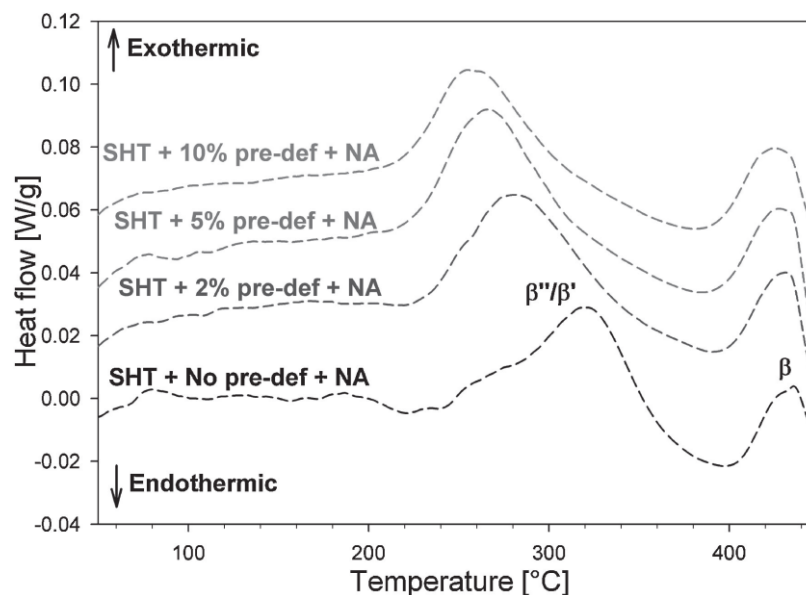
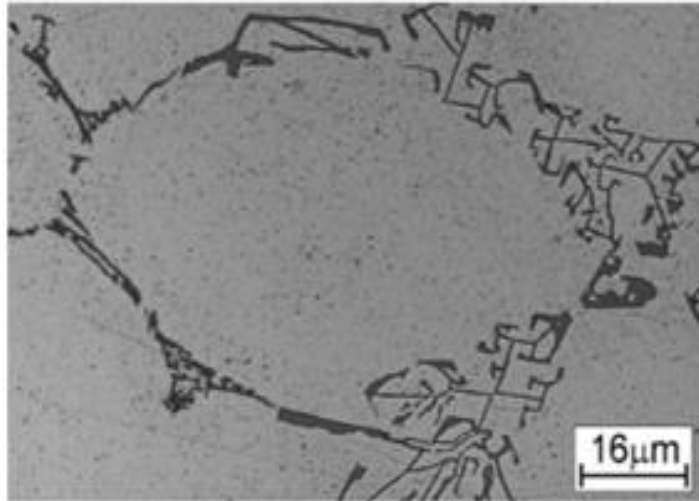


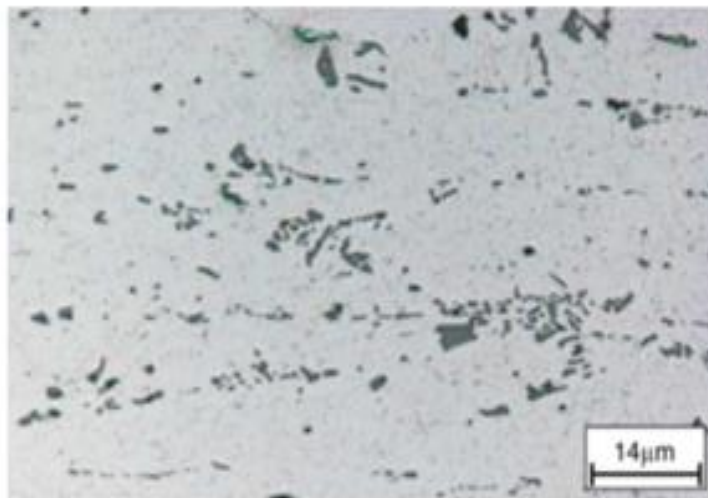
Figure 2.4-3 Effect of pre-deformation on DSC curves of solution heat treated AA6060 pre-deformed to various levels (0, 2, 5 and 10%) and naturally aged for 1 week (Kolar et al., 2011).

2.5 Inclusion Phase Transformation During Heat Treatments

Magnesium and silicon are two primary intentional alloying elements in 6XXX series aluminium alloys. Apart from these, additional elements, iron mainly and manganese, are normally introduced during casting process, which form Al-Fe, Al-Fe-Si and Al-Fe-Mn-Si intermetallic phases between the aluminium dendrites. The cooling rate and the Fe to Si ratio in the alloy determine the type of intermetallic compounds. Diverse inclusion phases exhibit varied atomic structures, morphologies, physical and mechanical properties. Solution heat treatment at 570⁰C, which is necessary to prepare as-cast billets well for hot extrusion, leads to intermetallic phase transformation. It has been discovered that interconnected plate-like β -Al₅FeSi intermetallics transform into more rounded discrete α -Al₁₂(FeMn)₃Si particles during homogenisation process, which enhances the material ductility. As it can be seen in Fig.2.5-1 (a), inclusions present in the interdendritic spaces of aluminium matrix solid solution. A mixture of β -AlFeSi and α -AlFeMnSi intermetallic phases precipitates at grain boundaries, connecting with coarse Mg₂Si second phases. From Fig.2.5-1 (b), it is found that inclusion particles arrange along plastic flow direction and thus form the band structures during aluminium alloy forming (Mrowka-Nowotnik & Sieniawski, 2005).



(a) Microstructure of examined as-cast 6082 alloys



(b) Microstructure of examined 6082 alloys after hot extrusion

Figure 2.5-1 Microstructure of examined AA6082 alloys (Mrowka-Nowotnik & Sieniawski, 2005).

CHAPTER III EXPERIMENTAL METHODS

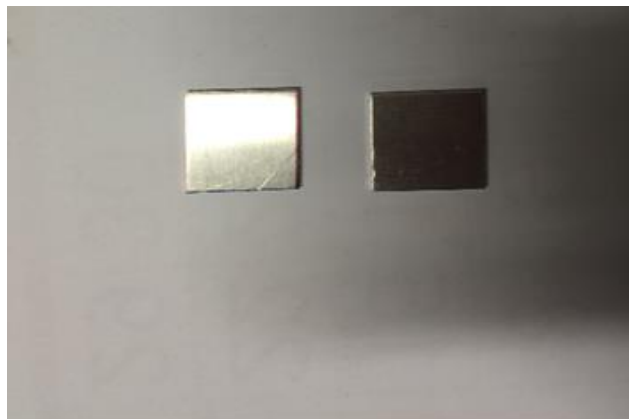
3.1 Materials and Sample Preparation

The material used in this research is AA6082 aluminium alloy sheet in T6 condition (solution heat treated and artificially aged). Plates with the dimension of 300×600×1.5mm purchased from Smiths Metal Centres Ltd are shown in Fig.3.1-1 (a). Due to the relatively large size of the supplied sheets, the required sample shapes were cut using the MORGAN RUSHWORTH shearing machine shown in Fig.3.1-2.

20mm×20mm square pieces shown in Fig.3.1-1 (b) were prepared for solution heat treatment tests.



(a)



(b)

Figure 3.1-1 As-received AA6082-T6 sheets (a) and 20mm × 20mm cutting specimens (b) used in solution heat treatment tests.



Figure 3.1-2 MORGAN RUSHWORTH shearing machine used to cut AA6082 as-received sheets.

180mm×40mm rectangular specimens were cut from the purchased large sheets before EDM cutting the dog-bone shaped samples designed for Gleeble tests. To fit the size of the sample fixture of the Gleeble equipment shown in Fig.3.1-3, the overall length of the dog-bone shaped samples is 150mm and the width is 25mm in the grip section. To fix the samples onto the Gleeble machine, two holes in the diameter of 5.1mm were drilled at the both end of the sample. In the width-reduction section, the gauge length is 70mm and the width is 15mm (Fig.3.1-3).

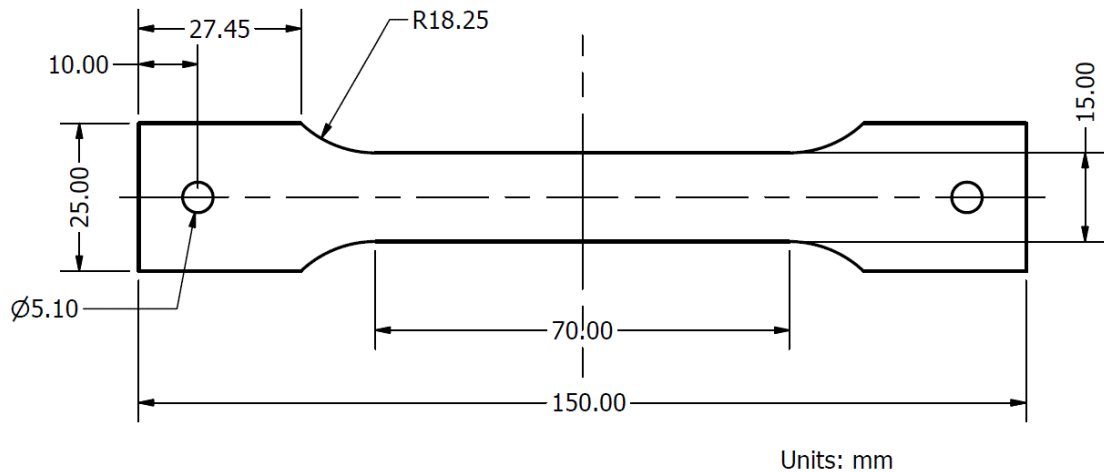


Figure 3.1-3 2D image of Gleeble test dog-bone shaped samples

Considering the complex shape of the dog-bone sample for Gleeble tensile test, wire EDM method was chosen as an optimal machining method as the EDM cut workpieces are accurate in both shape and size with good surface finish and burr-free edges (www.precisionmicro.com). Besides this, the wire imparts no physical pressure on the work piece and the clamping force of the holding parts is minimal, which are favourable conditions for tensile test samples (Moulton, n.d).

The equipment model is EDM CUT 20 produced by AgieCharmilles Company as shown in Figure.3.1-4 (a). The 180mm×40mm rectangular sheets were placed on top of each other, aligned and then fixed on the edge of work table of the EDM cutting machine by fastening devices as shown in Fig.3.1-4 (b). Considering the viscosity of materials and cutting wires, 10 to 12 prepared AA6082 rectangular sheets were cut together in a stack. As set in the system, the cutting wire entered from the top right of the rectangular samples, went along the path already designed as shown in Fig.3.1-3. The velocity of cutting wires was automatically set as 3.09mm/s. The dog-bone shaped samples cut by EDM are shown in Fig.3.1-4 (c)



(a)



(b)



(c)

Figure 3.1-4 (a) The AgieCharmilles CUT 20 P EDM equipment, (b) Samples are fixed on the workpiece before cutting, (c) EDM cutting dog-bone shaped tensile samples.

3.2 Heat Treatment

3.2.1 Solution Heat Treatment

Square AA6082 sheets in the size of 20mm×20mm (Fig. 3.1-1) were used for the solution heat treatments in ELITE laboratory chamber furnace (Fig.3.2-1). The furnace was heated to the target temperature at first at a heating rate of 8°C/min. Then the samples were loaded into the furnace when the furnace temperature reached the target temperature. When the designed holding time finished, the samples were taken out of the furnace and quenched in cold water quickly. The sample code and the detailed experimental parameters of solution heat treatments are shown in Table 9.

Table 9 Specimen code and experimental parameters for solution heat treatment.

Specimen Code	Temperature (°C)	Holding Time (min)
570-1	570⁰C	1
530-2	530⁰C	2
525-15	525⁰C	15
545-50	545⁰C	50
530-120	530⁰C	120
575-240	575⁰C	240

The solution heat treated samples were then ground and mounted for micro-hardness tests. The optimal solution heat treatment conditions were determined such that the treated samples showed the lowest hardness value. The identified optimum solution heat treatment conditions were used for the SHT of dog-bone shaped samples before the Gleeble tests.

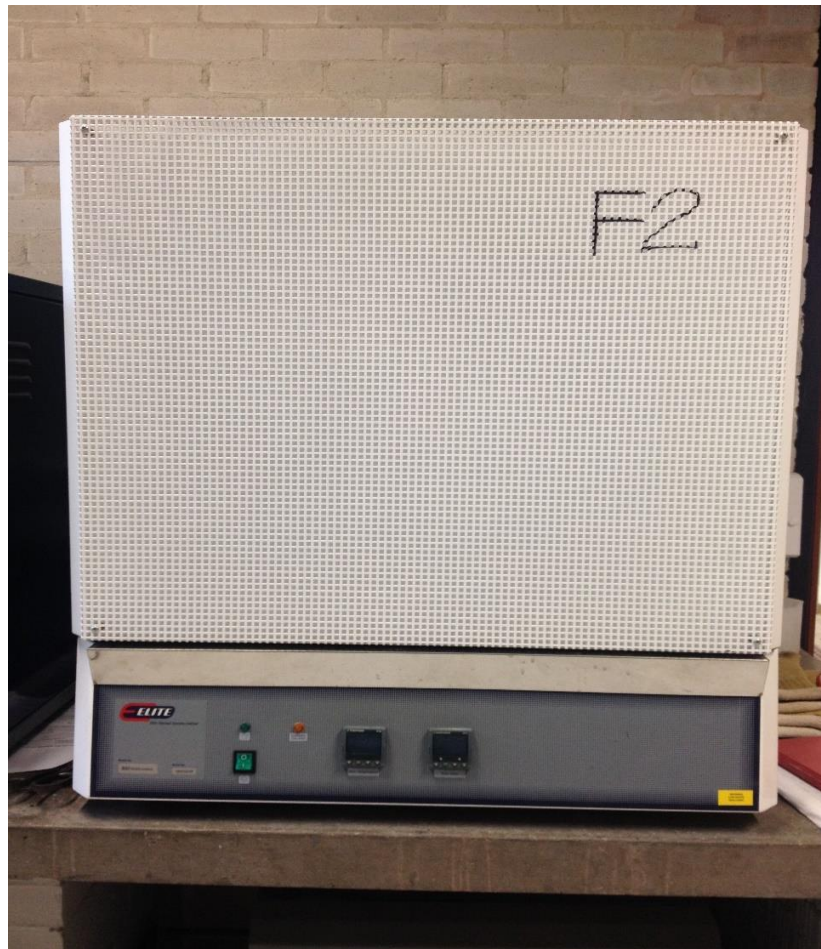


Figure 3.2-1 ELITE 1200°C laboratory chamber furnace

3.2.2 Aging Treatments

Aging treatment was applied to Gleeble-treated samples (see Section 3.3 for Gleeble testing). A ELITE laboratory tube furnace was used for the aging treatments (Fig.3.2-2). The cut samples were put into a ceramic tube container firstly. When the furnace was heated to the aging temperature of 180°C and stably maintained, the ceramic tube container with samples was sent into the middle of the furnace. Then the holding time started to count. When the aging time was up, the aged samples were taken out of the furnace and quenched in cold water quickly. After the aging treatment, the samples were cut and mounted; the cross-sections were ground and polished to obtain a good surface finish for micro-hardness measurements.

At first, some of the samples were aged at 180°C for 3h and 6h; then the aging time was adjusted according to the hardness values of the aged samples. Table 10 details all the aging conditions for Gleeble treated samples.



Figure 3.2-2 ELITE laboratory tube furnace

Table 10 Aging treatments parameters of varied samples.

Sample Code	Strain during Gleeble test	Age Holding Time at 180 °C/h
0% - 8	0	8
1% - 3	1%	3
1% - 6		6
1% - 7		7
1% - 8		8
5% - 3		5%
5% - 6	6	
5% - 7	5%	7
5% - 8		8
10% - 3	10%	3
10% - 6		6
10% - 7		7
10% - 8		8
15% - 3	15%	3
15% - 4.5		4.5
15% - 5		5
15% - 6		6
15% - 7		7
20% - 3	20%	3
20% - 4.5		4.5
20% - 5		5
20% - 6		6

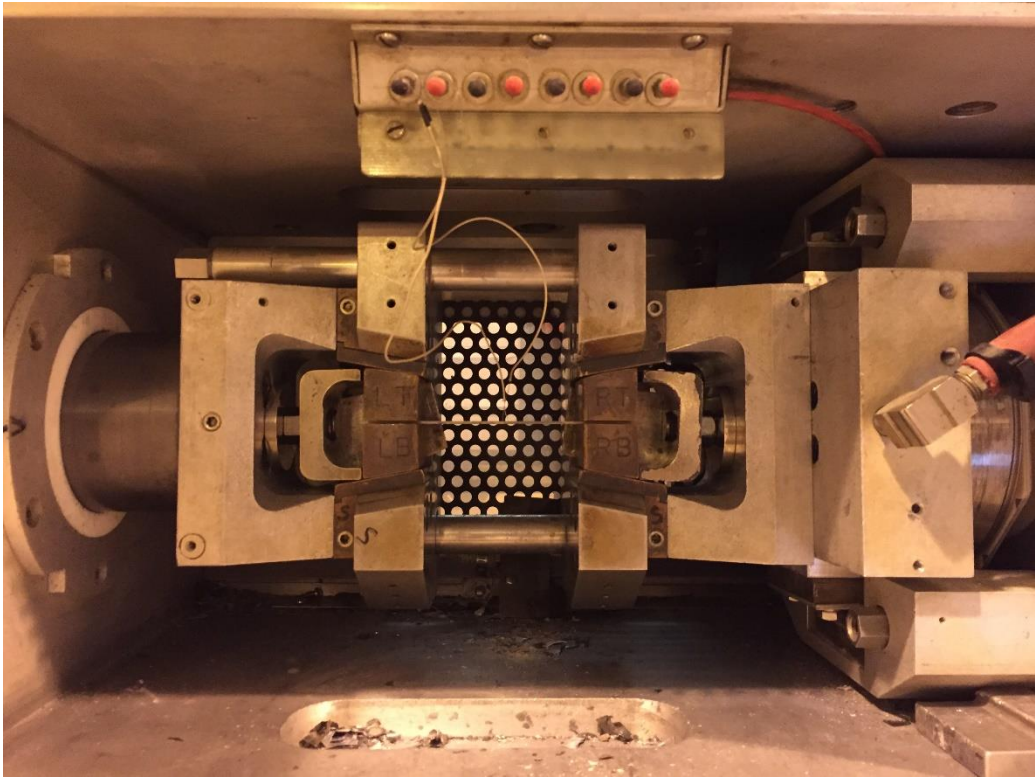
25% - 1	25%	1
25% - 2		2
25% - 3		3
25% - 3.5		3.5
25% - 6		6
30% - 1	30%	1
30% - 2		2
30% - 3		3
30% - 3.5		3.5
30% - 6	30%	6

3.3 Gleeble Test

3.3.1 Equipment and Sample Settings

In order to simulate the thermos-mechanical process of HFQ, Gleeble tests were carried out on the Gleeble 3800 with dog-bone shaped AA6082 samples (see Fig.3.1-4 (a)). As shown in Figs.3.3-1 (a) and (b), the sample was held horizontally by two copper jaws. Two blocks were fastened to grip the copper jaws in order to fix the sample. K-type thermocouples were welded by percussion welding on the centre of sample and connected to the thermometer to measure the actual temperature of the sample during Gleeble tests (Lippold et al., 2011). During the tests, the chamber door was closed and the sample was heated to the target temperature rapidly by electric current heating before the sample was stretched to the given stroke to produce a

specified deformation (or strain) for the sample. Once the stroke reached, the force loaded on sample was reduced to zero. The current was also switched off and the sample was cooled down within the chamber.



(a)



(b)

Figure 3.3-1 (a) Gleeble chamber with samples on and (b) K-type thermocouples welded on the centre of sample.

3.3.2 Evaluation of Temperature Difference

To simulate HFQ process, the operation temperature was set as 450°C. During current heating, the sample temperature decreases gradually with the distance to the centre of the sample, which affected deformation uniformity greatly. Hence, it is necessary to determine the actual effective region in the gauge section. To this end, three K-type thermocouples were welded on 3 positions of dog-bone shaped sample: the centre, 10mm to the centre and 15mm to the centre, and connected to the thermometer TC1, TC2 and TC3 separately. The target temperature of TC1 was set as 450°C and the temperature difference between the other 2 points (TC2, TC3) and the centre (TC1) was investigated and the test results are shown in Table 11.

Table 11 Temperature difference during heating in Gleeble tests.

Position	Centre	10mm To Centre	15mm To Centre	Target Temperature
Temp (°C)	450	425	350	450

As shown in Table 11 above, there is only 25°C difference as the distance to the centre increased to 10mm, which is acceptable. However, when the distance reached 15mm, the temperature dropped by 100°C, which would probably affected the following tension stage. Hence, the effective gauge length was shortened to 10mm to the centre, i.e. 20mm in total.

The specified strain (ϵ) of samples are chosen as 1%, 5%, 10%, 15%, 20%, 25% and 30%. An equation is used to calculate the final stroke difference (ΔL); $\epsilon = \ln\left(\frac{L_0 + \Delta L}{L_0}\right)$,

L_0 is 20mm, stands for the gauge length. The results are shown as Table 12.

Table 12 Stoke difference related to varied strains

Strain	Stroke(mm)
1.0%	0.20
5.0%	1.03
10.0%	2.10
15.0%	3.24
20.0%	4.43
25.0%	5.68
30.0%	7.00

3.3.3 Setting up of HFQ Simulation Tests

With the data above, the operation system of Gleeble test was ready to set up. As it can be seen in Fig.3.3-2, input sample gauge length l , thickness h and width w , set heating rate as 10°C/s , target temperature on TC1 450°C , holding time 30s. Strain rate was chosen as $0.1/\text{s}$ and stroke mode was applied. For instance, the sample 15% - 7 required 1.5s to complete the stroke process and the extension length was 3.24mm. To guarantee that sample is deformed uniformly with time, deformation time was divided into 10 equal time slots and the calculated related deformation amount for each time slot is shown in Fig.3.3-2. When the tension process finished, the force was removed and the sample was rapidly cool down by cold water spraying.

#	L	Time	Axis 1	Axis 2	Axis 3	Comment
1		System	Setup	Limits: Compression=-20mm, Force=50000kgf, Heat=100%		
2		Stress/Strain	Axial strain using Stroke, l = 20.00mm, h = 1.50mm, w = 15.00mm			
3		Acquire	Force	Force.line	PRam	PTemp Strain Stress Stroke TC1
4		*				
5		*				
6		*				
7		Start	<input checked="" type="checkbox"/> Mechanical	<input checked="" type="checkbox"/> High	<input checked="" type="checkbox"/> Thermal	
8		Mode	Force(kN)	Torsion(rev)	TC1(C)	
9		Sample	10.0Hz			
10		00:05.0000	0.2	0	0	
11		00:45.0000	0.2	0	450	
12		00:30.0000	0.2	0	450	
13		Zero	Stroke			
14		00:00.1000	0.2	0	450	
15		Sample	1000.0Hz			
16		Mode	Stroke(mm)	Torsion(rev)	TC1(C)	
17		00:00.1500	0.30	0	450	
18		00:00.1500	0.61	0	450	
19		00:00.1500	0.92	0	450	
20		00:00.1500	1.24	0	450	
21		00:00.1500	1.56	0	450	
22		00:00.1500	1.88	0	450	
23		00:00.1500	2.21	0	450	
24		00:00.1500	2.55	0	450	
25		00:00.1500	2.89	0	450	
26		00:00.1500	3.24	0	450	
27		Mode	Force(kN)	Torsion(rev)	TC1(C)	
28		00:00.0500	0.2	0	450	
29		Sample	10.0Hz			
30		00:00.0500	0.2	0	0	
31		01:00.0000	0.2	0	0	
32		End	<input type="checkbox"/> Mechanical	<input type="checkbox"/> High	<input type="checkbox"/> Thermal	

Figure 3.3-2 Gleeble test system setting up for 15% - 3 samples.

The recorded strain with time of 30% strain sample during stroke mode is presented in Fig.3.3-3 It can be seen that in the heating and holding stage from 0 to 80s, sample slightly expanded due to temperature rise. At 80s, the beginning of stroke mode, the strain returned to zero to eliminate the effect of temperature. The strain reached 30% in 3s and then the force was removed, and the temperature decreased also, thus leading to the slight drop of strain. Therefore, the strain caused by temperature change was mutually offset and the sample was 30% deformed.

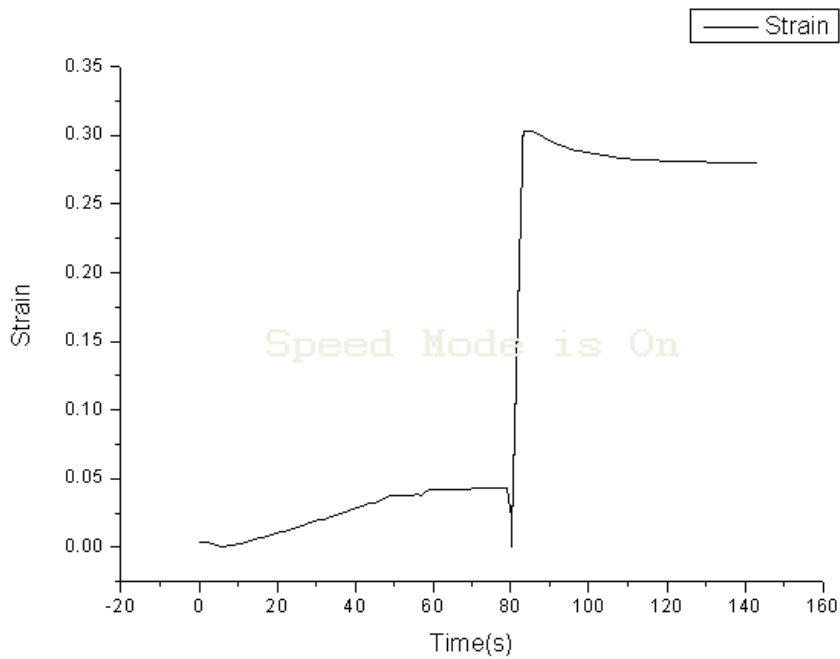


Figure 3.3-3 Strain VS Time (s) line chart during Gleeble test of 30% - 6 sample.

Two samples were Gleeble-tested for each strain, and thus 14 samples in total were tested. With the strain increased, the length of the sample increased as well. As it can be observed in Figure 3.3-4, sample strain rose from 1% to 30% from top to bottom, the overall length of Gleeble treated samples increased gradually. When drawn to 30% strain (sample at the bottom), the overall length of the sample increased to 157mm approximately, which is in consistent with the stroke of 7.0mm. This means that samples were drawn to the specified strain at 450°C during Gleeble test, which is an effective simulated process of HFQ. However, obvious necking was found on samples with strain at 20%, 25% and 30%.

However, error still exists in actual sample gauge length after Gleeble test compared with target stroke values as shown in Table 12. This is because the thermal expansion deformation during heating and holding process in Gleeble test was difficult, if not impossible, to offset completely after the whole equipment was cooled back to the

room temperature, but its effect would be quite limited. Therefore, the actual strain of each sample consisted with target strain and thermal strain.

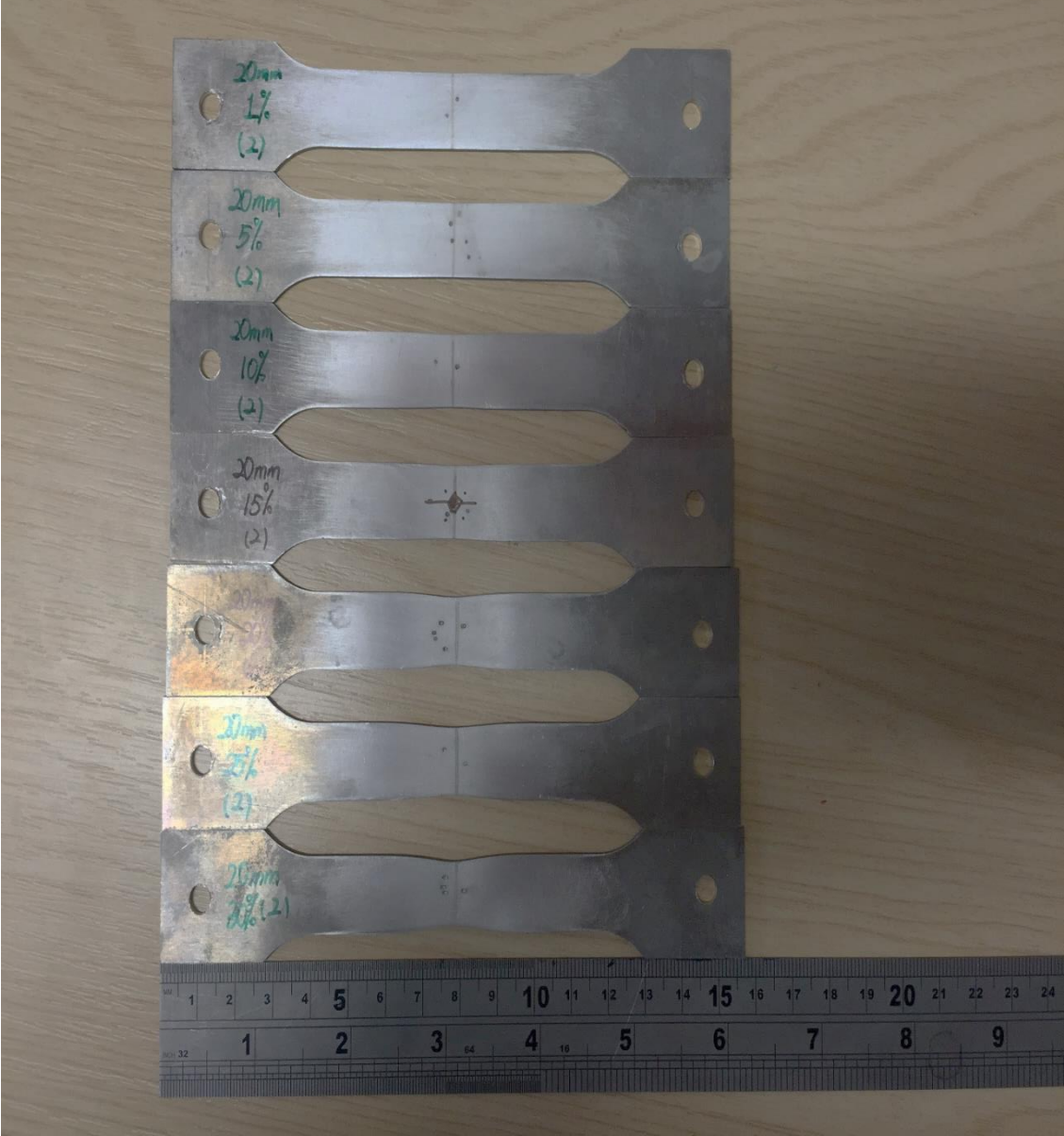


Figure 3.3-4 Gleeble-treated samples deformed from 1% to 30%.

3.4 Post-treatment Characterization

3.4.1 Sample Preparation for the Aging of Dog-bone Shaped Specimens

Owing to the fact that the effective gauge length is only 20mm, the area within the distance of 10mm to the sample centre from both sides was cut for following aging tests. As shown in Fig.3.4-1, the Gleeble tested sample was cut into 4 pieces along the centre line of the length and the width for undergoing aging tests under different conditions. The regions around the red points were marked for hardness tests. This is because it is the region to which a K-type thermocouples was contacted directly, and hence the temperature errors can be ignored. This region showed more reliable hardness results after Gleeble and aging tests than other regions.

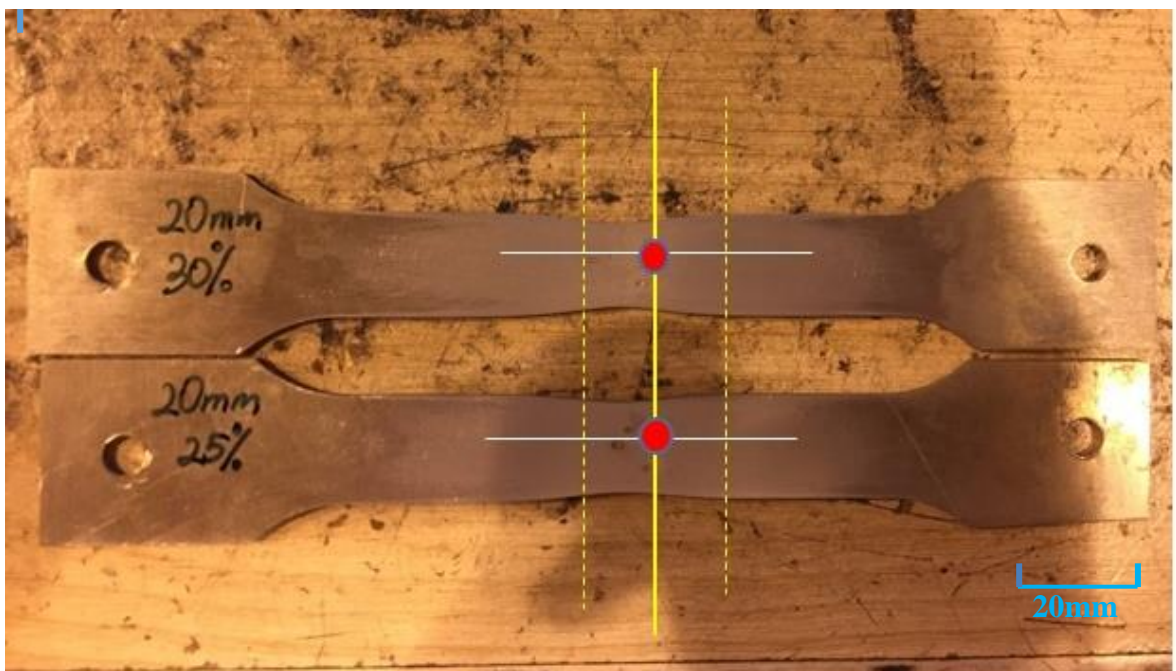


Figure 3.4-1 Schematic of cutting Gleeble-tested samples.

3.4.2 Micro-hardness Test

Micro-hardness test was applied on the cross-section of the centre area in Gleeble and aging tested samples with a load of 300g. Samples were mounted and ground to #1200 by silicon carbide grinding paper, as shown in Fig.3.4-2. Metal clips were used to fix samples. The vital purpose of aging is to improve the hardness or strength of material. Therefore, for the samples deformed at the same strain, the optimal aging conditions would produce the peak hardness.

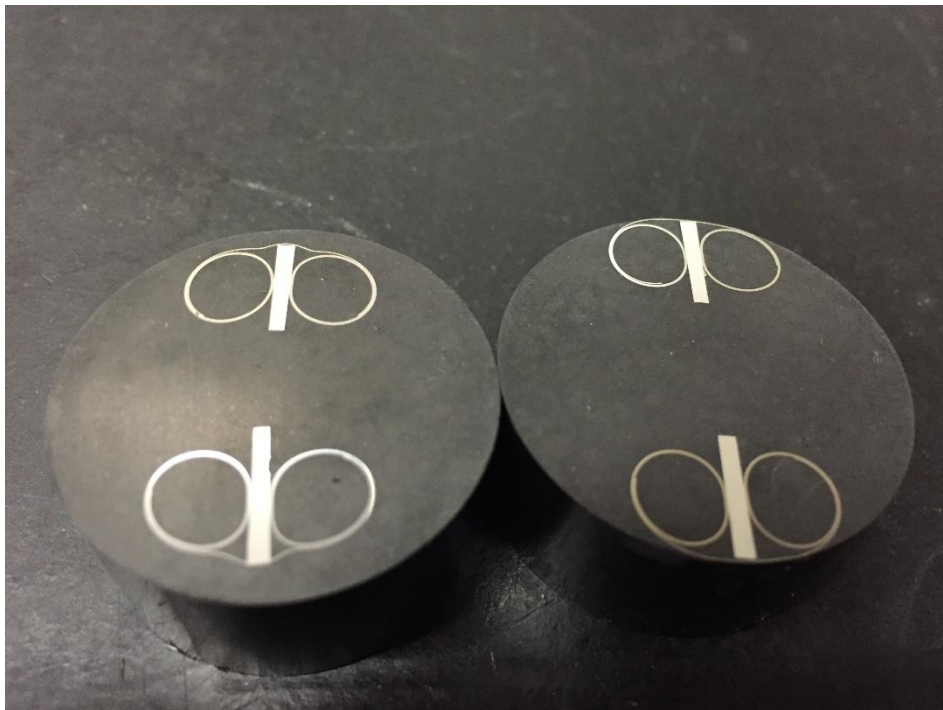


Figure 3.4-2 Mounted and ground samples for micro-hardness test.

3.4.3 Microstructure Characterisation

3.4.3.1 Optical Microscope Observation

The microstructure of the aluminium alloy aged samples investigated in this work was studied by optical microscopy to determine if the grains of aluminium were elongated along uniaxial direction. Samples 0%-8, 5%-8, 10%-8 and 20%-4.5 were ground and polished to 1 μ m. Keller's reagent containing 1% HF, 1.5% HCl, 2.5% HNO₃ and 95% water was used to etch the sample surfaces for 20s. Then, the etched samples were washed with flowing water and dried before observation.

3.4.3.2 SEM (EDS) Observation

To observe the size, distribution and amount of precipitate phase in AA6082 alloy, SEM was applied on ground and polished sample after aging tests. JEOL 6060 and EDS analysis were used to detect the composition of the particles observed. Due to the small size of the meta-stable magnesium silicide precipitates described in Table 8, TEM and XRD were used to detect rod-like β' and needle-like β'' phases and the details are given in Section 3.5.

3.5 XRD and TEM Detect

3.5.1 XRD Analysis

As discussed before, precipitate β'' , β' and equilibrium phase β possess different crystal structures. Also, precipitate phases in AA6082 alloy transform and the distribution and types of precipitates change during aging treatment. Thus, their corresponding characteristic peaks in XRD pattern separately are different. With the help of XRD analysis, it is possible to detect the types of existed precipitates and their proportion, in order to judge the status of aging test, for instance, under-aged, peak-aged or over-aged.

X-ray diffraction patterns were obtained using a Bruker D8 Advance X-ray Diffractometer. The angle was set from 0° to 90° . Detected samples are as-received AA6082 specimen in T6 condition, 1% - 3, 5% - 3, 10% - 3, 1% - 8, 5% - 8 and 10% - 8 samples, compared with SHT-treated sample on the condition of $545^\circ\text{C}\times 50\text{min}$. PANalytical X'Pert HighScore software was utilized to identify the phase composition. On account of the limitation of XRD analysis of small precipitates, TEM (transmission electron microscope) is required for fine structure analysis.

3.5.2 TEM Characterisation

3.5.2.1 Sample Preparation

The aged sheet samples were first ground to 200 μ m in thickness and then polished slightly. After that, the samples were punched into discs with 3mm in diameter, as shown in Figure 3.5-1.



Figure 3.5-1 Punched disc samples prepared for TEM

Twin jet polishing was applied on punched discs by Struers Tenupol-5 (shown in Fig.3.1-2). The electrolyte was prepared by mixing 70vol% nitric acid and methanol at 1:2. The electro-polishing took place at -30°C , using liquid nitrogen to cool down the environment at the beginning and supply in time to keep the temperature around -30°C . The voltage was set as 20V while the flow rate was about 35 (Granholt, 2012).

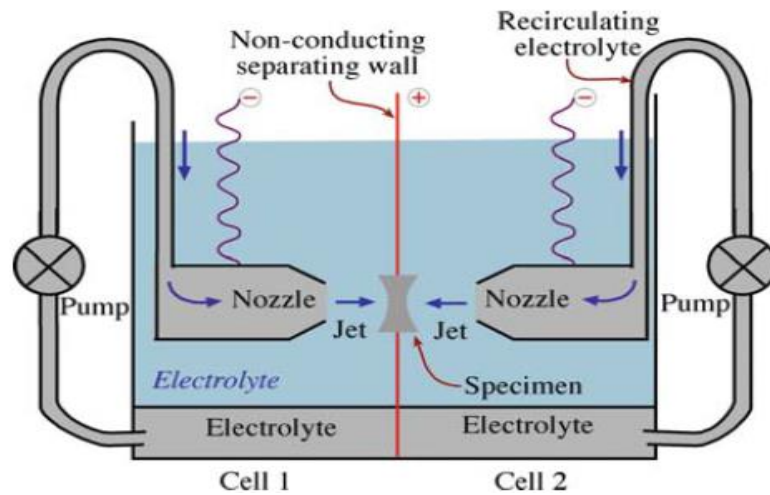


Figure 3.5-2 Schematics of twin jet polishing (Williams & Carter, 2008).

After electropolishing, a tiny hole existed in the middle of the sample. When the disc was penetrated, the samples were taken out from the bath, washed in methanol, then distilled water and finally methanol (Nicholson et al., 1957). The area around hole of the sample disc is the thinnest area, where electron beam can transmit through for TEM observation.

3.5.2.2 TEM Observation

TEM was conducted by JEOL 2100. Owing to the high resolution of TEM and the selected area diffraction function plus equipped EDS, the size, distribution and amount of precipitation phase, aluminium, magnesium silicide equilibrium phase and inclusions are able to be identified. Samples 15% - 3, 15% - 6, 15% - 7 and 0% - 8 were chosen to be observed via TEM JEOL 2100.

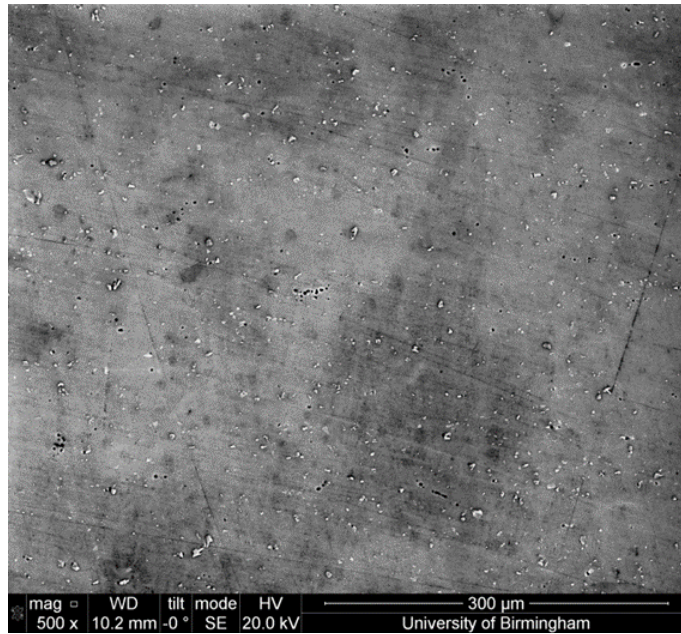
CHAPTER IV RESULTS

4.1 Characterisation of As-received Material

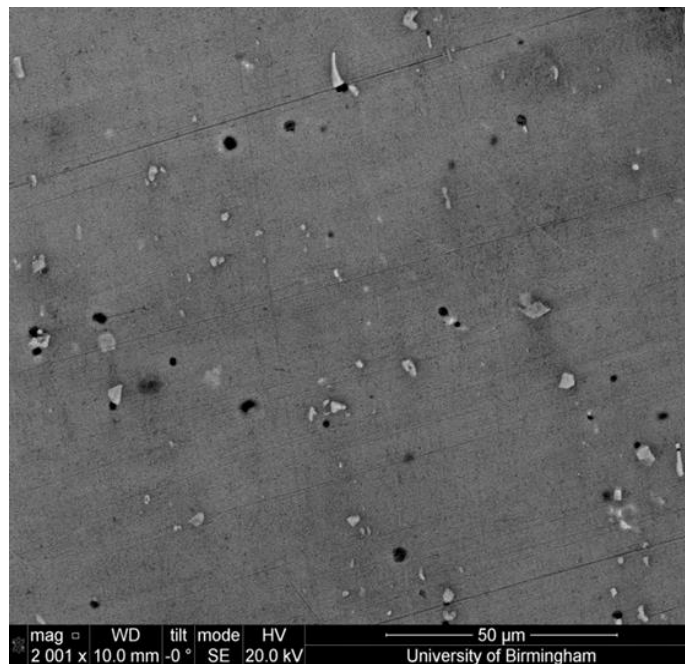
4.1.1 Microstructure of As-received AA6082 Samples

The microstructure of as-received 6082 aluminium alloy specimen on T6 condition was observed using Philips XL-30 SEM. It can be seen from Fig.4.1-1 (a) that black holes and white particles in varied shapes and sizes are dispersively, randomly distributed in grey background, which is known as Al matrix. In Fig.4.1-1 (b) with a much larger resolution, it is proposed that the black holes were formed when some white particles came off probably during polishing. Judging by the micrograph taken by XL-30 SEM, the white particles are considered to be inclusions rather than precipitates.

EDS analysis were applied on polished specimen surface via JEOL 6060 SEM to detect the chemical composition of the as-received AA6082 material. The actual elementary compositions are shown in Fig.4.1-2. It is discovered that, besides magnesium and silicon, manganese and iron are two main impurity elements, which are supposed to be in high contents in inclusions of the as-received AA6082 material.

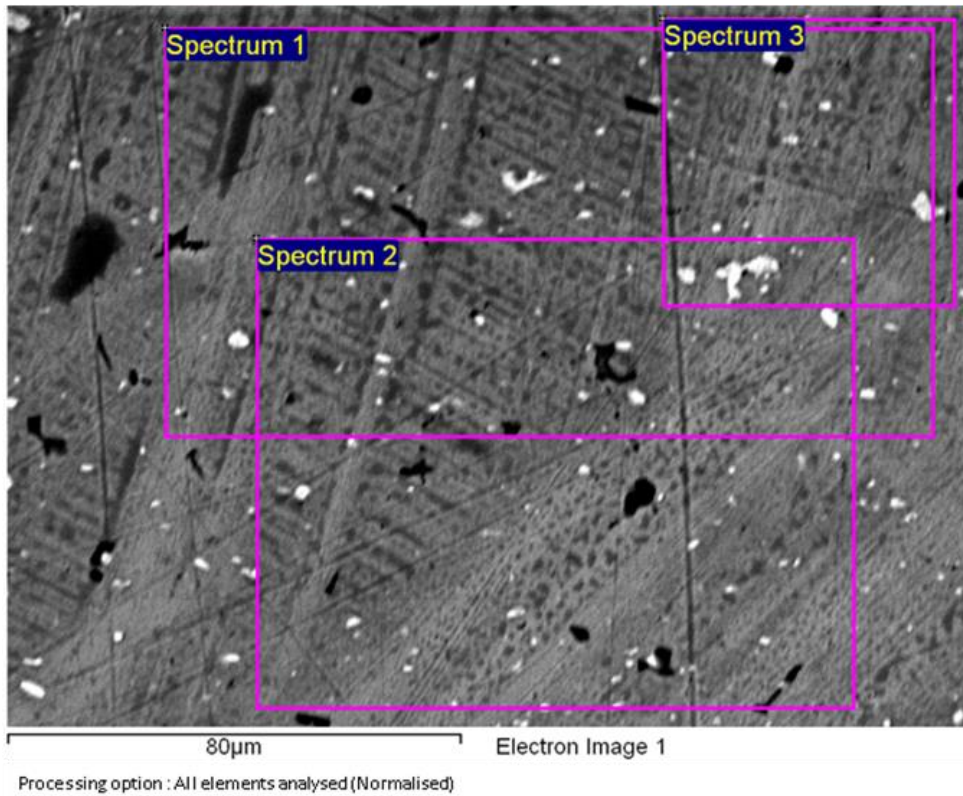


(a)



(b)

Figure 4.1-1 (a) & (b) SEM images of as-received AA6082 sample on T6 condition.



Spectrum	In stats.	Mg	Al	Si	Cr	Mn	Fe	Cu	Er	Total
Spectrum1	Yes	0.00	96.97	1.33	0.00	0.62	0.80	0.28		100.00
Spectrum2	Yes	0.22	96.71	1.69	0.00	0.61	0.76	0.00	0.00	100.00
Spectrum3	Yes	0.00	96.75	1.29	0.00	0.89	1.07	0.00		100.00
Max.		0.22	96.97	1.69	0.00	0.89	1.07	0.28	0.00	
Min.		0.00	96.71	1.29	0.00	0.61	0.76	0.00	0.00	

Figure 4.1-2 EDS analysis of as-received AA6082 material.

4.1.2 XRD and TEM characterisation

XRD pattern of as-received AA6082 material in T6 condition is shown in Fig. 4.1-3. It can be seen that only 5 significant peaks of α -Al matrix phase can be identified. No other phases could be detected although a few weak peaks can tentatively indexed to Mg_5Si_6 phase.

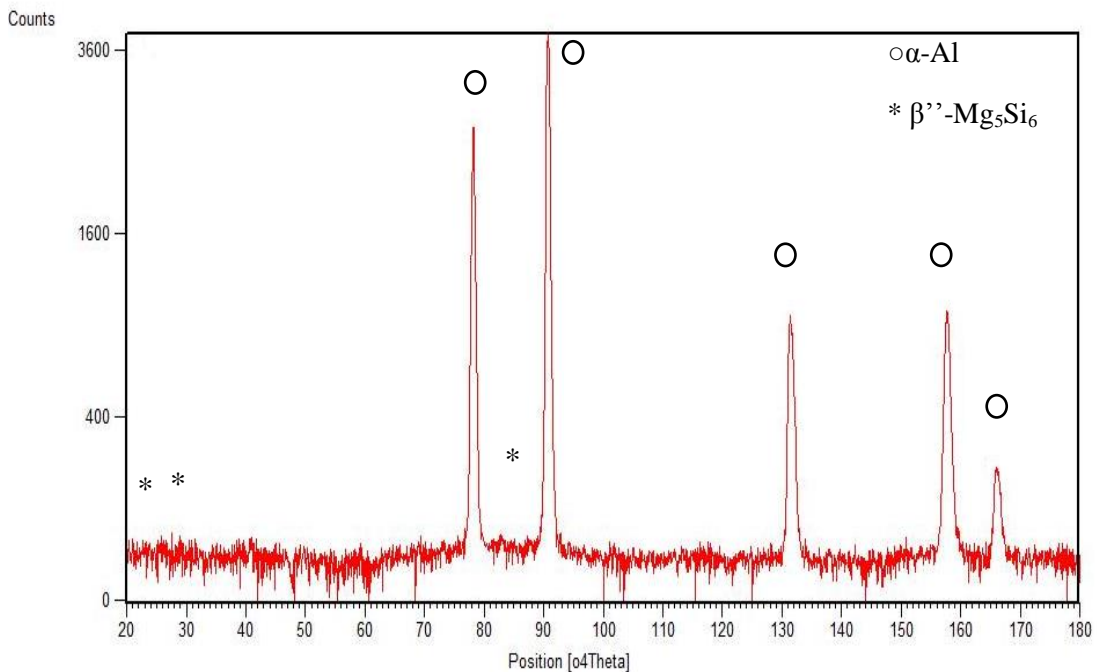
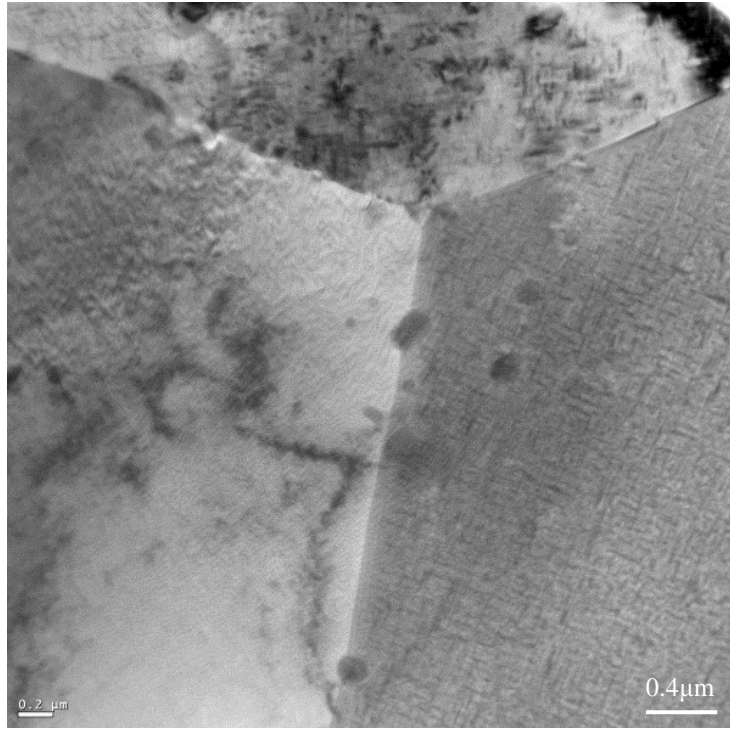


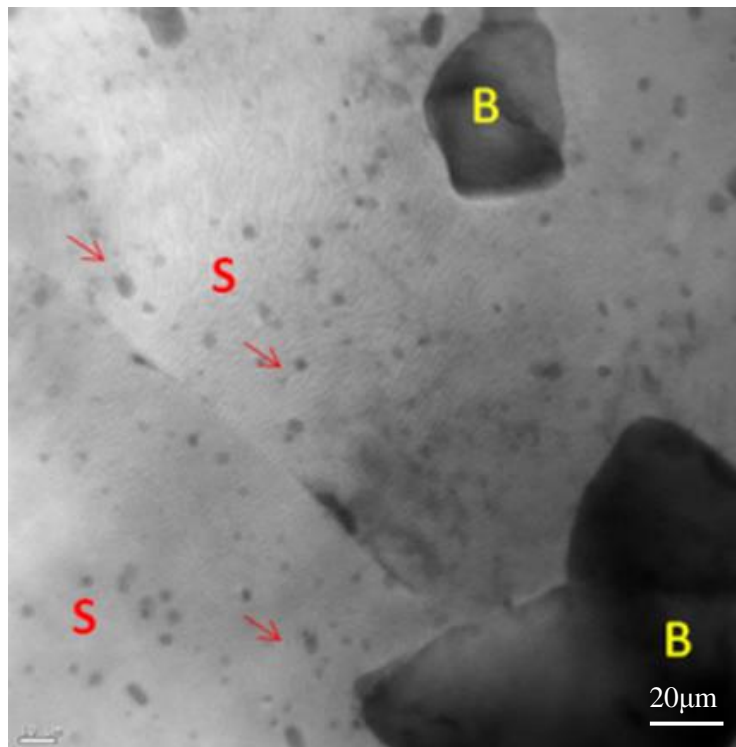
Figure 4.1-3 XRD pattern of as-received T6 AA6082 alloy.

To further study the microstructure of the T6 sample, TEM observation and EDX analysis were conducted. Bright field TEM images under low magnification (Fig.4.1-4) revealed α -Al grain boundaries, annular big sized particles and circular small particles. EDX chemical analysis on these big and small particles indicated relatively higher quantity of MnFeSi and MnSi composition than the matrix respectively, indicating inclusions of AlMnFeSi and AlMnSi for the big and small particles. As the melting point of these inclusions are above 700°C, the SHT soaking temperature was

not able to dissolve them but can round off some types of inclusions owing to phase transformation, possibly Al_5FeSi inter-metallic transforms into more rounded discrete $\alpha\text{-(Al}_{12}\text{(FeMn)}_3\text{Si)}$ particles as described in section 2.5 (Mrowka-Nowotnik & Sieniawski, 2005).



(a)



(b)

Figure 4.1-4 TEM images of (a) grain boundaries, (b) inclusions taken from as-received T6 AA6082 sample. AlMnFeSi inclusion is denoted as B, while AlMnSi inclusion particles are denoted as S and pointed by arrows.

Table 13 Chemical composition of inclusions in as-received T6 AA6082 material.

Spectrum	Mg	Al	Si	Cr	Mn	Fe	Cu	Total
From B (Si,Fe,Mn Inclusion)	0.43	71.71	22.95	0.21	1.55	2.88	0.28	100.00
From S (Si,Mn Inclusion)	0.51	63.75	31.57	0.35	3.31	0.33	0.19	100.00

*B-big, S-small particles in Fig 4.1-4.

High magnification TEM bright-field microstructure, Fig.4.1-5 (a), taken under direction of $B=[001]_{Al}$, (Fig.4.1-5 (b)), revealed fine precipitate β'' - Mg_5Si_6 for as-received T6 AA6082 specimen. As can be seen from Fig.4.1-5, β'' precipitates lie in cross perpendicularly and finely, homogeneously distributed in Al matrix along [100] and [010] directions. The [100] direction growth β'' precipitates are projected on the observation plane, seen as 'dots', denoted by arrows in Fig.4.1-5 (a).

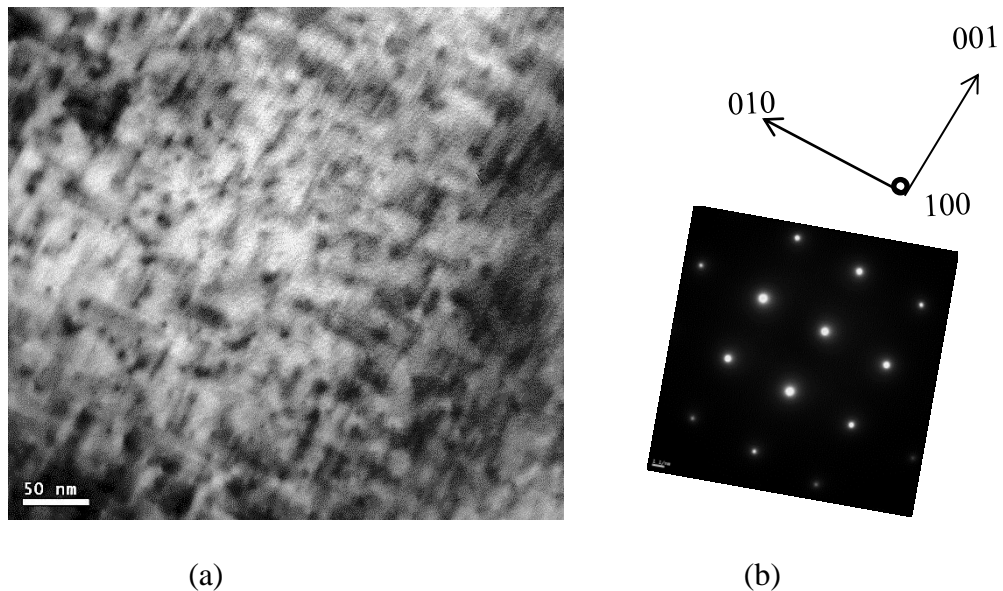


Figure 4.1-5 TEM microstructure of (a) fine β'' precipitates and (b) corresponding SAD pattern of matrix α -Al, $B=[001]$, taken from as-received T6 AA6082 sample.

4.2 Hardness of Solution Heat Treated Samples

In order to find a fully solution heat treated condition for AA6082 material, 6 treatments were tried. Some of the conditions were based on the previous study by group of Dr. Nan Li in Imperial College (Zhang, 2014). All the treatment temperatures were set below 595⁰C, which is solvus temperature of AA6082 materials. The treatment time varies from 1 minute to several hours. The measured hardness values of each SHT treated sample is shown in Table 14.

Table 14 Hardness Results of 6 Solution Heat Treatment Samples.

Specimen Code	SHT Condition	Test Hardness (HV)			Average Hardness (HV)
		Loads, 300g			
570-1	570 ⁰ C × 1min	77.9	78.3	78.4	78.20
530-2	530 ⁰ C × 2 min	80.1	81.2	79.4	80.23
525-15	525 ⁰ C × 15min	77.2	76.4	75.8	76.47
545-50	545 ⁰ C × 50min	48.8	49.6	49.8	49.40
530-120	530 ⁰ C × 2h	52.0	51.2	50.2	51.13
575-240	575 ⁰ C × 4h	53.3	54.2	54.6	54.03

Compared with solution heat treatment methods, it can be obviously seen that there are big differences in hardness between two groups. For conventional ones, sufficient time is provided to dissolve all the soluble precipitates into the aluminium matrix (Zhang, 2014). Hence, the hardness of treated AA6082 sample decreased from 120 HV on T6 condition to 50 HV approximately owing to softening mechanism of

solution heat treatment. However, in terms of fast SHT method, sample hardness only dropped to around 78 HV after treatment, which is nearly the same hardness as AA6082 alloy undergone 2 or 3 hours artificially aging treatment at 180⁰C (Zhang, 2014). The samples are under-heated thus not completely softened. Therefore, a conclusion can be made that 3 novel fast solution heat treatment methods are not able to dissolve the precipitates already existing in T6 condition AA6082 sample completely into Al matrix for quite short holding time (Zhang, 2014). The hardness values of fast SHT group are quite similar. Even though the holding time has slight differences, elevated temperature covers the shortage of diffusion time in solution heat treatment method. Therefore, it is also proved in this test that raising holding temperature and extend treatment time are able to achieve a similar effect in solution heat treatment.

However, it came to a completely different result for traditional SHT methods group. Higher treatment temperature and longer holding time lead to increase of AA6082 sample hardness after solution heat treatment test, which is unexpected for SHT softening mechanisms. It is inferred that slight growth of sample hardness in the last two tests was owing to over-heated phenomenon. Solution heat treatment test at 545⁰C lasting for 50 minutes shows the lowest hardness as 49.40 HV, which means all the soluble precipitates fully dissolved into aluminium matrix. Continuous homogeneous heating causes Al grains coarsening, as well as aggregation, growth and coarsening of fine silicon grains, which results in slight decrease in hardness (Shi et al., 2012). However, over-heating in solution heat treatment also contributes to dissolving Si from Al(MnFeSi) inclusions into Al matrix by diffusion. Meanwhile, Mn precipitates from super saturated solid solution (SSSS) and substitutes for Fe in Al(MnFe)Si inclusions. Inclusions in aluminium alloys transform to phases with

higher ratio of (Mn+Fe)/Si (Huang et al., 2012). Hence, based on 545⁰C, 50 minutes condition, when holding time increases (e.g. 2 hours or 4 hours), it is supposed that the transformation of interconnected plate-like β -Al₃FeSi intermetallics into more rounded discrete α_c -Al₁₂(FeMn)₃Si particles may occur (Mrowka-Nowotnik & Sieniawski, 2005). α_c -Al₁₂(FeMn)₃Si particles were finely, dispersively distributed in Al matrix, making a dispersion strengthening effect on whole AA6082 material. Therefore, hardness raised slightly. That is the reason that compared with sample 545-50, sample 530-120 and 575-240 were treated for much longer holding time but their hardness increases eventually. Considering efficiency, solution heat treatment test at 545⁰C lasting for 50 minutes is the optimum SHT condition for AA6082 alloy.

4.3. Effect of Pre-strain

4.3.1 Hardness of Aged HFQ-simulated Samples

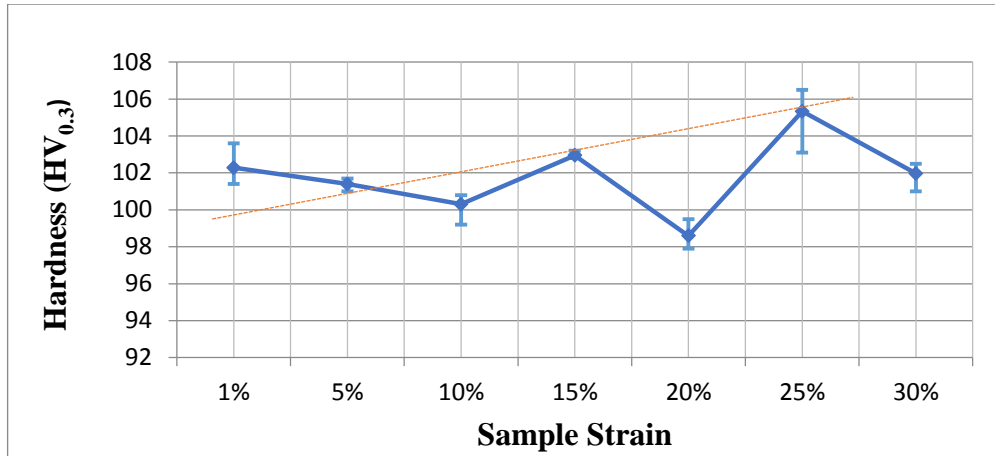
(a) Aging at 180⁰C for 3 hours

Aging treatments of Gleeble-processed samples with different strains were conducted at 180⁰C for 3 hours, 6 hours and 8 hours separately and the measured hardness results are demonstrated in Figs.4.3-1 (a), (b), (c) respectively. The line chart in Fig.4.3-1 (a) shows the hardness values of the Gleeble-processed samples after aging at 180⁰C for 3 hours as a function of their strains. It can be found that after aging at 180⁰C for 3 hours the Gleeble-processed sample with 25% strain, i.e. 25%-3, showed the highest hardness among all the samples. It is noticed that the 20% deformed sample 20%-3 showed the lowest hardness but the mechanism behind is not clear. If the particular hardness value of sample 20%-3 is ignored and taking account of potential

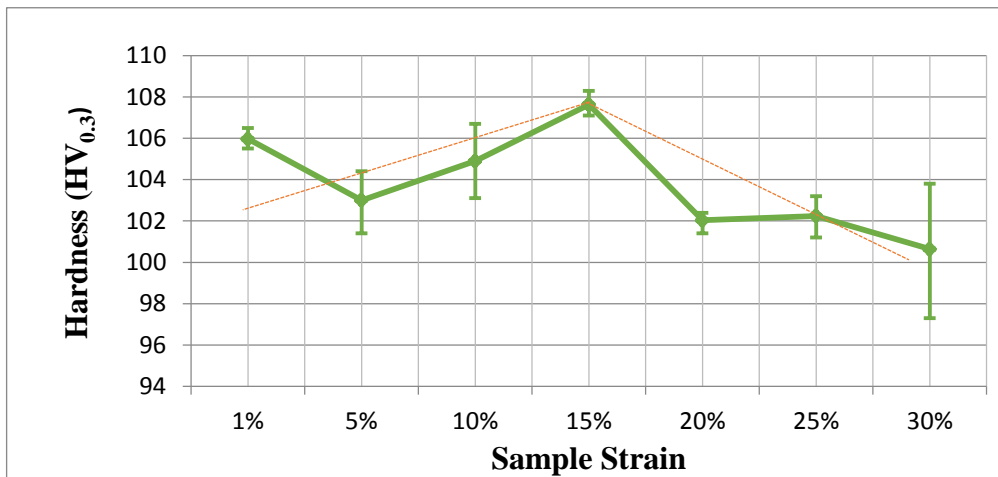
experimental errors, a general trendline of this line chart could be drawn by the orange dotted line in Fig.4.3-1 (a). It seems that under the aged condition at 180°C for 3h, the hardness of Gleeble-processed samples increased when the sample strain increased from 1 to 25%. This implies that the deformation introduced in HFQ process could promote the formation of metastable second phases β'' and β' . However, for sample 30%-3 further increase of strain to 30% led to reduced hardness. Hence, it is proposed that aging at 180°C for 3 hours is the optimum aging condition for sample 25%-3 but over-aging may have occurred to sample 30%-3.

(b) Aging at 180°C for 6 hours

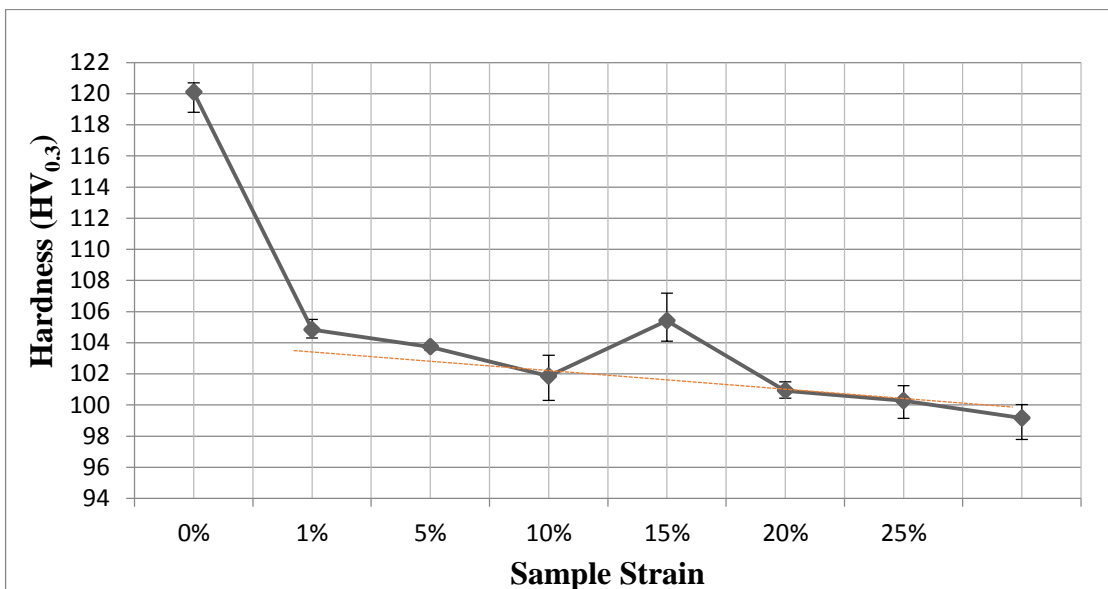
The response of Gleeble-processed samples with different pre-strains to aging at 180°C for 6 hours are summarised in Fig.4.3-1 (b). It can be observed that the sample pre-strained to 15% (i.e. sample 15%-6) displayed the highest hardness in the line chart. Except for sample 1%-6, two orange dotted overall trendlines could be drawn on Fig. 4.3-1(b). The hardness of the Gleeble-processed and aged samples first increased with the sample strain from 1% to 10%. This implies that deformation could promote the formation of β' and β'' phases. The hardness peaked at 15% for sample 15%-6 before it decreased with further increase of the strain from 20% to 30%. Due to the significant drop of hardness for sample 20%-6 as compared with sample 15%-6, it is reasonable to believe that over-aging may have occurred to sample 20%-6 when aged at 180°C for 6 hours. It is thus inferred that for Gleeble-processed samples with strain larger than 15%, the corresponding optimal aging time at 180°C would be shorter than 6 hours to avoid over-aging.



(a)



(b)



(c)

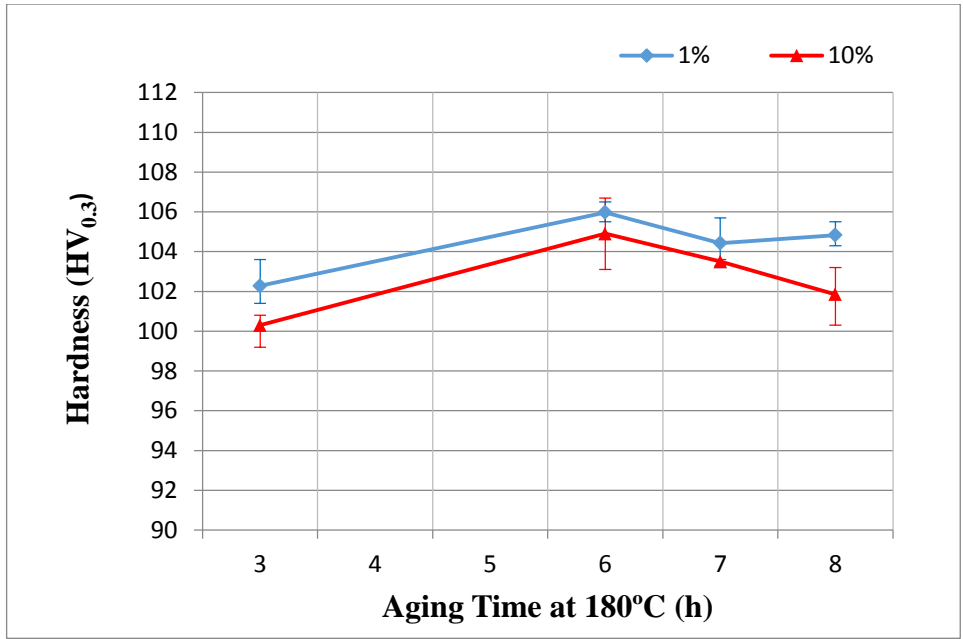
Figure 4.3-1 Line chart of all the Gleeble-processed samples hardness after (a) 3 hours, (b) 6 hours and (c) 8 hours aging treatment at 180°C separately.

(c) Aging at 180°C for 8 hours

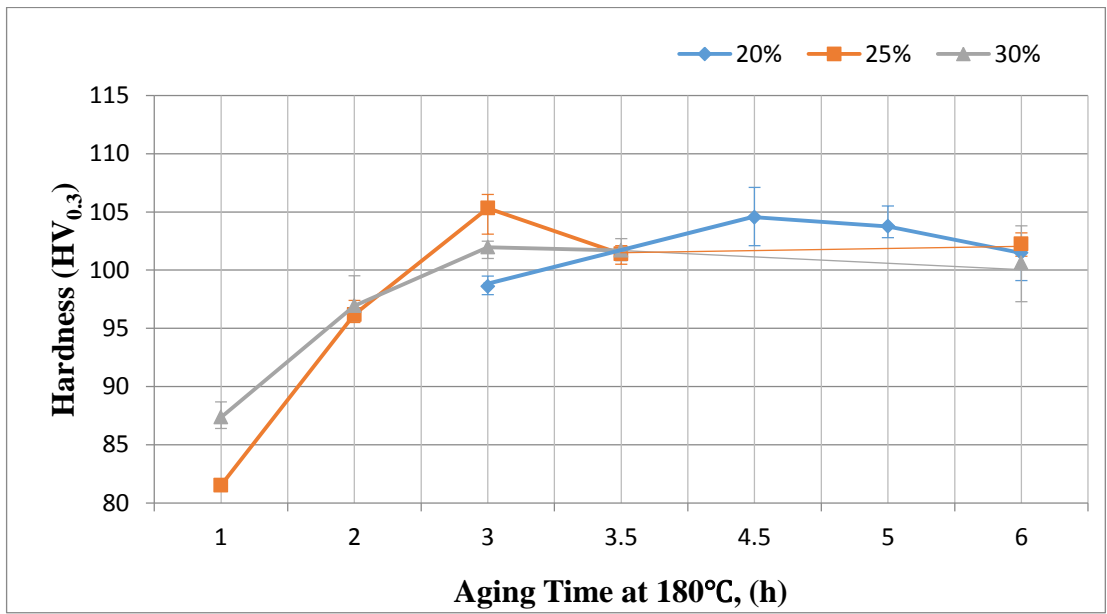
As shown in Fig.4.3-1 (c), after aged to the standard T6 condition of 180°C, 8 hours, non-deformed sample reached the peak hardness of 120HV. However, all the samples pre-deformed via Gleeble test to different strains showed a much lower hardness. Except for sample 15%-8, the general trendline marked as orange dotted line in the line chart depicts that after aging at 180°C for 8 hours the hardness of all the Gleeble-processed samples decreases with increasing the strain. Therefore, it is clear that the strain introduced by Gleeble test will reduce the maximum hardness after aging.

4.3.2 Optimal Aging Time for Peak Hardness

As reported in the previous section, when aged at 180°C for 3, 6 and 8 hours, the hardness of the aged samples are highly dependent on the strain induced by Gleeble tests. In general, the strain corresponding to the highest hardness after aging decreases with increasing the aging time. However, the optimal aging time for a given strain could be in between the time periods used for Section 4.3.1. Therefore, in order to identify the optimal aging time, more aging time periods were selected for some samples depending on the availability of Gleeble tested samples and the results reported in the section above. The results are shown in Fig.4.3-2 below.



(a)



(b)

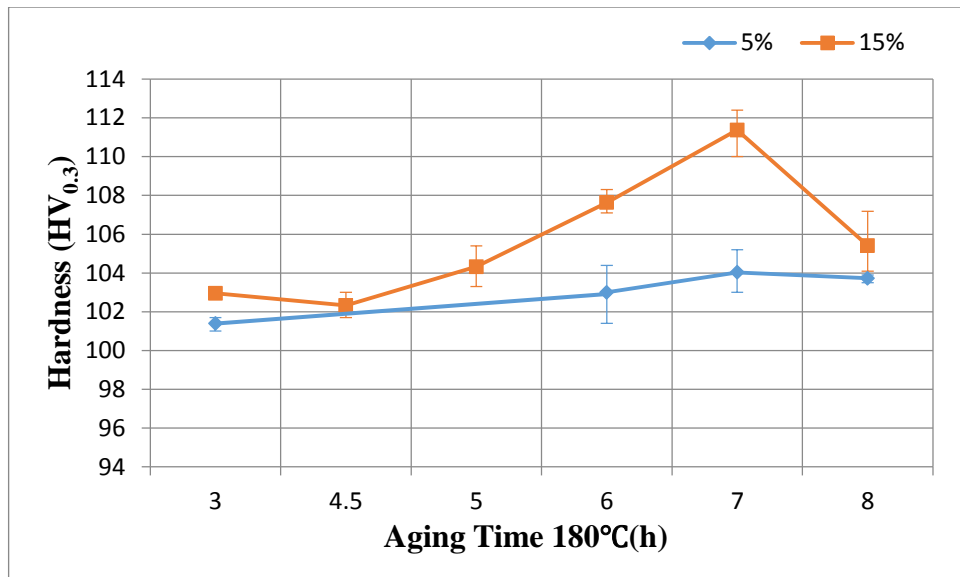


Figure 4.3-2 Hardness results of aging test after Gleeble for sample (a) 1% and 10%; (b) 20%, 25% and 30%; (c) 5% and 15%.

For samples deformed at 1% and 10%, due to their relatively low strains, the optimal aging time could be longer than 6 hours (see Section 4.3.1). As demonstrated in Fig.4.3-2 (a), however, further increasing the aging time to 7 hours has led to slightly reduced hardness probably due to the over-aging condition. Therefore, it is further confirmed that the optimal aging time for samples with such relatively low strains as 1 and 10%

For 20%, 25% and 30% samples, as discussed in Section 4.3.2, due to their larger strains, the corresponding optimum aging time could be shorter than 6 hours. A trend is founded in Fig.4.3-2 (b) that the hardness of the aged samples increases with the aging time before reaching the peak hardness and then descends with increasing the aging time. However, the optimal aging time differs for samples with different strains. For example, for Gleeble-processed samples deformed at 20%, the optimum aging time corresponding to the peak hardness is 4.5 hours, while the optimum aging time

for 25% and 30% deformed samples is 3 hours. Thus, it is also a proof that the accelerating effect of Gleeble test deformation on aging process enhances with increasing the strain.

However, for the samples with strain at 5% and 15%, the corresponding optimal aging time is 7 hours, which is close to the aging time for standard aging time (8 hours). It is also noted that the peak hardness of sample 15%-7 is much higher than that of sample 5%-7. In addition, the effect of the aging time is more significant for the 15% strained samples than for the 5% strained ones.

According to the hardness data shown in Figure 4.3-2, the optimum aging time and peak hardness of each Gleeble-processed sample are summarised in Table 15.

Table 15 Optimum aging time and maximum hardness value of Gleeble-processed samples.

Sample Deformation Rate	Optimum Aging Time /h	Maximum Hardness (HV, Loads 300g)
0	8	120.08
1%	6	105.97
5%	7	104.03
10%	6	104.90
15%	7	111.37
20%	4.5	103.90
25%	3	105.33
30%	3	101.97

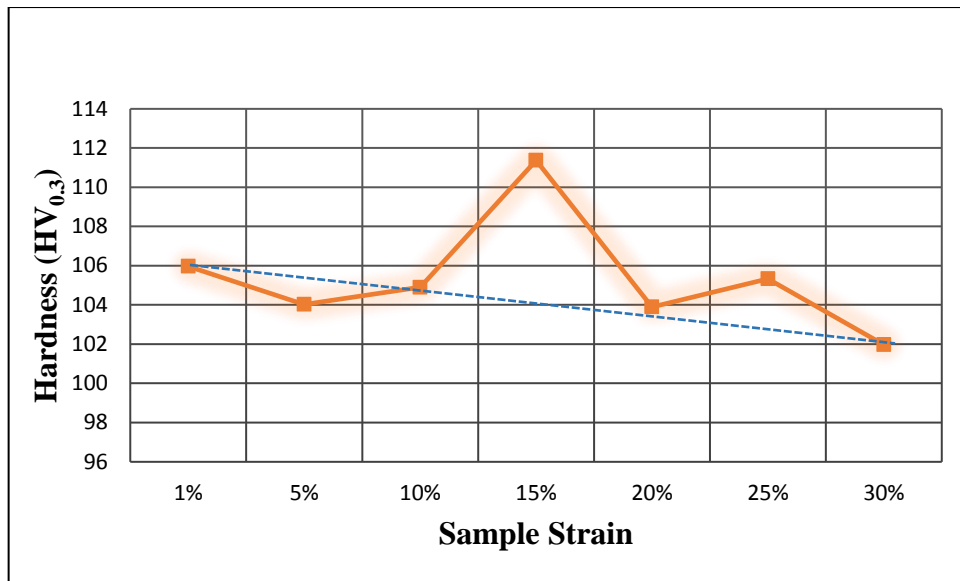


Figure 4.3-3 Peak hardness of each Gleeble-tested and aged samples.

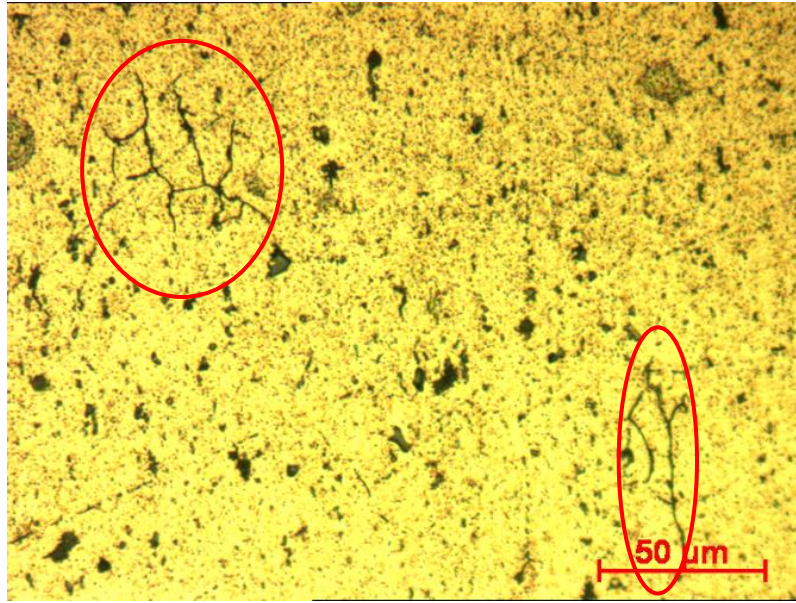
Peak hardness of all the Gleeble-processed and aged samples as a function of the pre-strain is shown in Fig.4.3-3. Sample 15%-7 shows a much higher peak hardness of 111.37 HV than any other samples and sample 30%-3 gives the lowest peak hardness as 101.97 HV. Regardless of sample 15%-7, which will be discussed later, sample 1%-6 possesses highest peak hardness among the left 6 samples. A trendline marked as blue dotted line in Fig.4.3-3 shows that sample peak hardness of optimum aging condition decreases with rising strain. In Table 15, with no regard to the particular optimum aging time of sample 1% and 15%, a general law is discovered that as strain goes higher, the corresponding optimum aging time descends from 6 hours to 3 hours. Therefore, a preliminary conclusion is made that deformation during Gleeble test, prior to aging, is able to shorten the aging process via accelerate the formation of β'' and β' precipitates. The sample optimum aging time decreases with increasing strains introduced during Gleeble test, however, it is at the cost of declining corresponding sample peak hardness.

4.4 Microstructure Characterisation of HFQ-simulated Samples

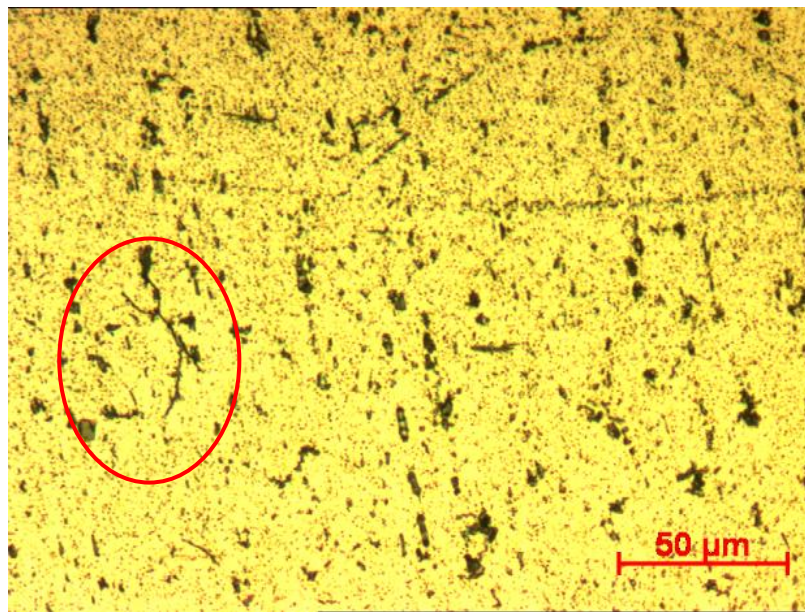
4.4.1 Optical and SEM microstructure

The optical microstructures of 3 Gleeble-treated and aged samples 5%-8, 10%-8, 20%-4.5 and the as-received AA6082 material in T6 condition with a 1:500 scale bar are shown in Fig.4.4-1. No clear grain boundaries can be observed from these samples except for some patches of discontinuous ones as shown in circled areas marked in red in Fig.4.4-1. It is supposed that the yellow background area stands for the aluminium matrix while the large dark spots in the images are inclusions and the tiny dots distributed all over the aluminium matrix are precipitates. Inclusions are in much larger size with varied shapes and clearer to be observed than the precipitates under optical microscope, which could be AlMnFeSi and AlFeSi inclusion particles according to the literature (Mrowka-Nowotnik & Sieniawski, 2005). It can be noticed that the fine precipitates are in larger quantities in heavily deformed samples than in the less deformed ones, as evidenced by the darker contrast in the substrate areas of the former (Fig.4.4-1(c)) than in the substrate areas of the later (Fig. 4.4-1 (b)).

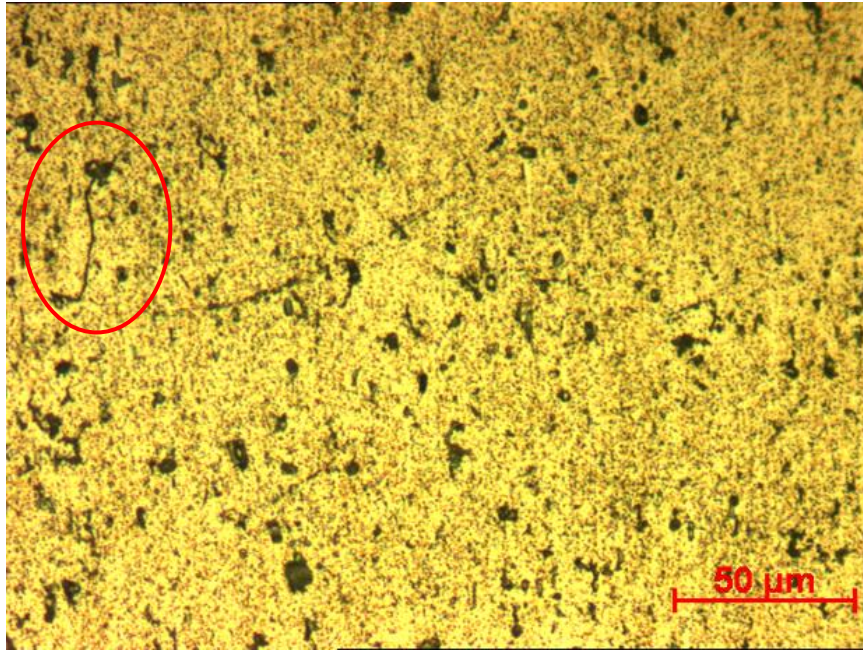
The force applied on the samples during the Gleeble tests was along the vertical direction of the micrographs in Figure 4.4-1. It can be found that some inclusions are elongated along the vertical direction and their shapes are changed from round to elliptical or rod (see Figs.4.4-1 (b) and (c)). Therefore, it is clear that the tensile stress applied during the Gleeble test resulted in plastic deformation of samples in uniaxial direction. This plastic deformation introduced during the Gleeble test has influenced the subsequent aging process of these samples and their eventual mechanical properties. SEM observation on these samples (Fig. 4.4-2) did not find any new features other than the ones observed by optical microscope.



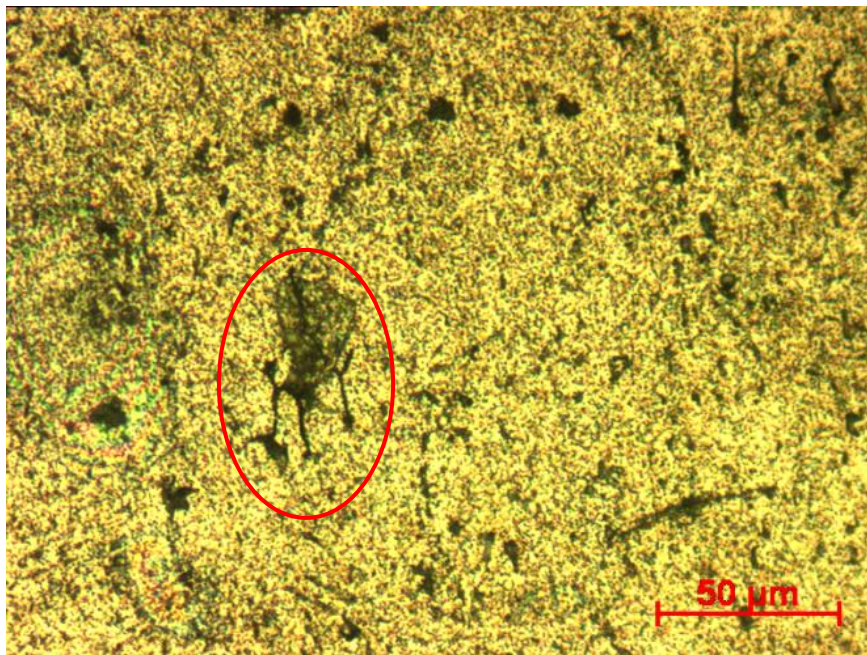
(a)



(b)

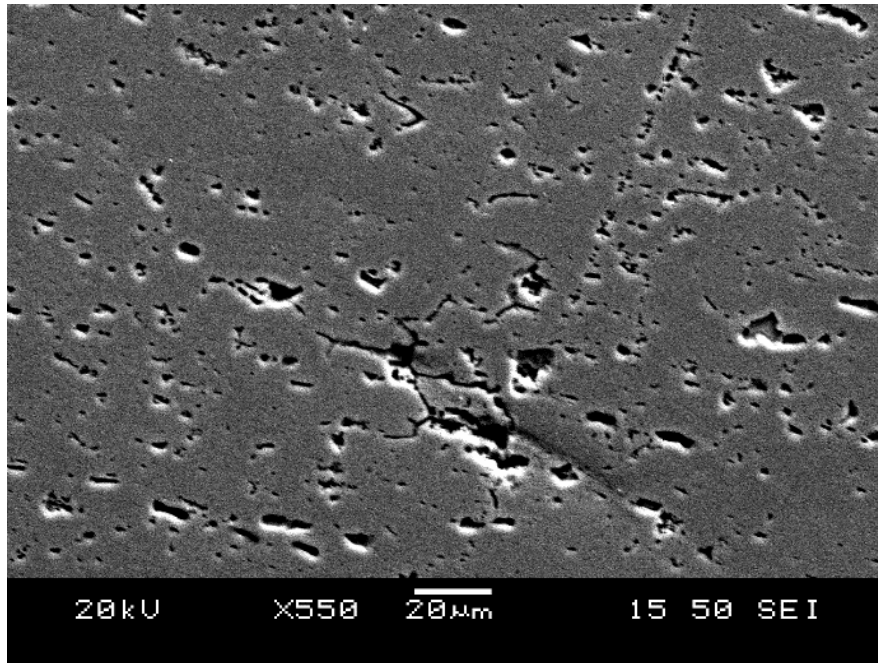


(c)

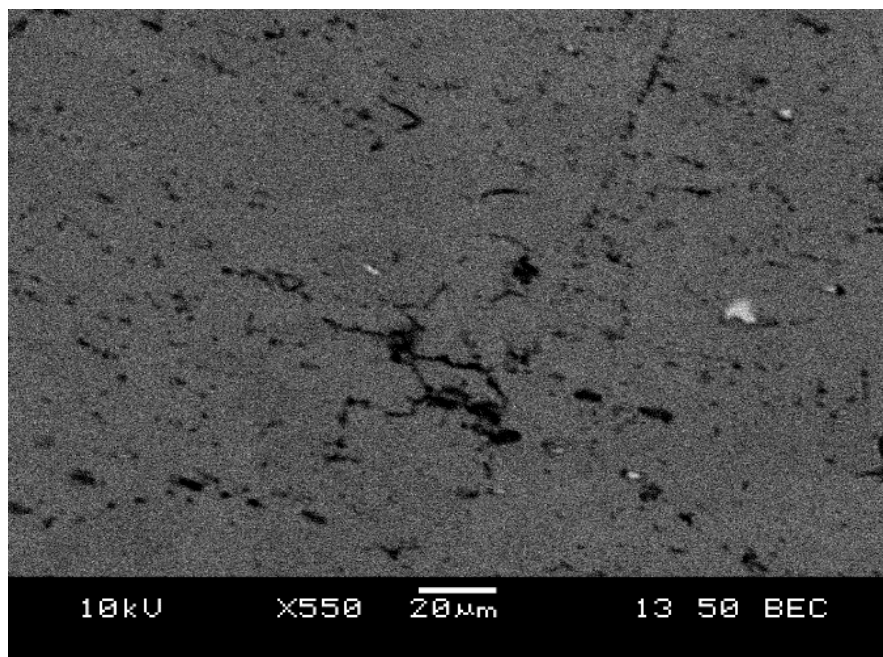


(d)

Figure 4.4-1 Microscope images of sample (a) 0%-8; (b) 5%-8; (c) 10%-8; (d) 20%-
4.5.



(a)



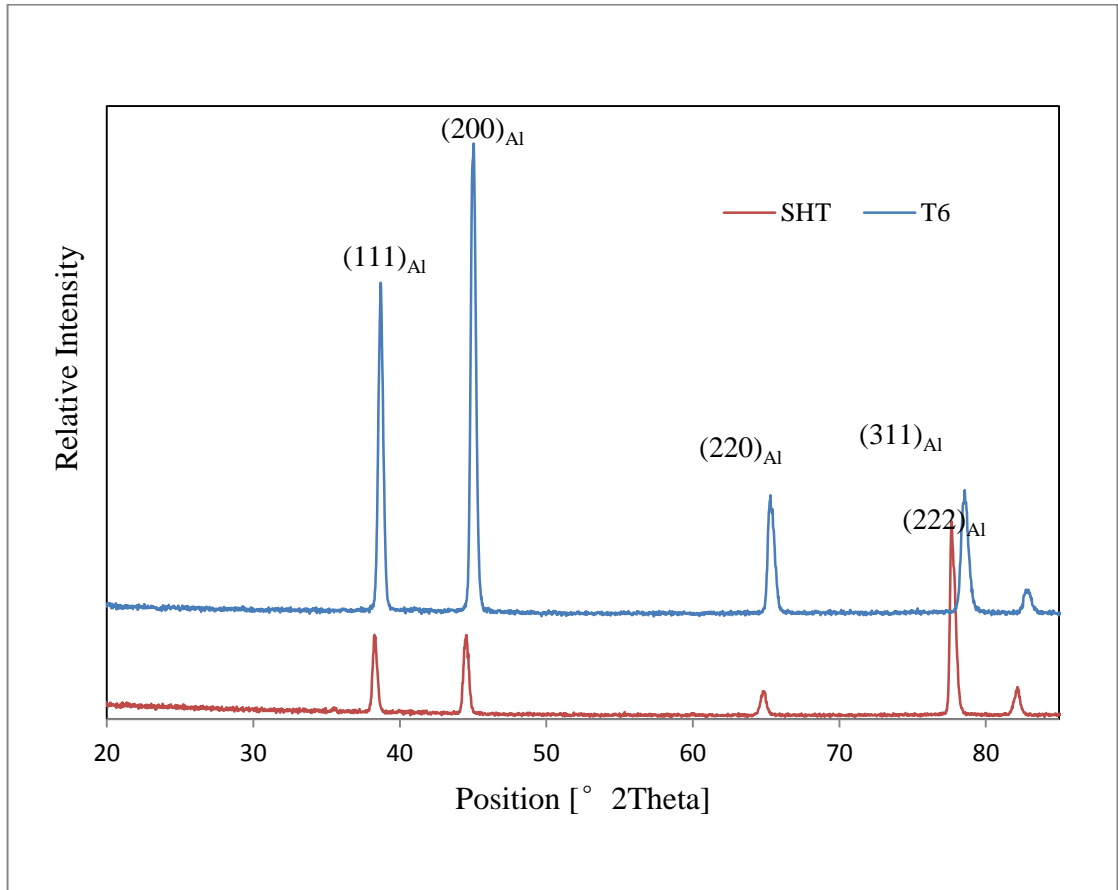
(b)

Figure 4.4-2 SEM images of 20%-4.5 sample: (a) SEI and (b) BSI.

4.4.2 XRD patterns of HFQ-simulated Samples

Fig.4.4-3 shows the XRD patterns measured from the samples of just undergone solution heat treatment and the as received T6 sample. No peaks of precipitates could be detected and only a set of f.c.c. peaks of the matrix α -Al phase was identified for both samples but with shifted 2 theta positions and altered peak intensities between these two patterns. It can be seen that the peaks of the SHT specimen shifted to the lower angles than the T6 ones, indicating expansion of α -Al d-spacing. This phenomenal approved that the solution heat treatment condition of 545 °C, 45min could make all the precipitates in T6 condition material dissolve into the aluminium matrix. The big atom size of Mg caused the expansion of the α -Al crystal size.

Figure 4.4-4 displayed XRD patterns of 1%, 5%, 10% strain rate deformed and 3, 8 hours aged samples. Sample 1%-3, 5%-3 and 10%-3 were under-aged, only very weak peaks of the β'' precipitate phase can be seen. While for 1%-8, 5%-8 and 10%-8 samples, the 8 hours aging time induces the magnesium silicide precipitates and the peak intensity of the precipitates are deformation rate dependant: the higher the deformation strain rate, the stronger the precipitates peak intensity. β'' -Mg₅Si₆ (ASTM 01-088-1207) was identified as the precipitate for 8 hours aged samples and a few weak peaks detected from sample 10%-8 can be identified as β' -Mg₂Si precipitate. This observation implies that deformation introduced defects in the specimen, where precipitates were nucleated and growth accelerated. Extended aging time could induce precipitate β'' transfer to β' . This assumption will be further investigated by TEM study in the following section.



Diffraction angle, 2θ

Figure 4.4-3 XRD patterns of SHT and T6 condition samples.

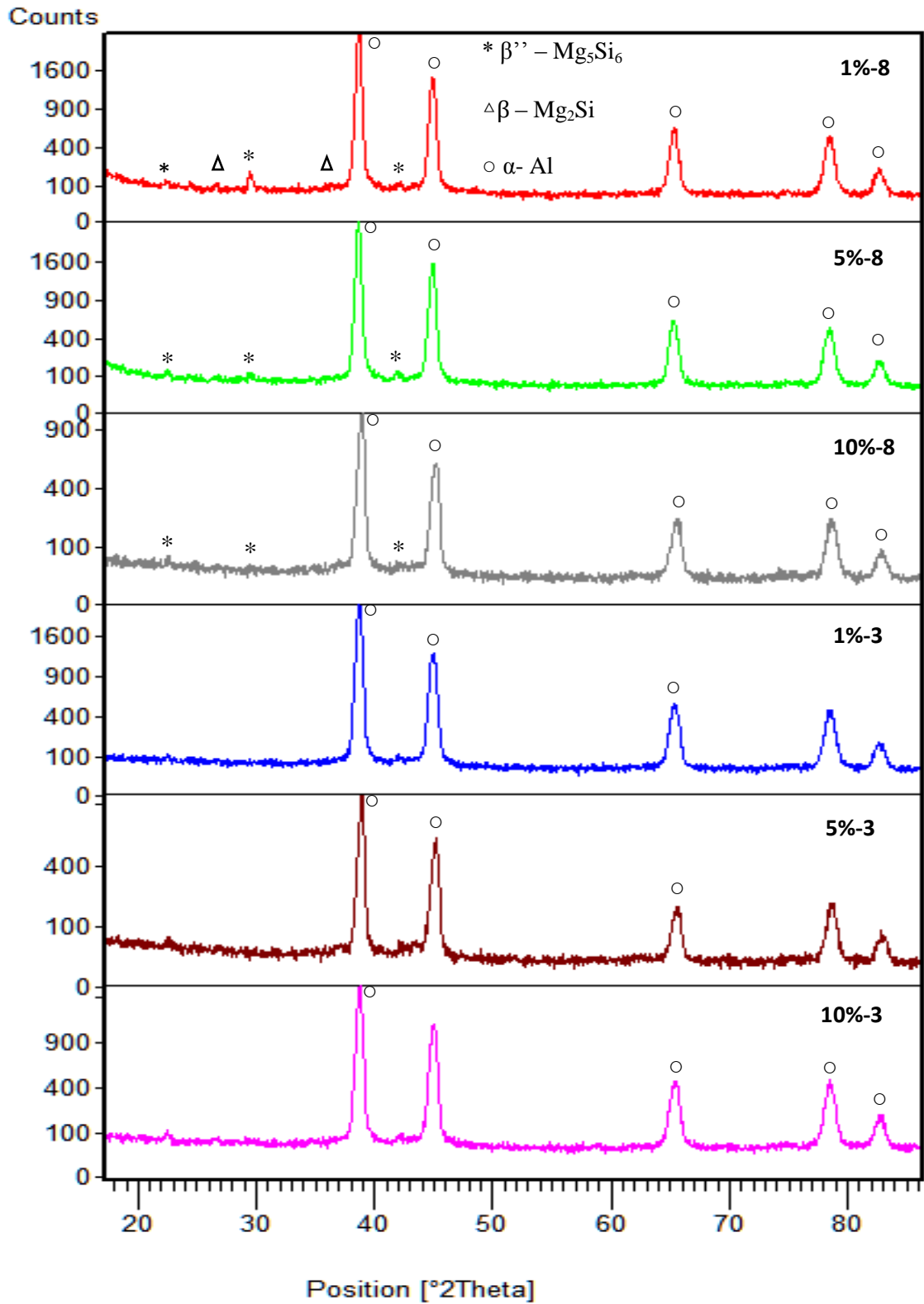


Figure 4.4-4 XRD patterns of 1%, 5%, 10% strain rate deformed and 3, 8 hours aged samples.

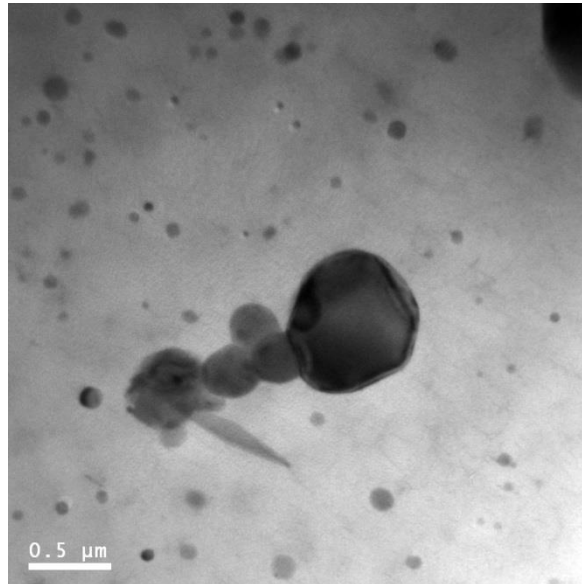
4.4.3 TEM and EDS Analysis

As mentioned in Section 4.4.1, SEM observations is not able to identify the precipitate features related to the deformation and the aging process due to its relatively low resolution. In this Section, the results of TEM observations on selected samples are reported. Due to the orientation and the coherency of the metastable phases of β'' and β' with respect to the aluminium matrix, all TEM investigations were performed in a $\langle 001 \rangle_{Al}$ type zone axis.

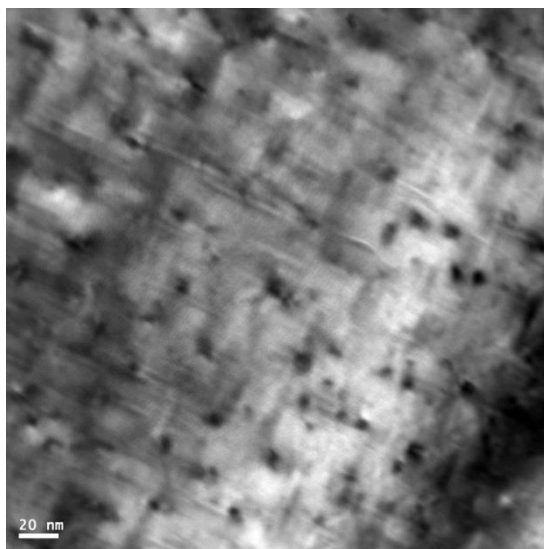
4.4.3.1 Solution Heat Treated and 180°C-8h Aged Sample

Figure 4.4-5 shows the TEM microstructures and corresponding selected area diffraction (SAD) pattern of $[001]_{Al}$ for sample 0%-8h. The low magnification TEM image in Fig.4.4-5 (a) displays inclusion particles in the aluminium substrate. The β'' precipitates could only be observed when the magnification was above 100kX (Fig.4.4-5 (b)). It can be seen that fine β'' phase in needle-like shape are precipitated along $\langle 100 \rangle_{Al}$ directions, lies in cross vertically or horizontally in the length of 28 ~ 40 nm and the distribution of the β'' precipitates are homogeneous. Compared with the TEM features of the as received AA6082 aluminium alloy sample in T6 condition as shown in Figure 4.1-5 (a), this SHT-treated and aged at 180°C for 8 hours sample revealed similar characteristics in terms of Al grain size, inclusion particles size, and the quantity and the size, density and distribution of β'' metastable phase. These similarities in microstructure of the as-received T6 sample and the 545°C × 50min SHT-treated (545-50) then 180°C-8h aged (0%-8) sample resulted in the same peak hardness of 120 HV for these two samples (Fig.4.3-1 (c)).

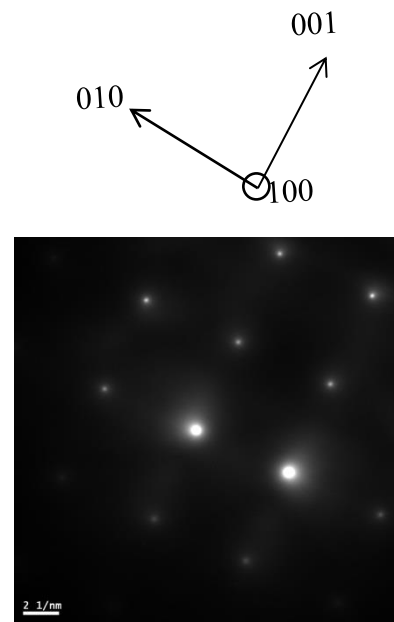
As all HFQ simulated samples were solution heat treated in the same condition of 0%-8 sample at 545°C for 50 minutes, their microstructures after aging for different time periods will be compared with sample 0%-8.



(a)



(b)



(c)

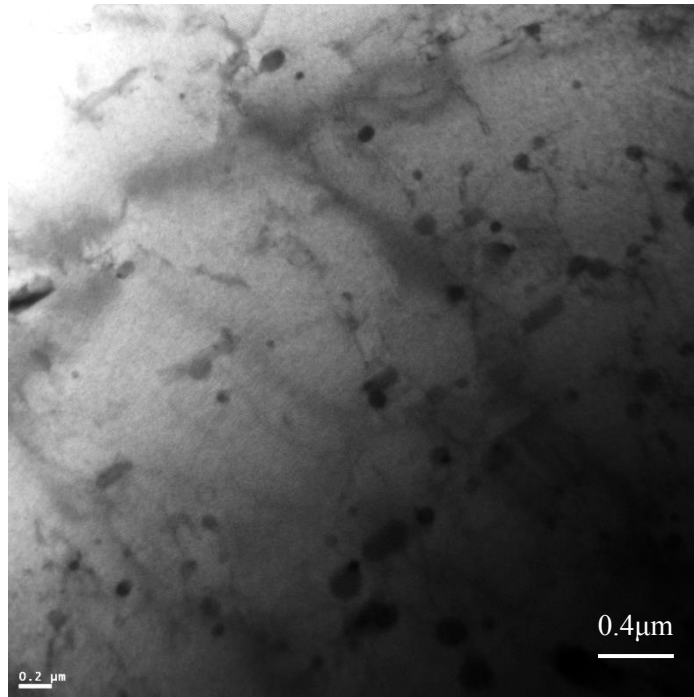
Figure 4.4-5 TEM images of sample 0%-8h. (a) inclusions; (b) β'' precipitates; (c) SAD pattern of precipitates.

4.4.3.2 HFQ Process Simulated AA6082 Samples

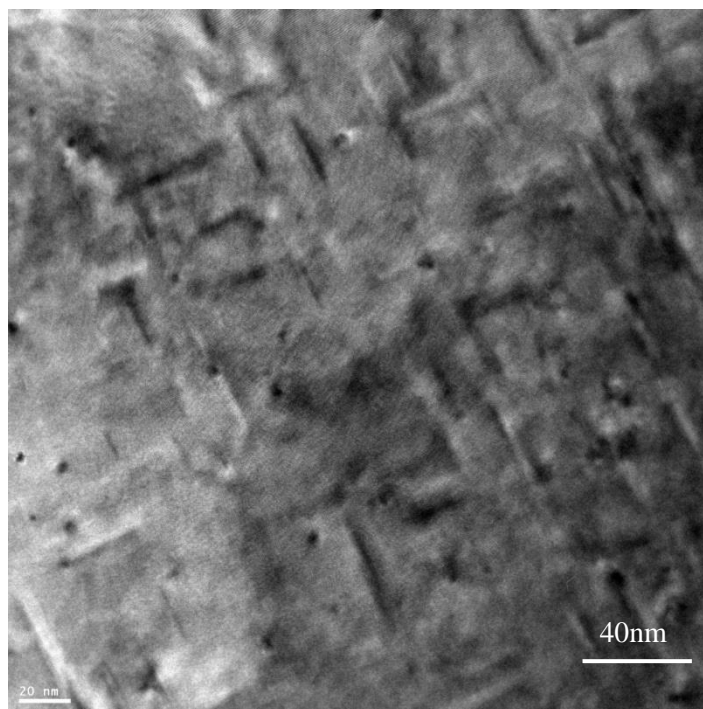
HFQ simulated samples produced by Gleeble-processing with 15% deformation strain aged for 3, 6 and 7 hours were studied by TEM in order to investigate the aging time effect on the formation and growth of precipitates.

As shown in Fig.48, a low density of β'' precipitates were observed in 15%-3 sample. This means that after 3 hours aging, a small quantity of needle-like fine β'' precipitates has already been formed for the 15% strained sample. When aged for 6 and 7 hours, some interesting phenomena were observed from the samples. Under a low magnification as shown in Fig.4.4-7 (a), some rod-like shaped or thick needles of β' precipitated along $\langle 100 \rangle$ direction of $\{100\}_{Al}$ zone can be clearly seen. When increasing the magnification to over 100K, fine β'' precipitates in needle-like shapes are able to be identified on the $\{100\}_{Al}$ zone along $\langle 100 \rangle$ directions for sample 15%-6 (Fig.4.4-7 (c)). Compared with the TEM images of sample 15%-3 in Fig.4.4-6 (a), β'' precipitates increase significantly in quantity and density as a result of longer aging time. The changes in fine metastable precipitates also lead to a significant increase in sample hardness as shown in Fig.4.3-2 (c).

For sample 15%-7, because of the increased holding time at 180°C during aging, TEM observation revealed that the rod-like shape of β' phases are longer and thicker in shape and the fine needle-like β'' precipitates are denser than those presented in 15%-6 sample (Fig.4.4-8 vs Fig 4.4-7). Therefore, the density and quantity of the fine needle-like β'' precipitates reached the highest value, thus contributed to the peak hardness of sample 15%-7.

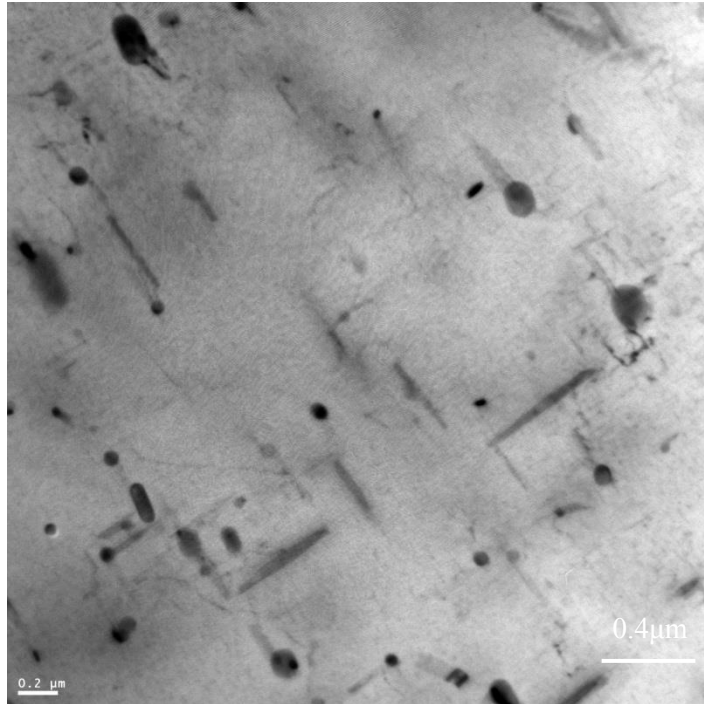


(a)

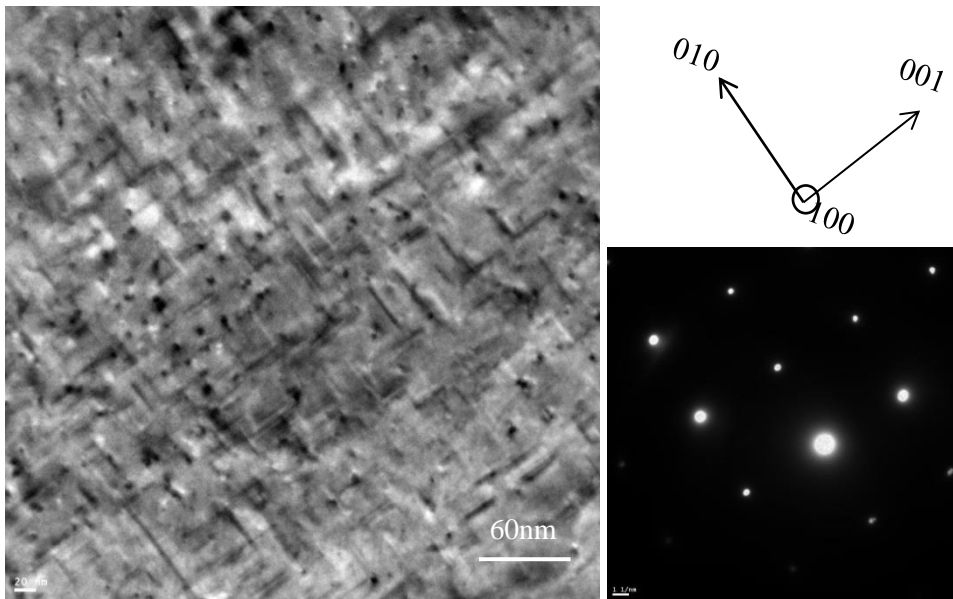


(b)

Figure 4.4-6 TEM images of 15%-3 sample (a) inclusions; (b) precipitates.



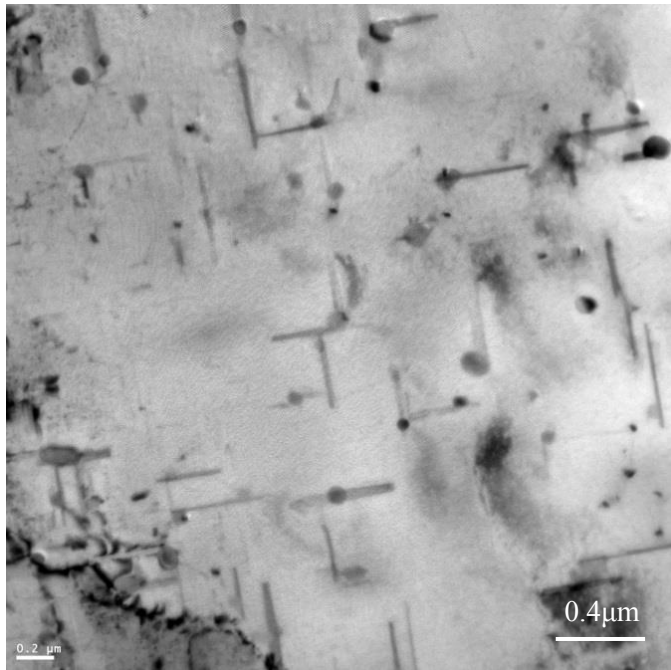
(a)



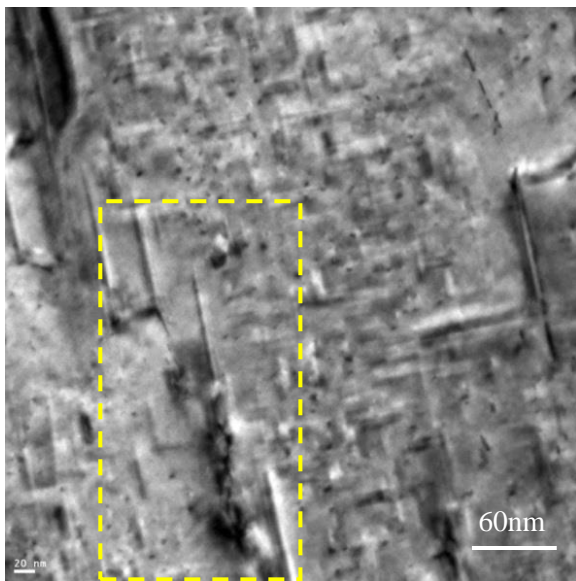
(b)

(c)

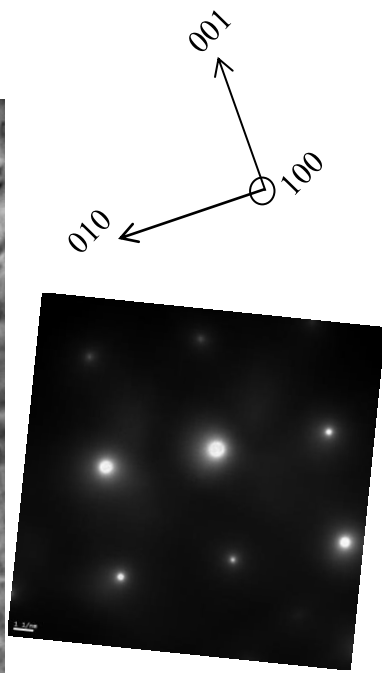
Figure 4.4-7 TEM images of sample 15%-6 (a) precipitates under low resolution; (b) precipitates at higher resolution; (c) SAD pattern of precipitates.



(a)



(b)



(c)

Figure 4.4-8 TEM images of precipitates in sample 15%-7(a) precipitates under low resolution; (b) precipitates at higher resolution; (c) SAD pattern of precipitates.

Table 16 Quantification of the precipitates and inclusions for the four samples TEM studied

Sample Code	β' , Length (nm)		β''				Inclusions, Diameter (nm)	
			Length (nm)		Number Density $1/4000\text{nm}^2$		Mean	SD
	Mean	SD	Mean	SD				
0%-8	-	-	32.46	7.51	81	92.75	28.31	
15%-3	-	-	32.18	3.63	40	96.01	25.77	
15%-6	81.05	27.26	30.59	7.21	55	116.00	30.54	
15%-7	475.12	83.06	31.36	7.72	58	89.05	30.20	

Table 16 summarises the size of the metastable second phases β'' , β' and AlFeMnSi inclusions of samples 0%-8, 15%-3, 15%-6 and 15%-7 by quantifying the TEM images with ImageJ software. After manually marking the precipitates on each image, the ImageJ analysis tool was used for computing the average cross-section area, length and number density of area fraction of the precipitates and the inclusions. The average characteristics of the precipitates and the inclusions were calculated from about 50 counts for each sample treated under 4 different conditions. Phases were identified based on their dimensions and the crystallographic orientations.

It can be observed from Table 16 that the size of the inclusions has no apparent difference for the four chosen treatment conditions of the TEM samples; the length of the precipitated β'' metastable second phase is in the similar range of 32 nm (± 8 nm) for the four TEM samples. The major differences are the number density of β'' is higher and the size of β' phase is larger in sample 15%-7 than in sample 15%-6. This is consistent with the hardness difference in these two samples.

An interesting phenomenon was also discovered by careful TEM observation of Gleeble processed and aged samples. As shown in Fig.4.4-8, long and wide rod-like β' precipitates tended to be form along severely deformed areas (as marked by yellow rectangle) while needle-like β'' precipitates were finely and homogeneously dispersed in aluminium matrix.

Due to the high strain and hence high energy level in these severely deformed areas, metastable phase β'' and β' would form preferentially in the vicinity of these heavily deformed areas. Therefore, it is inferred that plastic deformation introduced by the Gleeble test, as well as HFQ process, form areas with highly concentrated strain. In these areas, the formation of metastable precipitates β'' and β' could be accelerated, thus speeding up the aging process.

Therefore, fine needle-like β'' precipitates are formed in homogeneous regions but the preferentially formed precipitates β'' in the severely deformed areas will transfer to wide and long β' phase. The growth of the β' phase depleted the element Mg and Si adjacent to it, which would eliminate the formation of β'' precipitates. This is evidenced by the fact that there are only few β'' precipitates around the β' thick rods in the area highlighted by the yellow rectangle in Fig.4.4-8 (b).

Therefore, although sample 15%-7 possessed the highest density of β'' precipitates among the deformed four samples, the preferential grown of coarse β' precipitates in the severely deformed areas would reduce the peak hardness due to local over aging. This could be reason way the peak hardness of HFQ-simulated and aged sample is much lower than that of as-received T6 AA6082 material. This also explains the reason for the shorter aging time for HFQ-simulated material than for un-deformed material.

CHAPTER V DISCUSSION

5.1 The Relationship between Optimum Aging Time and Strains

As has been reported in Section 4.3.2, in general the optimal aging time corresponding to peak hardness for HFQ-simulated samples decreased with increasing the strain introduced by Gleeble test (see Fig.5.1-1) except for sample 15%-7.

As shown in Fig.5.1-1, the optimum aging time for the sample without Gleeble test and hence with no pre-deformation is 8 hours, which is the same as for T6 condition. While the optimal aging time dropped to 3 hours when the strain introduced by Gleeble test increased to 25% and 30%. Owing to the deformation prior to aging, the time taken for achieving peak hardness has decreased by about 37.5%.

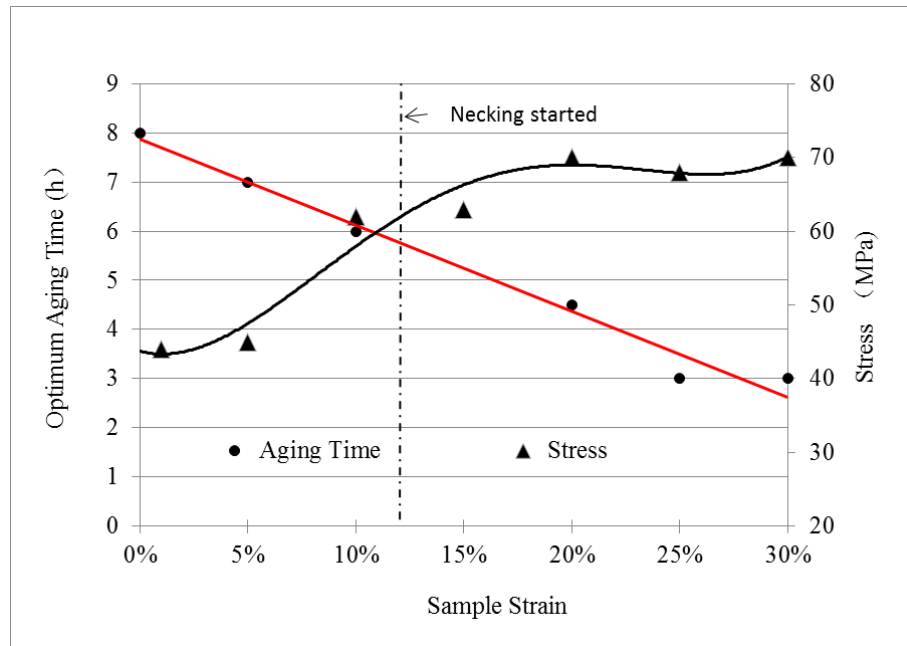


Figure 5.1-1 The relationship between sample strain and optimum aging time (h).

As discussed in Section 2.2.4, the formation of magnesium silicide precipitates from a homogeneous super-saturated solid solution starts with two solute atoms clustering together (Granholt, 2012). The clusters formation requires excess vacancies (Zhang, 2014). The clusters continue to grow by the alloying elements diffusing through the voids of the vacancies and condensate on the clusters. This process is known as the formation of Gunier – Preston (GP) zones, as well as the nucleation of the precipitates. Therefore, it is inferred that the plastic deformation introduced by Gleeble treatment enhances the concentration of voids in super saturated solid solution, thus accelerates the formation of GP zones, as well as the process of metastable second phase precipitation and aging treatment.

It has been discovered in previous various theoretical and experimental studies on dual phase steels that void initiation occurs under the combined influence of stress state and plastic deformation. The cohesion of the inclusion to the matrix is the vital factor affects the essential extent of plastic deformation to initiate a void. The primary sites of void initiation tend to be around non-metallic inclusions and hard second phase particles. Because nearly all the precipitate phases are dissolved after solution heat treatment, inclusions in AA6082 alloy become vital. The incoherent inclusions lead to initiate voids at a small plastic deformation (Barnby et al., n.d). Hence, even though the deformation rate only reaches 5%, the subsequent aging treatment is shortened from 8 hours to 7 hours at 180 °C as shown in Fig.5.1-1. For sample deformed at 1% in Gleeble test, the optimum aging time also decreases compared with as-received AA6082 samples.

However, the linear relationship between the strain and the optimal aging time almost lost once the strain is reached 15% or above. There is no linear relationship between

the optimum aging time of HFQ-simulated samples and the strain introduced by Gleeble test when the strain is beyond 10%.

This scientifically interesting phenomenon could be explained by careful observation of the samples after Gleeble test. As can be observed from Fig.3.3-4 mild necking started to appear when the strain reached 15% and severe necking was observed for the samples deformed at strain 25% and 30% as evidenced by the clearly reduced section in the middle of these samples. Necking is a kind of locally concentrated deformation and the stress state will be changed from uniaxial homogeneous tensile deformation to complicated three dimensional deformation. The strain in the neck is more complex and is under the influence of strain rate sensitivity, coalescence of voids, strain hardening and ductile rupture. This is evidenced by the fact that, as shown in Fig.5.1-1, before necking the stress increased with the strain; the stress is almost flatted when clear necking occurs. Clearly, the change of stress/strain state has caused complex influence on the following aging process of the Gleeble-tested samples.

In sum, dislocations and voids introduced by plastic deformation during Gleeble test provide more vacancies for GP-zones to form and thus shorten the aging time. The pre-aging deformation after solution heat treatment accelerates the formation of metastable phase β'' and β' . Therefore, the sample optimum aging time decreases with increasing the pre-strain. However, because of the complex effect of necking when the strain exceeds 15%, there is no linear relationship between sample strain induced by HFQ-simulated process and the corresponding optimum aging time.

5.2 Reduced Peak Hardness of HFQ-simulated Samples After Aging

It has been reported that cold forming after solution heat treatment can effectively enhance the precipitation behaviour and hence age hardening of age-hardenable Al alloys, especially Al-Cu-Mg based and Al-Cu based alloys (Kubora et al., 2004). It is supposed that additional dislocations are introduced into the supersaturated solid solution by cold working and thus preferred heterogeneous nucleation sites are offered for the formation of metastable second phases. Al-Mg alloys were then chosen as experimental materials to explore the influence of pre-aging cold working on the aging process. In the first experiment, 5% strain was applied to a Al-8% Mg (mass) sample by stretching, and it has been detected that the peak hardness after age treatment was enhanced as cold reduction increased (Kubora et al., 2004). It is also known that, in terms of metastable precipitate phases, preferred nucleation sites are offered by pre-existing dislocations in super saturated solid solution (SSSS), and hence the plastic deformation post solution heat treatment is able to manipulate the distribution and density of dislocations and thus second phases. Thus, in order to improve the aging behaviour of heat-treated hardenable aluminium alloys, an effective way is proved to form identity pre-existing dislocations, their distributions and hence the as-quenched microstructures. However, the above study is focused on cold forming of Al-Cu-Mg and Al-Cu based alloys and no similar study has been reported for Al-Mg-Si 6082 alloy.

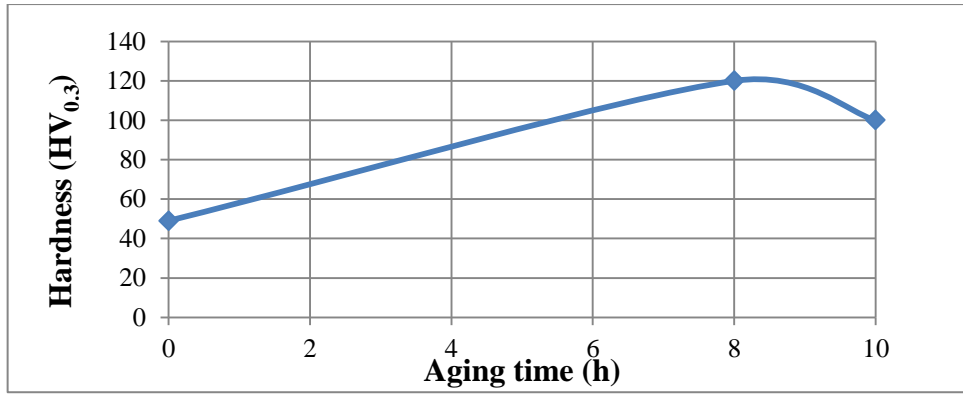
As reported in Section 4.3, the deformation induced by Gleeble test after solution treatment (i.e. simulated HFQ) was under hot conditions, which resulted in reduced rather than increased peak hardness as compared with the hardness of solution treated and peak-aged sample 0%-8 in T6 condition (see Fig.4.3-1(c)). This phenomenon was

also observed for the HFQ processed and aged components as displayed in Fig.1-1. Decrease in sample peak hardness after aging means that the amount, size and distribution of meta-stable phases in the HFQ-simulated samples would be different as in 0%-8 sample after the aging.

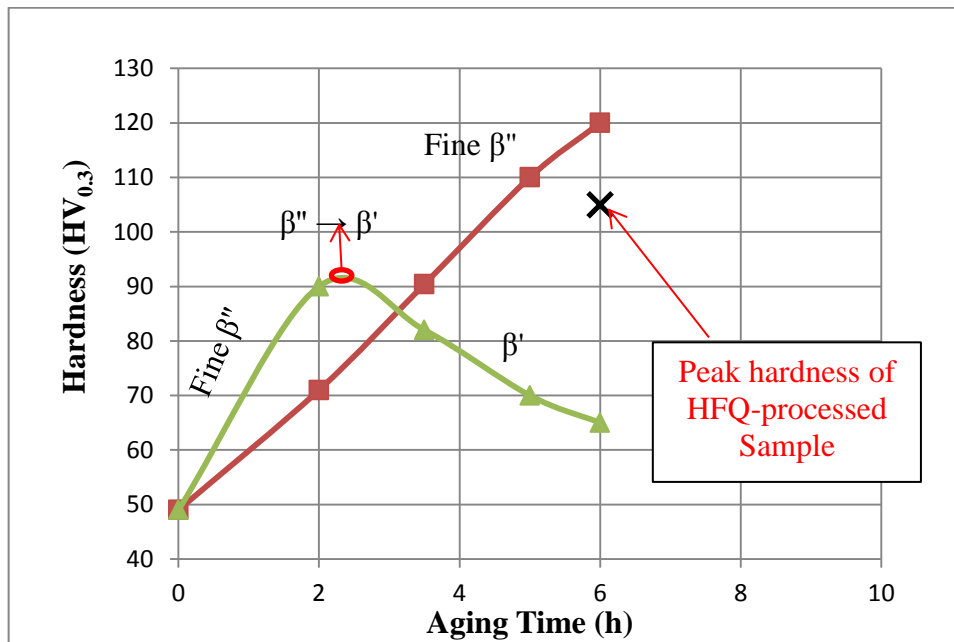
As discussed in Section 5.1 plastic deformation prior to aging is able to introduce defects and dislocations into homogeneous Al matrix, which then provide preferred nucleation sites for clusters and GP zones. Thus, the formation of metastable β'' phase is promoted in AA6082 alloys. However, TEM observation revealed that the deformation is not homogenous and as depicted in Fig.4.4-8 and Table 16, large rod-like β' precipitates are developed in severely deformed areas (as marked by yellow rectangle) while needle-like β'' precipitates were finely and homogeneously dispersed in majority of aluminium matrix.

This presumably because the high strain and hence high defect density in these severely deformed areas facilitated the formation of metastable phase β'' and β' . Therefore, in these local plastic deformation areas, introduced by the Gleeble test or HFQ process, form of metastable precipitates β'' is accelerated. Accordingly, whilst fine needle-like β'' precipitates are formed in the majority of homogeneous regions. β' phase transformed from the β'' phase formed preferentially in the severely deformed areas. The β' phase rapidly grows to thick and long rods leads to the depletion of Mg and Si in the adjacent area, thus eliminating the formation of β'' precipitates around. This assumption is supported by the observation that there are only few β'' precipitates around the β' thick rods in the area highlighted by the yellow rectangle in Fig.4.4-8 (b).

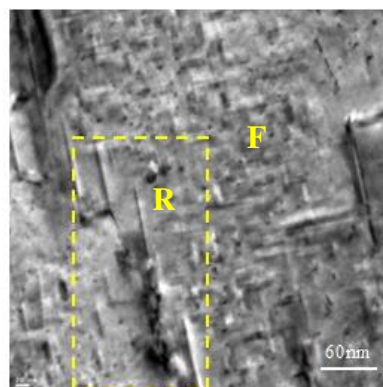
It is well known that the peak hardness of AA6082 alloy is achieved by aging to allow metastable β'' phase to be precipitated finely without transferring to the β' -Mg₂Si phase. As the transfer of the metastable β'' to the β' phase loses its coherency with the matrix, the hardness starts to drop as soon as the transformation is underway. Therefore, the preferential growth of coarse β' precipitates in the severely deformed areas would reduce the peak hardness due to local over aging. Figure 5.2-1 schematically illustrated the effect of β'' and β' precipitates on the hardness of the HFQ-processed (10%) material during aging. As illustrated in Fig.5.2-1 (a), for undeformed material, tempered in T6 condition, a peak hardness of 120 HV can be reached after 8 hours artificial aging. While for HFQ processed and aged material, the hardness is determined by the two precipitates observed by TEM characterisation: fine metastable needle-shaped β'' and rod-shaped β' phases (Fig.5.2-1 (c)). As shown in Fig.5.2-1 (b), the precipitation of fine β'' will increase the hardness to its peak value after 6 hours aging for the 10% deformed sample, as the deformation induced dislocations led to an acceleration in β'' precipitation kinetics, as discussed in section 5.1. While for the 'R' sites (see Fig.5.2-1(c)) of the material, where the deformation is introduced heavily, the transformation of β'' to β' occurred rapidly, thus resulting in low hardness locally. Therefore, the overall hardness of the material after the aging depends on the combined effect of these two lines and hence the hardness of the 10% deformed sample reduced to 105 HV.



(a)



(b)



(c)

Figure 5.2-1 Schematics of (a) hardness of AA6082 alloy against aging time; (b) effects of fine homogeneous β'' phase (marked as F in (c)) and rod β' phase (marked as R in (c)) to the hardness of deformed AA6082 alloy; (c) TEM images of deformed sample (e.g. 15%-7).

5.3 Optimised Aging Condition Applied in HFQ-processed AA6082 Alloy

In real automotive moulding process including HFQ, a car component is pressed with varied strain in different areas. However, after HFQ processing, the component has to go through aging treatment to increase its strength. As discovered in the present work, the optimal aging condition for pre-deformed AA6082 Alloy is highly strain dependent. Hence, it is impossible to find an optimal aging condition to reach the peak hardness for all the part of the component. As a result, different areas of the component will show varying hardness. On the other hand, the service stress and hence the requirement for material strength also vary with the different parts of components.

Hence, it is important to determine and make sure the risk area or key zone in a large whole component, and then the objective of subsequent aging treatment after HFQ process is to ensure that the risk area or key zone can reach the maximum hardness HFQ and aging. Owing to the different deformation strains in moulding, the other parts of the component probably are under-aged or over-aged with relatively low hardness but still meet the workpiece requirement. Therefore, the large whole component with different hardness values at different areas can meet the application requirement and is allowed to be assembled in vehicles.

An example is given here to demonstrate that different parts on automotive panels have different product hardness requirements. A body-in-white specimen is shown in Fig.5.3-1, different from this project, different types of aluminium alloys are chosen to meet different requirements on each part. For instance, outer body panels requires high strength and good hemming performance, thus AA6016 alloy in T6 condition is used with hardness as 107 HV (asm.matweb.com). While for inner structures such as

seat structures, there is no strict constraint on material strength but requires high surface quality (www.hydro.com, 2014), hence O tempered AA5182 alloy with hardness as 84 HV meets the requirement (AZoM, 2013). However, in this project, changes on component hardness requirement are able to be met via different aging conditions of AA6082 alloys.



Figure.5.3-1 Automotive body-in-white moulded by aluminium alloys (www.hydro.com, 2014).

HFQ process is a kind of highly-efficient and cost-effective forming technologies, not only reduces production steps, but also facilitates the production of high precision and complex-shaped parts using high strength aluminium alloys (5xxx, 6xxx and 7xxx series) (LoCoLite, 2013). However, these advantages are at the price of reduced peak hardness with a reduction of 14% approximately for AA6082 aluminium alloy, which generally drops to 104 HV from 120 HV. Thus, if the component hardness is required no more than or close to 104 HV, complex component can be HFQ-processed high efficiently by AA6082 alloy and then artificially aged using optimal conditions. A

table of optimum aging condition corresponding to varied strain in a certain area of workpiece with target hardness reachable is show in Table 17.

Table 17 Optimum aging condition and target peak hardness corresponded to a certain strain.

Key Area Strain	Optimum Aging Condition	Target Peak Hardness (HV_{0.3})
< 5%	180 °C×7h	106
5% ~ 10%	180 °C×6h	105
10% ~ 25%	180 °C×4.5h	104
> 25%	180 °C×3h	102

Table 17 is the standard reference table which is able to be utilized in practice during HFQ process and the following age treatment in automotive manufacture applications. For special requirement, such as workpiece with large strain but high hardness over corresponding reachable peak hardness, it is a better choice to divide the workpiece into more parts with much lower strain, which is able to be treated as non-deformed sheets, using traditional aging condition holding at 180 °C for 8 hours, aged then welded or connected and fixed with bolts and caps to assemble an integrated large component.

CHAPTER VI CONCLUSIONS AND SUGGESTED FUTURE WORK

6.1 Summary and Conclusions

An innovative solution heat treatment, forming and in-die quenching (HFQ) process has been developed by Lin et al (LoCoLite 2013) for high strength aluminium alloys (such as AA6082). The HFQ process combines die forming and quenching in one operation to reduce thermal distortion and spring back effects. The deformed aluminium alloy parts are artificially aged afterwards. However, the preliminary work has revealed that the hardness of aged HFQ processed AA6082 components varied with the positions on the component formed due to the varying strain across the whole component during HFQ forming and that the peak hardness of the product is lower than AA6082 in T6 condition. However, no work has been conducted to investigate the mechanisms involved, to study the effect of HFQ-strain on aging response and to develop the optimal aging treatment condition for HFQ processed AA6082, which formed the theme of this research work.

To this end, a Gleeble machine was used to simulate HFQ process to produce deformed AA6082 specimens with the strain ranging from 0 to 30%; a wide range of aging time at 180°C was employed to identify the optimal aging time for a given strain; and a series of materials characterisation techniques were used to investigate the mechanism involved including XRD, optical microscopy, SEM, EDX, TEM. Based on the experimental results obtained from the research, the following conclusions can be drawn.

- 1) The microstructure of the as-received AA6082 material in T6 condition consist of fine β'' - Mg_5Si_6 precipitates homogeneously distributed in α -Al matrix along [100] and [010] directions together with the inclusions of large annular AlMnFeSi particles and small circular AlMnSi particles.
- 2) When hot deformed by Gleeble tensile testing at 450°C at a strain rate of 0.1/s, homogenous deformation occurred when the strain produced by the Gleeble test is less than 10%; appreciable necking can be observed when the applied strain is reached 15% or above.
- 3) The pre-deformation introduced by Gleeble tensile testing after solution heat treatment has a significant impact on the response of the deformed AA6082 material to subsequent aging at 180°C in terms of the maximum hardness (i.e. peak hardness) after aging and the optimal aging time to achieve the peak hardness.
- 4) The optimum aging time for the sample without Gleeble tensile test and hence with no pre-deformation is 8 hours, which is the same as for T6 condition. In general, the optimal aging time corresponding to the peak hardness for HFQ-simulated samples decreases with increasing the strain introduced by Gleeble test. The optimal aging time dropped to 3 hours when the strain introduced by Gleeble test increased to 25% and 30%.
- 5) The strain caused Gleeble test can introduce defects (dislocations in particular) into supersaturated solid solution structure of AA6082 alloy. As a results, the

plastic deformation introduced by Gleeble tensile test enhances the concentration of voids, thus accelerates the formation of GP zones, as well as the process of metastable second phase precipitation and aging treatment.

- 6) The deformation induced by Gleeble test after solution treatment (i.e. simulated HFQ) resulted in reduced peak hardness (100-106HV_{0.3}) as compared with the hardness of solution treated and peak-aged sample 0%-8 in T6 condition (120HV_{0.3}). Decrease in sample peak hardness after aging is related to change in the amount, size and distribution of meta-stable phases.
- 7) TEM observation revealed that the deformation is not homogenous and large rod-like β' precipitates are formed in severely deformed areas while needle-like β'' precipitates are finely and homogeneously dispersed in aluminium matrix. The preferential growth of coarse β' precipitates in the severely deformed areas reduce the peak hardness due to the local over aging.
- 8) The peak hardness reachable and the optimum aging time at 180°C of Gleeble-processed and aged samples are strain dependent. If the strain is less than 5%, the optimum aging time is 7 hours and the peak hardness reached is 106 HV. When the strain is between 5% and 10%, the optimum aging time decreases to 6 hours and the peak hardness is 105 HV. If the strain lies in the range of 10% to 25%, the peak hardness of 104 HV requires 4 hours to reach. When the strain is increased to more than 25%, the optimum aging time decreases to 3 hours with the corresponding hardness being only 102 HV.

- 9) To apply HFQ process in industry practice, it is important to determine and make sure the risk area or key zone in a large whole component, and then the objective of subsequent aging treatment after HFQ process is to ensure that the risk area or key zone can reach the maximum hardness HFQ and aging.

- 10) Different from cold rolling, if the strain is more than 20% in HFQ process for AA6082 aluminium alloy, severe necking would take place which is not beneficial to form a shape the peak hardness is only about 102HV. Hence, it is recommended that the strain applied in HFQ process for AA6082 had better be set less than 20%.

6.2 Recommendations for Future Work

- 1) In this project, strains at 1%, 5%, 10%, 15%, 20%, 25% and 30% in HFQ-simulated test were investigated. However, in practice, the strains across a HFQ processed components are diverse. To obtain more useful aging time data, more strains in between the two adjacent values of the strains investigated in this project could be added, especially in the range of 0% to 20% at which severe necking do not take place.

- 2) Also, in the current research into the optimal aging conditions, only the effect of aging time was studied as the aging temperature is set as a constant of 180 °C. However, apart from T6 aging condition of 180°C × 8h for AA6082 alloy, other age treating methods are also able to enhance the peak hardness to 120 HV. Therefore, the effect of aging temperature should also be investigated in future work.

REFERENCES

- Aluminium Alloy – General Information – Introduction to Aluminium and Its Alloys.* (n.d.) Available from: http://www.aalco.co.uk/datasheets/Aluminium-Alloy_Introduction-to-Aluminium-and-its-alloys_9.ashx [Accessed on 8 May 2015].
- Aluminium Alloys* (n.d.) Available from: <http://www.aluminiumdesign.net/design-support/aluminium-alloys/> [Accessed on 7 March 2016].
- Aluminium Properties and Applications.* (2014) Available from: <http://www.constellium.com/technology-center/aluminium-alloy-properties> [Accessed on 8 August 2016].
- Aluminium – Specifications, Properties, Classifications and Classes, Supplier Data by Aalco.* (2005) Available from: <http://www.azom.com/article.aspx?ArticleID=2863#13> [Accessed on 7 May 2016].
- Aluminium 6061-T6; 6061-T651.* (n.d.) Available from: <http://asm.matweb.com/search/SpecificMaterial.asp?bassnum=MA6061t6> [Accessed on 3 April 2016].
- Annealing of Aluminium and Aluminium Alloys.* (2006) Available from: <http://www.totalmateria.com/Article139.htm> [Accessed on 5 June 2015].
- AZoM. (2004) *Aluminium and Aluminium Alloys - Heat Treatment of Aluminium and Aluminium Alloys.* Available from: <http://www.azom.com/article.aspx?ArticleID=2540> [Accessed on 28 May 2016].
- AZoM. (2013) *Aluminium 5182 Alloy (UNS A9158).* Available from: <http://www.azom.com/article.aspx?ArticleID=8652> [Accessed on 5 May 2016].
- Barnby, J.T., Flavell, C.J., Nadkarni, A.S. & Shi, Y.W. (n.d.) *Void Nucleation and Growth During Tensile Deformation in Steel.* Available from: <http://www.gruppofrattura.it/ocs/index.php/ICF/ICF6/paper/viewFile/3094/8156> [Accessed on 26 July 2016].
- Bay, N. (1997) ‘Cold Forming of Aluminium-State of the Art’. *Journal of Materials Processing Technology*, 71: 76-90.
- Benzerga, A.A. & Leblond, J. (2010) ‘Ductile Fracture by Void Growth to Coalescence’. *Advanced in Applied Mechanics*, 44: 169-305.
- Biról, Y. (2006) ‘DSC Analysis of the Precipitation Reactions in the Alloy AA6082 Effect of Sample Preparation’. *Journal of Thermal Analysis and Calorimetry*, 83: 219-222.
- Brown, R.D., Ambrose, F., Monragna, D. (1985) *Separation of Cast and Wrought Aluminium Alloys by Thermomechanical Processing.* Available from: file:///C:/Users/cissy/Downloads/cdc_10698_DS1.pdf [Accessed on 15 April 2016].

Cobden, R., Alcan & Banbury. (1994) *Aluminium: Physical Properties, Characteristics and Alloys*. Available from: <http://core.materials.ac.uk/repository/eaatalat/1501.pdf> [Accessed on 28 July 2016].

Cold Working and Annealing. (n.d.) Available from: <http://gatesolution-metallurgicalengineering.blogspot.co.uk/2011/07/cold-working-and-annealing.html> [Accessed on 5 May 2016].

Data Sheet AA6082 (n.d.) Available from: <http://www.aviometal.com/en/aa6082.php> [Accessed on 3 June 2016].

EU project LoCoLite. (n.d.) Available from: <http://www.localite.net/ProjectArea1/2014-news> [Accessed on 5 May 2015].

Fakir, O.E., Wang, L., Balint, D., Dear, J.P., Lin, J. & Dean, T.A. (2014) 'Numerical Study of the Solution Heat Treatment, Forming, and In-Die Quenching (HFQ) Process on AA5754'. *International Journal of Machine Tools & Manufacture*, 87: 39-48.

Fang, X., Song, M., Li, K. & Du, Y. (2010) 'Precipitation Sequence of An Aged Al-Mg-Si Alloy'. *J. Min. Metall. Sect. B-Metall.*, 46 (2) B: 171-180.

Galindo-Nava, E.I. (2013) *Thermostatistical Theory of Plastic Deformation in Metals*. BSc Thesis. Mexico City, Mexico: National Autonomous University of Mexico [published].

Garrett, R.P., Lin, J. & Dean T.A. (2005) 'An Investigation of the Effects of Solution Heat Treatment on Mechanical Properties of AA 6xxx Alloys: Experimentation and Modelling'. *International Journal of Plasticity*, 21: 1640-1657.

Granholt, J.D.D.A. (2012) *Precipitate Structure Changes During Overaging in an Al-Mg-Si Alloy*. MSc Thesis. Trondheim, Norway: Norwegian University of Science and Technology [published].

Han, L., Yang, M., Shen, Q. & Zhang, L. (2008) 'Reaction Sintering of Magnesium Silicide Thermoelectric Material by the Spark Plasma Sintering Technique'. *Journal of the Chinese Ceramic Society*, 36 (3): 337-340.

How Deformation Affects the Mechanical Properties of Aluminum Forgings. (2003) Available from: <http://apac.totalmateria.com/page.aspx?ID=CheckArticle&site=ktn&NM=89> [Accessed 8 July 2016].

Huang, J., Sun, Y., Zhao, Y., Yan, S. & Huang, Z. (2012) 'Effect of Homogenization Treatment Temperatures on Microstructure and Properties of 6082 Aluminum Alloys'. *Journal of Central South University (Science and Technology)*, 43 (3): 911-917.

Jensrud O. & Pedersen, K. (1998) 'Cold Forging of High Strength Aluminium Alloys and the Development of New Thermomechanical Processing'. *Journal of Materials Processing Technology*, 80-81: 156-160.

Juneja, B.L. (2010) *Fundamentals of Metal Forming Processes*. New Delhi: New Age International Pvt Ltd Publishers.

- Kolar, M., Pedersen, K.O., Gulbrandsen-Dahl, S., Teichmann, K. & Marthinsen, K. (2011) 'Effect of Pre-Deformation on Mechanical Response of an Artificially Aged Al-Mg-Si Alloy'. *Materials Transactions*, 52 (7): 1356-1362.
- Kubora, M., Nie, J.F. & Muddle, B.C. (2004) 'Characterisation of Precipitation Hardening Response and As-Quenched Microstructures in Al-Mg(-Ag) Alloys'. *Materials Transactions*, 45 (12): 3256-3263.
- Larsen, M.H., Walmsley, J.C., Lunder, O., Mathiesen, R.H. & Nisanciolu, K. (2008) 'Intergranular Corrosion of Copper-Containing AA6xxx AlMgSi Aluminium Alloys'. *Journal of The Electrochemical Society*, 155 (11): C550-C556.
- Lang, P. (2009) *Simulation of the Precipitation Sequence in Al-Mg-Si Alloys*. Available from: http://www.tuwien.ac.at/forschung/lehrstuhl_fuer_werkstofftechnik/projekte/abgeschlossen/peter_lang/ [Accessed on 23 June 2015].
- Lippold, J., Bollinghaus, T. & Cross, C.E. (eds.) (2011) *Hot Cracking Phenomena in Welds III*. Berlin: Springer Science+Business Media.
- 'LoCoLite: Scientific and/or Technical Quality' (2013)
- Marciniak, Z., Duncan, J.L. & Hu, S.J. (2002) *Mechanics of Sheet Metal Forming* (2nd edn.). Oxford: Butterworth Heinemann.
- Mansourinejad, M. & Mirzakhani, B. (2012) 'Influence of Sequence of Cold Working and Aging Treatment on Mechanical Behaviour of 6061 Aluminium Alloy'. *Trans. Nonferrous Met. Soc. China*, 22: 2072-2079.
- Meng, C. (2010) *Effect of Preheating Condition on Strength of AA6060 Aluminium Alloy for Extrusion*. M.Eng Thesis. Auckland, New Zealand: Auckland University of Technology [published].
- Moulton, D.B. (2013) *Wire EDM 'The Fundamentals'*. Available from: <http://www.edmnetwork.com/wire-edm-the-fundamentals-by-donald-b-moulton> [Accessed on 28 July 2016].
- Mrowka-Nowotnik, G. & Sieniawski J. (2005) 'Influence of Heat Treatment on the Microstructure and Mechanical Properties of 6005 and 6082 Aluminium Alloys'. *Journal of Materials Processing Technology*, 162-163: 367-372.
- Mrowka-Nowotnik, G., Sieniawski, J. & Nowotnik, A. (2009) 'Effect of Heat Treatment on Tensile and Fracture Toughness Properties of 6082 Alloy'. *Journal of Achievements in Materials and Manufacturing Engineering*, 32 (2): 162-170.
- Nicholson, R.B. (ed.) (1957) 'A technique for obtaining thin foils of aluminium and aluminium alloys for transmission electron metallography'. *British Journal of Applied Physics*, 9: 25-27.

Paulraj, P. & Garg, R. (2015) 'Effect of Intermetallic Phases on Corrosion Behavior and Mechanical Properties of Duplex Stainless Steel and Super-duplex Stainless Steel'. *Advances in Science and Technology Research Journal*, 9 (27): 87-105.

Polmear, I.J. (1995) *Light Alloys: Metallurgy of the Light Metals* (3rd edn.). London: Halsted Press.

Properties of Aluminium. (n.d.) Available from: <http://www.aluminiumdesign.net/why-aluminium/properties-of-aluminium/> [Accessed on 3 March 2015].

Raugei, M., Fakir, O.E., Wang, L., Lin, J. & Morrey, D. (2014) 'Life Cycle Assessment of the Potential Environmental Benefits of A Novel Hot Forming Process in Automotive Manufacturing' *Journal of Cleaner Production*, 83: 80-86.

Recrystallization and Grain Growth. (2014) Available from: <http://www.hhallberg.com/?tag=nucleation> [Accessed on 26 May 2016].

Remoe, M.S. (2014) *The Effect of Alloying Elements on the Ductility of Al-Mg-Si Alloys*. MSc Thesis. Trondheim, Norway: Norwegian University of Science and Technology [published].

Sellers, J. (2013) *Shaping the Future of Aluminium.* Available from: <https://lotusproactive.wordpress.com/2013/11/11/shaping-the-future-of-aluminium/> [Accessed on 20 March 2016].

Shi, L., Wang, Y.Q., Wang, Y., Su, H. & Zhen, L.L. (2012) 'Effect of Solution Treatment on Microstructure and Mechanical Properties of Quasi Eutectic Al-Si Alloy'. *The Chinese Journal of Nonferrous Metals*, 22 (12): 3373-3377.

Siefert, K., Merklein, M., Nester, W. & Grunbaum, M. (2011) 'Enhancement of Forming Limits of Aluminium Alloys Using An Intermediate Heat Treatment'. *AIP Conference Proceedings*; Paris, France: 24-27 October 2010. New York: American Institute of Physics.

Steinbrunner, D.L., Matlock, D.K. & Krauss, G. (1988) 'Void Formation during Tensile Testing of Dual Phase Steels'. *Metallurgical Transactions A*, 19A: 579-589.

Steinacher, M., Dragojevic, V. & Smolej, A. (2011) 'Influence of the Heat Treatment and Extrusion Process on the Mechanical and Microstructural Properties of the AlSi1MgMn Alloy'. *RMZ – Materials and Geoenvironment*, 58 (3): 329-338.

Strengthening/Hardening Mechanisms. (n.d.) Available from: <https://www.nde-ed.org/EducationResources/CommunityCollege/Materials/Structure/strengthening.htm> [Accessed 9 May 2016].

Strip and Sheet for Body. (2014) Available from: <http://www.hydro.com/en/Products/Rolled-products/Strip-and-sheet-for-automotive/Aluminium-strip-and-sheet-for-Body/> [Accessed on 5 October 2016].

Takata, K. (2013) 'Warm Forming of Aluminium Alloys'. *Nippon Steel Technical Report* 103: 104-109.

Tan, E. & Ogel, B. (2007) 'Influence of Heat Treatment on the Mechanical Properties of AA6066 Alloy'. *Turkish J. Eng. Env. Sci.*, 31: 53-60.

Umeda, J., Kondoh, K., Kawakami, M. & Imai, H. (2008) 'Solid State Synthesis of Mg₂Si/MgO Composites from an Elemental Mixture Powder of Magnesium and Rise Husk Silica'. *Transactions of JWRI*, 37 (1): 113-117.

Understanding the Alloys of Aluminium. (n.d.) Available from: <http://www.alcotec.com/us/en/education/knowledge/techknowledge/understanding-the-alloys-of-aluminium.cfm> [Accessed on 10 May 2016].

Wenner, S. (2014) *Transmission Electron Microscopy and Muon Spin Relaxation Studies of Precipitation in Al-Mg-Si Alloys*. PhD Thesis. Trondheim, Norway: Norwegian University of Science and Technology [published].

Wenner, S., Marioara, C.D., Ramasse, Q.M., Kepaptsoglou, D., Hage, F.S. & Holmestad, R. (2013) 'Atomic-resolution Electron Energy Loss Studies of Precipitates in An Al-Mg-Si-Cu-Ag Alloy'. *Scripta Materialia*, 74: 92-95.

Wenner, S., Marsuda, H.M., Nishimura, K., Matsuzaki, T., Tomono, D., Pratt, F.L. & Marioara, C.D. (2012) 'Probing Defects in Al-Mg-Si Alloys Using Muon Spin Relaxation'. *Physical Review B*, 86: 59-65.

Wenner, S., Nishimura, K., Matsuda, K., Marsuzaki, T., Tomono, D., Pratt, F.L., Marioara, C.D. & Holmestad, R. (2013) 'Muon Kinetics in Heat Treated Al (-Mg)(-Si) Alloys'. *Acta Materialia*, 61: 6082-6092.

Williams, D.B. & Carter, C.B. (2008) *Transmission Electron Microscopy: A Textbook for Materials Science*. New York: Springer Science+Business Media.

Wire EDM: Features & Benefits. (n.d.) Available from: <http://www.precisionmicro.com/74/features-&-benefits/other-processes/wire-edm> [Accessed on 6 April 2016].

Woodford, C. (2016) *Aluminium.* Available from: <http://www.explainthatstuff.com/aluminum.html> [Accessed on 30 April 2016].

Woodward R. (2001) *Aluminium and Aluminium Alloys Designations*. Available from: <http://www.azom.com/article.aspx?ArticleID=310> [Accessed on 18 February 2016].

Worrall, E. (2015) *Are Stringent Vehicle Emissions Standards Driving a Surge in Coal?* Available from: <https://wattsupwiththat.com/2015/11/22/are-stringent-vehicle-emissions-standards-driving-a-surge-in-coal/> [Accessed on 4 April 2016].

Xue, H. (2012) *Assessment of U-shape Springback*. BEng Thesis. London, UK: Imperial College London [published].

Zhang, C. (2014) *Study on the Solution Heat Treatment of Aluminium Alloy 6082*. MSc Thesis. London, UK: Imperial Collge London [unpublished].

Zhang, Z. & Chen, D.L. (2006) 'Consideration of Orowan Strengthening Effect in Particulate-reinforced Metal Matrix Nanocomposites: A Model for Predicting Their Yield Strength'. *Scripta Materialia*, 54 (7): 1321-1326.

Zheng, J. (2014) Investigation of Fast Ageing Process for AA6082. MSc Thesis. London, UK: Imperial Collge London [unpublished].

Zhu, J., Wang, W., Lin, M., Liu, W., Wang, J. & Zhou, B. (2008) '3D Atom Probe Characterization of Precipitation of Cu-rich Clusters in Pressure Vessel Model Steel'. *Journal of Shanghai University (Natural Science)*, 14 (5): 525-530.

Zou, Y., Tao, H., Xu, G., Li, Y. & Zhu, H. (2007) 'Research on Heat Treatment Parameters of 6082 Aluminium Alloy'. *Heat Treatment of Metals*, 32 (10): 71-76.

1200°C - Laboratory Chamber Furnaces. (n.d.) Available from: <http://www.elitefurnaces.com/eng/products/furnaces/1200%20Laboratory%20Chamber%20Furnaces.php> [Accessed on 5 July 2016].